Technische Universität München
Fakultät für Chemie
Lehrstuhl für Technische Chemie II

Selective Oxidation of Methane to Methanol on Cu-Based Catalysts Supported on Microporous Materials

Takaaki Ikuno

Vollständiger Abdruck der von der Fakultät für Chemie der Technischen Universität München zur Erlegung des akademischen Grades eines

Doktors der Naturwissenschaften (Dr. rer. nat.)

genehmigten Dissertation.

Vorsitzender:	Prof. Dr. Dr. h.c. Bernhard Rieger
Prüfer der Dissertation:	Prof. Dr. Johannes A. Lercher
	Prof. Dr. Roland A. Fischer

Die Dissertation wurde am 25.07.2019 bei der Technischen Universität München eingereicht und durch die Fakultät für Chemie am 02.09.2019 angenommen.

“Patience is bitter, but its fruit is sweet.”

Hideyo Noguchi (1876-1928)

Acknowledgements

It has been a foggy, winding path throughout my doctoral research. However, as I know from my cycling experience, the harder and the steeper the climb is, the more beautiful and victorious scenery is awaiting. I have struggled a lot, and therefore, with the support of many people, I could learn and grow, and I am finally standing here.

I would like to thank Prof. Dr. Johannes A. Lercher for providing the opportunity to conduct research on a challenging and competitive topic. Through scientific discussion with you, I have learned how to do rigorous science. You were always not only patient and open during discussion with me, but also sharp and critical to misleading ideas and hypotheses. Discussion with you have been always inspiring and I am glad to have been able to work with you.

My special gratitude goes to Dr. Maricruz Sanchez-Sanchez, who has supervised me throughout my doctoral study. You have been always very open, trustful and supportive, and am very glad that I had many opportunities to discuss with you, even on very small issues. It was a lot of fun and learning to have scientific exchange. This dissertation could not have been completed without your help.

I thank Prof. Dr. Andreas Jentys for his support in research, especially in XAS. Your deep understanding in spectroscopic techniques helped in driving my research ahead. Your funny stories from good old times were definitely a nice entertainment especially during intense beamline trips full of tiredness and desperation.

My collaborators, especially Dr. Evgeny Pidko, Dr. Jian Zhen and Dr. John Fulton are acknowledged for their scientific input and fruitful and constructive discussion. Especially I have learned really a lot on XAS from John, and I am glad to have had beamline trips with you.

Deutsche Forschungsgemeinschaft (DFG) and International Graduate School of Science and Engineering (IGSSE) at TUM are acknowledged for the financial support on the project.

I am grateful to the administrative staffs, Stefanie Seibold, Kateryna Kryvko, Ulrike Sanwald and Bettina Federmann for all the support in my life at the chair. Technical

staffs at TC2, Franz-Xaver Hecht, Andreas Marx and Martin Neukamm are acknowledged for the technical support in the lab.

Dr. Sebastian Grundner introduced me to this research topic and to different experimental techniques at the beginning of my doctoral research. It certainly helped me with finding ways to answer scientific questions. I really appreciate the time spent with my project colleagues and also friends, Insu Lee, Matteo Ranieri and Lei Tao. I had a lot of fun having scientific discussion, as well as fun time outside of work.

I would also like to thank students who have worked with me, especially Xiao Han for her good work during her Master's thesis. My acknowledgement also goes to all the former and current colleagues at TC2. I had a good time in the old office as well as in CRC. Even the hard beamline trips were also fun with nice people at the chair.

My life in Munich has become much better and with friendship with Ricardo Bermejo-Deval, Stanislav Kasakov, Moritz Schreiber and Marco Peroni. True friendship will live forever, and I am looking forward to the fun time that we will have together in the future.

Finally yet importantly, I want to thank my family for their unconditional support and encouragement for whole my life. And of course Daria for being my family here in Germany and for supporting me in any difficult situations.

Takaaki Ikuno

September 2019

Abbreviations

3QMAS NMR	Triple-quantum magic angle spinning nuclear magnetic resonance
AAS	Atomic absorption spectroscopy
ALD	Atomic layer deposition
BAS	Brønsted acid site
bypm	2,2’-bipyrimidinyl
CN	Coordination number
CTF	Covalent triazine-based framework
d6r	Double-6-ring
DFT	Density-functional theory
dmap	Dimethylamino-2-propoxy
DME	Dimethyl ether
DSC	Differential scanning calorimetry
DW	Debye-Waller
EFAl	Extra-framework Al
EXAFS	Extended X-ray absorption fine structure
FAl	Framework Al
FT	Fourier-transformed
FTC	Framework type code
ICP-AES	Inductively coupled plasma-atomic emission spectroscopy
IR	Infrared
IZA-ZC	Structure Commission of the International Zeolite Association
LAS	Lewis acid site
LMCT	Ligand-to-metal charge transfer
MAS NMR	Magic-angle spinning nuclear magnetic resonance

MMO	Methane monooxygenase
MMOB	Regulatory protein in soluble methane monooxygenase
MMOH	Hydroxylase in soluble methane monooxygenase
MMOR	Reductase in soluble methane monooxygenase
MOF	Metal-organic framework
MR	Membered-ring
MS	Mass spectrometry
MTH	Methanol to hydrocarbon
pMMO	Particulate methane monooxygenase
SCR	Selective catalytic reduction
sMMO	Soluble methane monooxygenase
STEM	Scanning transmission electron microscopy
TBAPy	1,3,6,8-tetrakis(p-benzoic acid)pyrene
TGA	Thermogravimetric analysis
TOF	Turnover frequency
TPR	Temperature-programmed reduction
UV-Vis	Ultraviolet-visible
XANES	X-ray absorption near-edge structure
XAS	X-ray absorption spectroscopy
XRD	X-ray diffraction
ΔH^o	Standard enthalpy of reaction

Abstract

Formation of Cu trimers hosted in mordenite, which oxidize methane selectively into methanol, occurs via thermally driven mobilization of Cu^+ species, followed by their facile oxidation. Reactivity of Cu-oxo clusters is affected by their location in the zeolite micropore structure and by interaction with adjacent extra-framework Al species. Therefore, control of both extra-framework Al formation and Cu speciation is critical for synthesizing active Cu-zeolites. Supports suitable to host active Cu-oxo clusters provide structural confines, well-defined pore structure and anchoring sites as well as thermal stability and oxidation resistance.

Zusammenfassung

Die Bildung von Cu-oxo-Trimeren in Mordenit, die Methan selektiv zu Methanol oxidieren, erfolgt durch thermisch induzierte Mobilisierung von Cu^+ Kationen, gefolgt von Oxidation zu mindestens Cu^{2+}. Die Reaktivität der Cu-oxo-Trimere wird durch ihre Position im Zeolithen und durch die Wechselwirkung mit Aluminiumoxid Clustern in den Poren beeinflusst. Für Synthesewege zu definierten Katalysatoren sind daher sowohl die Anwesenheit der Aluminiumoxid Cluster als auch der Form und Nuklearität der Cu-Oxo-Cluster entscheidend. Trägermaterialien, die geeignet sind, aktive Cu-Oxo-Cluster zu stabilisieren, müssen wohldefinierte Nanoporen besitzen, sowie Bindungszentren, die thermisch stabil und gegen Oxidation geschützt sind.

Table of Contents

1. General Introduction

1.1. Challenges in Utilization of Methane

Natural gas is growing its abundancy as a primary energy source due to the surge of shale gas reserve.[1] Many natural gas reserves are dispersed and located remotely from the existing infrastructure,[2-3] thus the transport of the natural gas requires the construction of expensive gas pipelines or its liquefaction. However, due to very low boiling point of its primary component methane (-161.5 °C), liquefaction of the natural gas is highly energy intensive. As a consequence of these challenges in the transportation, more than 140 billion cubic meters of natural gas is estimated to be annually flared in addition to fugitive emission and routine venting and leaking of natural gas into the environment.[4] Such emission of carbon dioxide and methane as greenhouse gases has greatly negative impact on the current situation of global warming. Therefore, to be integrated in the existing infrastructure for economical transportation of the natural gas, it has to be converted to easily condensable chemicals.

Methane is the main component of natural gas, accounting for up to approximately 90% of the gas volume.[5] Hence, the conversion of methane plays a very important role in the utilization of natural gas as a feedstock. However, due to the high symmetry of methane molecule as well as its high C-H bond dissociation energy of 439 kJ/mol, severe reaction conditions are often applied to methane conversion processes, resulting in undesired energy intensive processes.

1.2. Conventional Route of Methane Conversion

Production of synthesis gas (syngas) from methane is to date the most applied processes for methane utilization. This is achieved by steam or dry reforming of methane (equations 1.1, 1.2). Because of the endothermic character, conversion of methane is favored at high temperature.

$$CH_4 + CO_2 \rightleftharpoons 2CO + 2H_2 \qquad \Delta H^o_{298K} = 247 \text{ kJ/mol} \qquad (1.1)$$

$$CH_4 + H_2O \rightleftharpoons CO + 3H_2 \qquad \Delta H^o_{298K} = 206 \text{ kJ/mol} \qquad (1.2)$$

Dry reforming produces CO rich syngas typically on Ni or noble metal based catalysts [6], and it is suitable for the further production of higher hydrocarbons and chemicals. However, the catalysts tend to suffer deactivation due to coke deposition and sintering of catalyst caused at high reaction temperatures (550-1000 °C).[7-8]

On the other hand, steam reforming produces more H_2 utilizing Ni-based catalysts at high temperatures (outlet temperature of 800-950 °C). While coke formation is suppressed by adjusting the reaction gas compositions and catalysts[9], sintering of catalyst particles at high reactions temperatures as well as sulfur poisoning of the catalysts are the major cause of catalyst deactivation.[10]

Produced syngas can be further converted to higher hydrocarbons via Fischer-Tropsch synthesis at relatively mild temperatures (200-300 °C) and moderate pressures (10-40 bar) using Fe or Co catalysts.[11] Formation of hydrocarbons from syngas is exothermic (~165 kJ/mol_{CO}). Alternatively, syngas can be also converted to methanol via methanol synthesis and subsequently to higher hydrocarbons by methanol-to-hydrocarbon (MTH) processes. Methanol synthesis is carried out typically on Cu/ZnO/Al_2O_3 catalysts at moderate temperatures and pressures of 200-300 °C and 50-150 bar.[12] Methanol synthesis proceeds as the sequence of water-gas shift reaction (equation 1.3) and hydrogenation of CO_2 (equation 1.4).

$$CO + H_2O \rightleftharpoons H_2 + CO_2 \qquad \Delta H^o_{298K} = -41.2 \text{ kJ/mol} \qquad (1.3)$$

$$CO_2 + 3H_2 \rightleftharpoons CH_3OH + H_2O \qquad \Delta H^o_{298K} = -49.5 \text{ kJ/mol} \qquad (1.4)$$

Cu/ZnO/Al_2O_3 catalysts suffer from deactivation in the presence of sulfur by the formation of inactive Cu surface sulfide. Additionally, sintering of Cu particles is the

major cause of deactivation, and the presence of chorine accelerates this process, possibly by the formation of volatile Cu and Zn chloride phases.[12]

As shown, conventional methods of converting methane into other value-added chemicals include energy intensive methane reforming processes. Endothermic processes make it uneconomical to downscale the reactor, despite dispersed natural gas reserves. To tackle the current situation, selective oxidation of methane into methanol is a promising. Since the reaction is exothermic (equation 1.5), the process is suitable to be run at smaller scales.

$$CH_4 + 1/2\ O_2 \rightleftharpoons CH_3OH \qquad \Delta H^o_{298K} = -128\ kJ/mol \qquad (1.5)$$

However, due to the higher reactivity of methanol than methane, it is challenging to maintain a high selectivity to methanol.

1.3. Selective Oxidation of Methane to Methanol

Various homogeneous as well as heterogeneous catalysts have been investigated to achieve selective oxidation of methane to methanol.

Periana et al. discovered Hg(II) to be able to catalyze the selective oxidation of methane at a moderate temperature of 180 °C.[13] H_2SO_4 was found to be able to function as oxygen transfer-agent in the presence of Hg(II)-based catalysts, and the following reactions were proposed to take place during catalytic reaction cycles.

$$CH_4 + 2H_2SO_4 \xrightarrow{Hg(II)} CH_3OSO_3H + 2H_2O + SO_2 \quad (1.6)$$

$$CH_3OSO_3H + H_2O \longrightarrow CH_3OH + H_2SO_4 \quad (1.7)$$

$$SO_2 + 1/2O_2 + H_2O \longrightarrow H_2SO_4 \quad (1.8)$$

Pt(II) amine complexes were found to be more active compared to Hg(II) salt in catalyzing selective oxidation of methane, using concentrated H_2SO_4 as an oxidant.[14] The obtained methyl bisulfate can be hydrolyzed to obtain methanol as the final product. Activation of C-H bond occurs at Pt(II), while Pt(IV) species formed via oxidation in concentrated H_2SO_4 was found to be inactive for reaction with methane. Further mechanistic study on such “Periana Catalytica” system has found out that stable catalytic systems with higher TOF can be obtained by increasing the rate of oxidation of Pt(II) to Pt(IV).[15] Reaction of over-oxidized Pt(IV) species with Pt(II)-CH_3 species results in the formation of methyl bisulfate and the regeneration of catalytically active Pt(II) species. Similar behavior was observed in the system found by Shilov et al., where Pt(IV) functions as stoichiometric oxidant while the overall reaction is catalytic in Pt(II).[16-17] Despite remarkable progress in the activation of methane in the Periana-Catalytica system, the use of noble metal as well as the harsh reaction conditions, such as the use of concentrated H_2SO_4, make the process difficult to be run at a large scale.

In nature, bacteria known as methanotrophs are able to convert methane into methanol under ambient temperature and pressure using environmental O_2 by employing enzymes called *methane monooxygenases* (MMOs).[18] Two different forms of MMOs are known: one is soluble MMO (sMMO) which contains diiron centers as an active site, and the other one is membrane-bound particulate MMO (pMMO) which contains

copper in its active center and is able to activate methane at a turnover frequency (TOF) = 1 s^{-1}.[19]

Structure and mechanism of CH_4 reaction on sMMO are well established due to its high stability after purification.[20] sMMO consists of hydroxylase (MMOH), reductase (MMOR) and a regulatory protein (MMOB), and MMOH, where hydroxylation of methane is carried out, contains diiron center (Figure 1-1).[20-21] Catalytic oxidation of methane occurs as a series of reaction steps, which consists of (i) the reduction of diiron(III) center with the aid of MMOR, (ii) activation of diiron(III) center with O_2, (iii) structural transformation of peroxo intermediate into the key intermediate which oxidizes methane into methanol, and (iv) regeneration of diiron(II) center upon release of methanol and H_2O.[18]

The structure of pMMO, on the other hand, is under debate due to its low stability in the purification process.[22-23] As a result, the structure of pMMO is still under debate, while copper center is known to play a key role in the oxidation of methane.[18, 22-24] Dicopper[24-25] as well as tricopper[18, 23, 26] centers are proposed to be the active sites, however, reaction mechanism of methane in pMMO remains unclear.

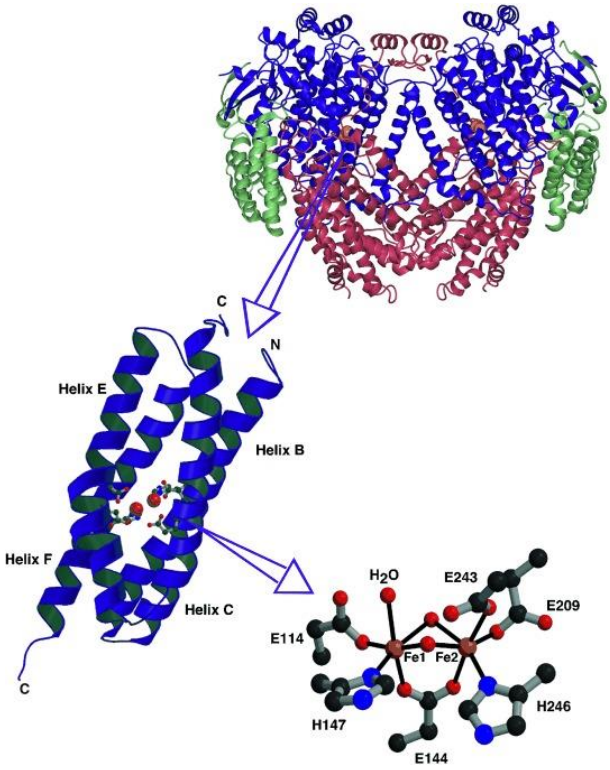

Figure 1-1. Three structural levels of hydroxylase (MMOH) in sMMO (adapted with permission from ref [20]).

Based on the existing knowledge on pMMO, synthesis of trinuclear copper catalysts[27-28] as well as the fabrication of printable biocatalytic polymer by embedding pMMO in polyethylene glycol diacrylate hydrogel[29] were carried out. Even though selective oxidation of methane into methanol was successfully observed at ambient temperature, catalyst longevity as well as the usage of expensive reagents in the preparation of catalysts or reaction remain as challenges.

Excellent activity and methanol selectivity of MMOs inspired scientists to investigate Cu- and Fe-catalysts supported on zeolites as well as other transition metal-exchanged zeolites.[30-34] While Fe-zeolite catalysts requires activation in N_2O,[31] Cu- and other transition metal-exchanged zeolites can be activated using O_2 as an oxidant.[35-36] Moreover, methanol yield on Cu-zeolite catalysts have drastically improved in the last decade among different transition metal-exchanged catalysts.[37] These facts make Cu-zeolite catalysts promising candidates for industrial applications.

Methane oxidation on Cu-zeolite catalysts are often carried out in three-step, where activation of the catalyst at high temperatures, reaction of methane on the activated catalyst, and product desorption are carried out separately, resulting in a single turnover at an active site. Continuous catalytic reaction in gas phase only yields low TOF or selectivity to methanol,[38-39] while in aqueous phase, the usage of expensive H_2O_2 is required.[34, 40] These challenges keep Cu-zeolite catalysts from application to selective oxidation of methane to methanol. However, despite these drawbacks, Cu-zeolites remain attractive due to the high thermal stability and low production cost of these materials. In addition to zeolites, active Cu can be hosted in other porous materials, such as mesoporous silica and metal-organic framework (MOF).

1.4. Zeolites

1.4.1. Structure of Zeolites

Zeolites are a series of crystalline microporous aluminosilicate materials, which consist of TO_4 (T denotes tetrahedrally coordinated Si and Al) tetrahedra as elementary building unit (Figure 1-2). Different arrangement of the TO_4 tetrahedra results in different topologies. Structures of the zeolites are often classified according to their framework topology as Framework Type Code (FTC), assigned by Structure Commission of the International Zeolite Association (IZA-SC). 245 structures have been assigned to date.[41] Zeolites can also be classified according to their pore size, which is denoted as the number of T-atoms consisting the pore. 8 membered-ring (MR), 10 MR and 12 MR can be typically found in zeolites, and they are called small-pore, medium-pore and large-pore zeolites, respectively.

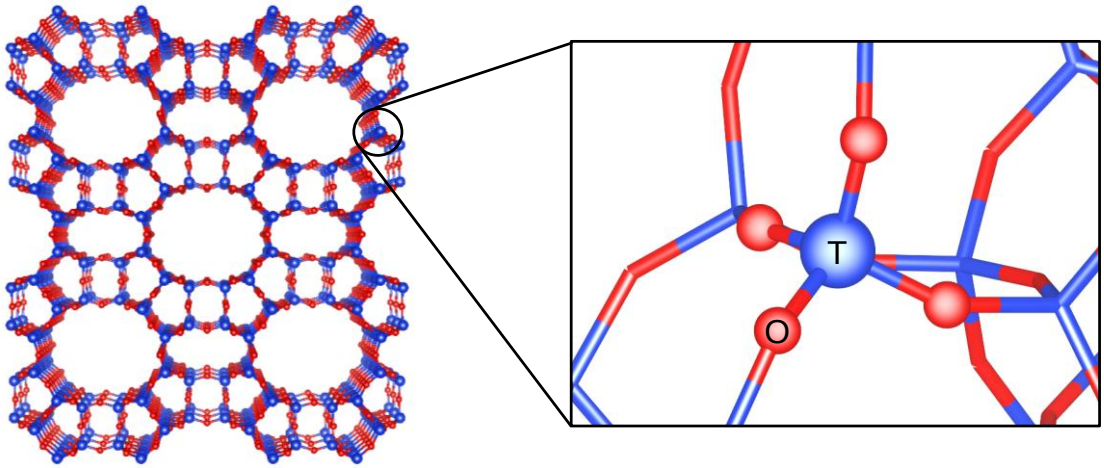

Figure 1-2. Structure of MOR-type zeolite consisting of TO_4 elementary building unit.

Due to high thermal stability, microporosity and highly organized unique structures, zeolites are suitable for heterogeneous catalysts. Among various zeolites, structures of MOR, MFI, MEL, FER and CHA are described in detail below due to their relevance to this study.

MOR is a large-pore zeolite which possesses 1-dimensional 12 MR straight channels (6.5 x 7.0 Å) with 8 MR side pockets perpendicular to the 12 MR main channel, consisting of 4 and 5 MR wall (Figure 1-3). Entrance of the 8 MR side pockets are sized 3.9 x 5.7 Å, and they are interconnected with a restricting 8 MR. Since the size of the

interconnecting 8 MR is small, MOR is regarded as a zeolite with 1-dimensional channel structure. 8 MR channels (2.6 x 5.7 Å) are also present along the 12 MR main channel.

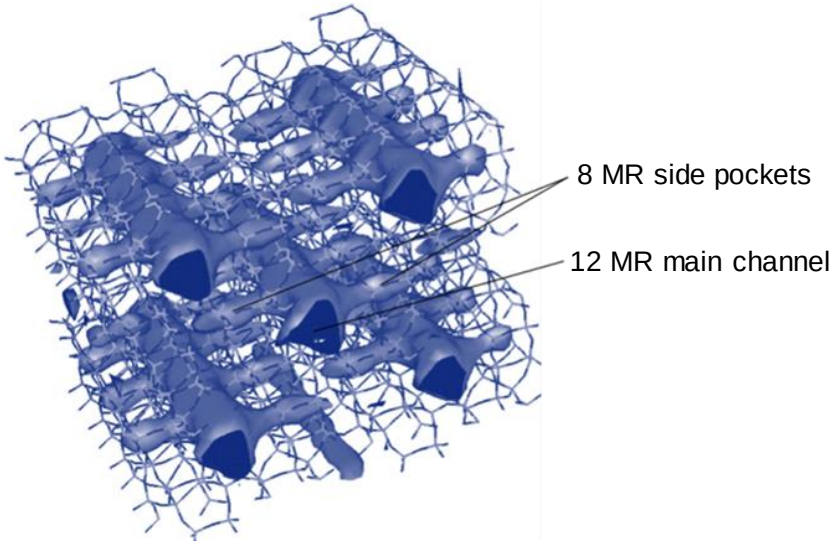

Figure 1-3. Channel structure of MOR consisting of 12 MR main channel and 8 MR side pockets.

MFI (also ZSM-5) is a medium-pore pentasil zeolite possessing interconnected 10 MR straight channels (5.3 x 5.6 Å) and sinusoidal channels (5.1 x 5.5 Å), resulting in 3-dimensional pore structure (Figure 1-4). Intersection of two 10 MR channels is large enough to include a sphere with 6.36 Å diameter. MFI plays an important role in petrochemical industry due to its shape selective effect in cracking and methylation of aromatics.[42-45]

MEL (also ZSM-11) possesses interconnected straight 10 MR channels (5.3 x 5.4 Å), creating 3-dimensional pore structure, and the walls of the 10 MR channels have shallow dents of 8 MR. Since its pore size is similar to MFI, MEL is often used as a reference to study the effect of pore structure on the shape selectivity in catalysis.[46]

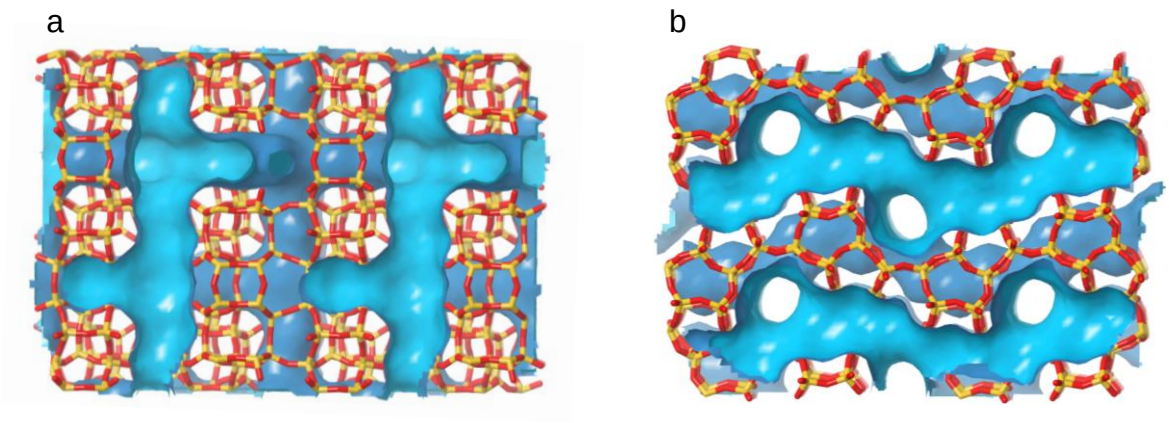

Figure 1-4. Framework and pore structure of MFI viewed along [010] (a) and [001] (b), representative of straight and sinusoidal 10 MR channels, respectively.[41]

FER has straight 10 MR channels (4.5 x 5.4 Å) along [001], that are connected with cages with 8 MR openings (3.5 x 4.8 Å) to the direction of [010], resulting in 2-dimensional pore structure (Figure 1-5 (a), (b)). FER is an important catalyst in skeletal isomerization of olefins.[47-48]

CHA is a small-pore zeolite, constructed by stacking of cha-cage and double-6-ring (d6r), resulting in a highly symmetric structure (Figure 1-5 (c)). Though cha-cage can include a sphere with a diameter of 7.37 Å, diffusion is limited by 8 MR (3.8 x 3.8 Å). Cu ion-exchanged CHA catalysts, such as Cu-SSZ-13 (aluminosilicate framework) and Cu-SAPO-34 (silicoaluminophosphate framework), attract great interests due to the superior performance in selective catalytic reduction (SCR) of NO_x for automotive exhaust gas purification.[49-50]

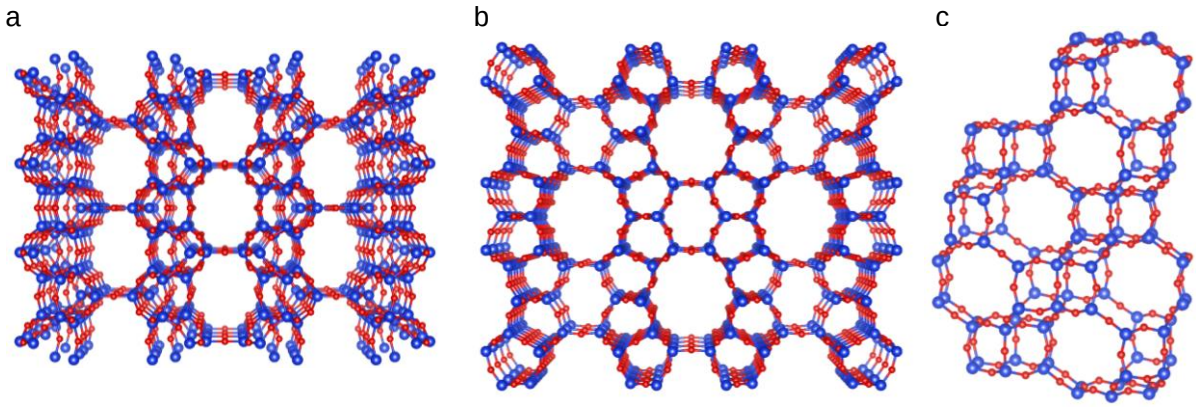

Figure 1-5. Framework structure of FER viewed along [010] (a) and [001] (b), and the structure of CHA viewed normal to [001] (c).

1.4.2. Ion exchange of Zeolites

Substitution of Si^{4+} in tetrahedron with Al^{3+} introduces a negative charge at a neighboring O atom. Isomorphous substitution of T-sites is governed by Löwenstein's rule, which indicates that Al-O-Al bond cannot be formed in zeolite framework. This results in the minimum framework Si/Al ratio of 1. Brønsted acid sites (BAS) can be created by balancing the negatively charged framework Al sites with protons, resulting in a bridging OH group[51] (Figure 1-6), and it is able to catalyze various reactions. Other cations, such as alkaline and alkaline earth metal cations as well as different transition metal cations, can also balance the negative charge (Figure 1-6). This results in the formation of Lewis acid sites (LAS), and it is the basis of ion-exchangeability of zeolite. Transition metal exchanged in zeolites can also act as active sites for catalysis, such as olefin dimerization on Ni-exchanged zeolites[52] and selective catalytic reduction of NO_x on Fe- and Cu-exchanged zeolites.[49-50, 53]

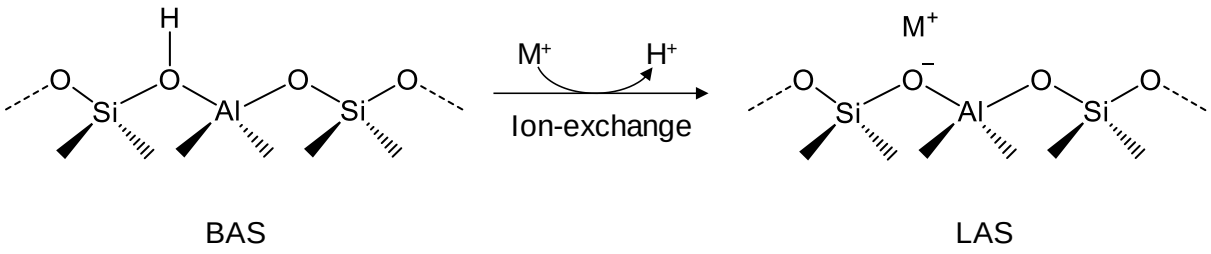

Figure 1-6. Structure of BAS and its ion-exchange by a metal cation (denoted as M^+) resulting in the formation of LAS.

Distribution of BAS and LAS are known to play a crucial role in catalysis. For instance, Na^+ cations selectively exchange BAS in 8 MR side pockets of H-MOR, resulting in a significant decrease in TOF of *m*-xylene isomerization, suggesting that BAS with stronger acidity are present in 8 MR side pockets, rather than in 12 MR main channel.[54] It is also reported that BAS location in H-MFI catalysts affects not only the activity and selectivity in paraffin cracking and disproportionation of aromatic compounds, but also lifetime of the catalysts.[55]

Dedecek et al. have reported that the concentration of "paired" Al sites can be determined by Co^{2+}-exchange of Na-form of the zeolites in aqueous phase.[56] Under well-controlled conditions, exclusive presence of $[Co(H_2O)_6]^{2+}$ can be guaranteed both

in aqueous phase and in hydrated zeolites.[57-58] While such cobalt hexaaquocomplex can compensate a paired Al sites which is described as Al-O-(Si-O)$_n$-Al with n = 1, 2, it cannot compensate an isolated Al sites (n > 2). When Co^{2+}-exchanged MOR is dehydrated, several different sites can be occupied by Co^{2+}. By X-ray diffraction (XRD) study, five different sites are determined to be occupied by different cations such as K^+, Cs^+, Ca^{2+} and Ba^{2+} (Figure 1-7).[59]

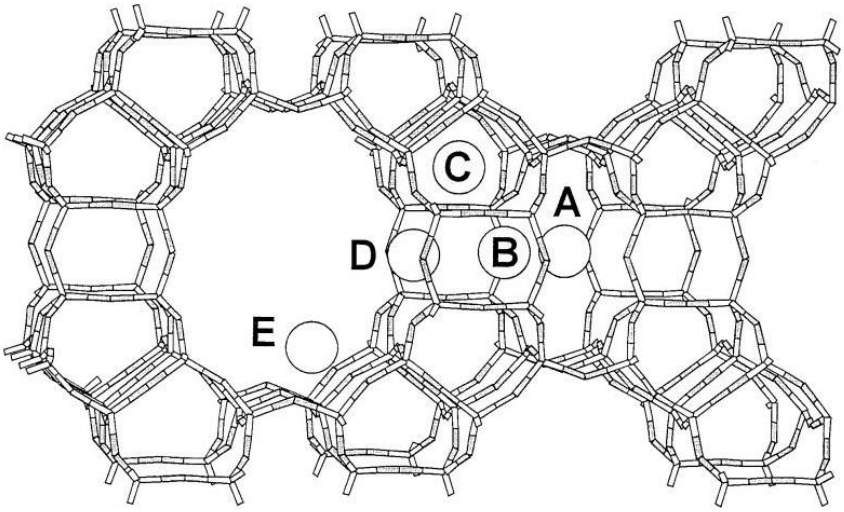

Figure 1-7. Cationic sites in dehydrated MOR (adapted with permission from ref [60]).

Among five different cationic sites, sites A, C and E are plausible to be occupied by Co^{2+}, since sites B and D are too large to coordinate dehydrated Co^{2+}.[60] While site C can be only occupied at high Co^{2+} loading due to the lowest stabilization energy of Co^{2+}, occupation of sites A and E depends on the conditions of ion-exchange and dehydration procedure.

It is often reported that transition metal cations exchanged in Si-rich zeolites form metal-oxo clusters when dehydrated in oxidative conditions. For instance, oxidative activation of Co- and Cu-exchanged zeolites form Co-oxo and Cu-oxo clusters, which can be active in the oxidation of light alkanes.[36, 61] As a consequence of the formation of larger metal-oxo clusters, the locations of such species are strongly affected by conditions of activation and sample preparation, as well as by local arrangement of Al in zeolite framework. Dedecek et al. have shown that the different distribution of Al in MOR results in different locations of exchanged Cu cations, which strongly affects the reducibility of Cu^{2+} into Cu^+.[62]

Infrared (IR) spectroscopy with the aid of probe molecules is suitable to determine the location of BAS in zeolites. In the case of H-MOR, adsorption of *n*-hexane covers BAS in 12 MR main channel, while it is not able to access 8 MR side pockets.[63] It was observed during stepwise dosing of *n*-hexane that the position of the band corresponding to BAS red-shifted upon adsorption of *n*-hexane, suggesting that the band has contribution from two distinguishable bands at 3612 cm^{-1} and 3590 cm^{-1}, attributed to BAS located in 12 MR main channel and 8 MR side pockets, respectively (Figure 1-8). On the other hand, pyridine, which is commonly used as a probe molecule to quantify BAS and LAS in zeolites, cannot access acid sites located at the bottom of 8 MR side pockets in MOR.[54]

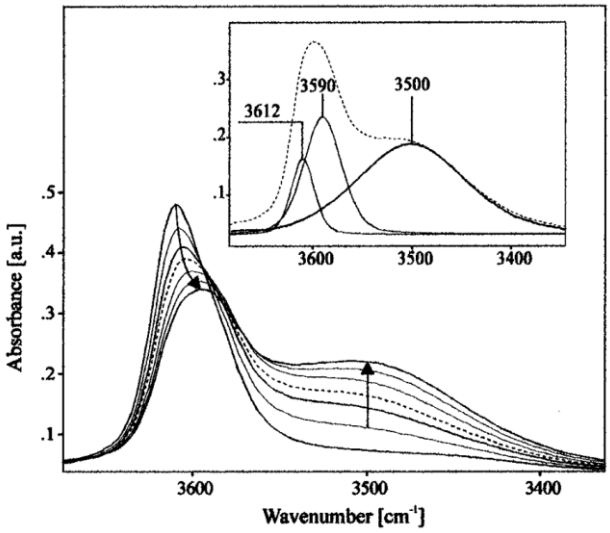

Figure 1-8. IR spectra of H-MOR in O-H vibration region during adsorption of *n*-hexane (adapted with permission from ref [63]).

1.5. Application of Cu-Exchanged Zeolites in Catalysis

1.5.1. Selective Catalytic Reduction of NO_x

Besides noble metal and metal oxide catalysts, Cu-exchanged Y zeolites have been first found to be able to carry out catalytic decomposition of NO into N_2 and O_2.[64] Activity of the catalyst in such systems was improved by excessive Cu-exchange of MFI.[65] It was proposed that Cu^+ species take part in the reduction of NO and transformed into $[Cu\text{-}O\text{-}Cu]^{2+}$ and CuO clusters.[66] Formation of such multinuclear Cu clusters suggests that the closely located Cu species are responsible for NO decomposition.[67] $[Cu\text{-}O\text{-}Cu]^{2+}$ species can be reduced to a pair of Cu^+ at elevated temperature in inert atmosphere.[68]

In the standard SCR reaction, decomposition of NO in the presence of NH_3 and O_2 forms N_2 and H_2O as products. It is known that different reactions mechanisms govern in different temperature regimes.[69] While Cu ions are fully solvated by NH_3 at temperatures below 350 °C as mobile monomeric Cu species, at temperatures above 350 °C, Cu cations are anchored at Al sites in zeolites.[70] Decrement of SCR activity at temperature lower than 250 °C is proposed to be due to the limitation in the activation of O_2 to regenerate Cu^{2+} species which is able to activate NO. It is reported that Si/Al ratio and Cu/Al ratio of the catalysts affect the location and redox properties of exchanged Cu^{2+}.[71] Increase of Cu/Al ratio results in the increasing reducibility of Cu^{2+} possibly due to the formation of oxo-bridged Cu dimer species. BAS in the zeolite also takes part in the reaction, functioning as a reservoir to provide active NH_3 molecules to Cu sites.

1.5.2. Selective Oxidation of Methane to Methanol

Methane oxidation on Cu-zeolites is typically carried out in three-step reaction conditions, consisting of (i) thermal activation of the catalyst in strongly oxidizing atmosphere (e.g. O_2, N_2O) at high temperature (450-600 °C), (ii) reaction of methane on the activated catalyst at moderate temperatures (150-200 °C) and (iii) H_2O steam-assisted product desorption in gas phase or liquid phase extraction in polar solvents. After desorption of the products, activation of the catalyst at high temperature has to be carried out again to achieve the second turnover of methane. Regeneration of the catalyst in inert atmosphere is also reported.[72-73] Sufficiently long reaction time of

methane enables the quantification of the active Cu species in the catalyst, and the activity of the catalyst can be formulated as Cu efficiency, which is defined as [activated CH_4]/[Cu].

Selective oxidation of methane to methanol on Cu-zeolites was first reported in 2005 on Cu-exchanged MFI and MOR.[30] Na-type of zeolites were used as starting materials for Cu-exchange. The catalysts were activated in O_2 flow at 450 °C, followed by reaction with CH_4 at 125-225 °C. During the reaction of the catalyst with methane, decrement of a ultraviolet-visible (UV-Vis) band at 22700 cm^{-1} was observed, and it was assigned to bis(μ-oxo)dicopper center (Figure 1-9 (a)) which is able to activate methane. Further studies on Cu-MFI and Cu-MOR catalysts with the aid of different techniques such as Raman spectroscopy and extended X-ray absorption fine structure (EXAFS) study combined with density-functional theory (DFT) calculation proposed that mono(μ-oxo)dicopper cluster (Figure 1-9 (b)) is responsible for methane oxidation, while bis(μ-oxo)dicopper species was ruled out.[74-76]

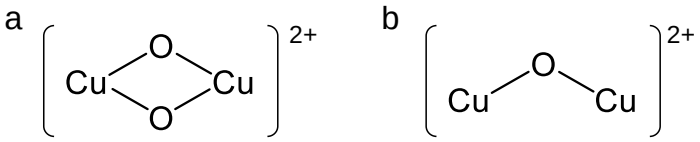

Figure 1-9. Structures of bis(μ-oxo)dicopper center (a) and mono(μ-oxo)dicopper center (b).

On the other hand, a tricopper-oxo cluster is also reported as an active species in methane activation. High homogeneity of the tricopper-oxo cluster formation was achieved at various Si/Al ratios and Cu loadings of Cu-MOR catalysts by Grundner et al., resulting in a high yield of methane oxidation.[77] Based on IR spectroscopy characterization, it was proposed that three Cu atoms are anchored to two framework Al sites at the pore mouths of 8 MR side pockets of MOR. EXAFS analysis of the catalyst, combined with DFT calculation of stable structure for Cu-oxo clusters, revealed that $[Cu_3(\mu\text{-}O)_3]^{2+}$ (Figure 1-10) is a single-site active species in such Cu-MOR catalysts.[77]

Even though structural characterization of the dimeric Cu species is extensively carried out, studied Cu-zeolite catalysts typically possess spectator species, which is not active in CH_4 activation. This indicates that the spectroscopic characterization of Cu centers gives convoluted information on both active and inactive Cu species.

Therefore, the nature of active Cu species is still under debate. Recently, it was found that the properties of parent H-MOR (synthesis protocols and Si/Al ratio) affects the Cu speciation in the catalyst. For instance, pH during Cu-exchange has to be controlled below 5.7 in order to avoid unselective precipitation of CuO and $Cu(OH)_2$ nanoparticles, which results in the activity drop.[78] Presence of alkaline or alkaline-earth cations, such as Na^+, K^+ and Ca^{2+}, in the parent MOR also depletes the activity of Cu-MOR catalysts.[78]

Cu-exchanged small-pore zeolites, such as CHA, AEI and AFX, have also been reported to oxidize methane into methanol, however, relatively low Cu efficiency of the catalysts suggests the formation of important concentrations of inactive Cu species in such catalysts.[79-80]

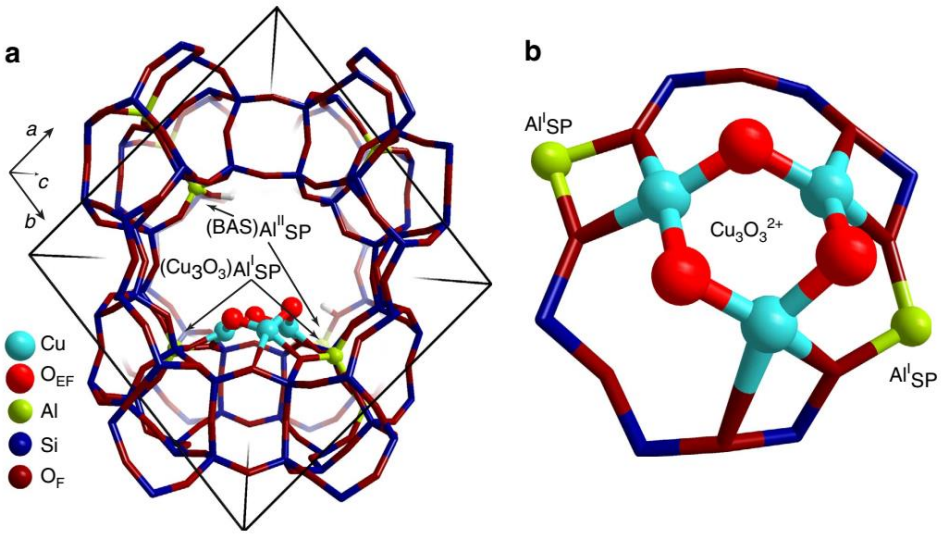

Figure 1-10. DFT-optimized structure of $[Cu_3(\mu\text{-}O)_3]^{2+}$ stabilized by two framework Al sites and located at the pore mouth of 8 MR side pocket in MOR (adapted with permission from ref [77])

In addition to the catalyst properties, reaction conditions also strongly affect the yield of CH_4 oxidation on Cu-zeolite catalysts. Sheppard et al. have demonstrated isothermal CH_4 oxidation on Cu-MFI catalyst with NO and N_2O as oxidants.[81] By using NO as an oxidant, activation temperature was reduced to 150 °C while retaining methanol yield, though it is lower compared to thermal activation in O_2. Increasing methanol yield with increasing activation temperature was also observed on Cu-MOR and Cu-CHA catalysts.[79, 82] Positive effect of CH_4 loading pressure on methanol yield was observed during isothermal reaction on Cu-MOR catalyst at 200 °C under high pressure up to 36 bar, while O_2 pressure during activation did not show a dramatic

effect on methanol yield.[83] Increasing methanol yield with increasing CH_4 partial pressure was also observed on Cu-CHA catalysts under atmospheric pressure.[79] These observations on different catalysts strongly suggest the importance of activation as well as CH_4 reaction conditions in order to achieve high methanol yield.

Oxidation of methane to methanol in catalytic mode was also achieved by feeding CH_4 in presence of H_2O with trace amounts of O_2.[38] It was suggested that Cu species formed by rearrangement of mobile, hydrated Cu species are responsible for the methane oxidation activity in continuous catalytic conditions. 70% methanol selectivity was achieved on a CuNa-MFI catalyst, while observed TOF normalized to Cu concentration was as low as 10^{-3} h^{-1}.[38] Higher TOF up to 4.8 h^{-1} was achieved on Cu-CHA catalyst with using N_2O as an oxidant, however, tradeoff of methanol selectivity at higher CH_4 conversion was clearly observed.[39]

1.6. Metal-Organic Frameworks

1.6.1. Properties of Metal-Organic Frameworks

Metal-Organic Frameworks (MOFs) are microporous and/or mesoporous crystalline organic-inorganic composites, consisting of linking organic molecules and metal cations as nodes. Variety of selection for organic linkers and metal nodes enables the synthesis of huge variety of MOFs, resulting in more than 20000 different materials with different physicochemical properties.[84] Surface area of MOFs is typically much higher than conventional porous materials such as zeolites due to their high porosity, ranging from 1000 to 10000 m^2/g.[84] However, MOFs with high thermal and chemical stability are very limited despite wide variety of materials with different properties. Zr_6-based MOFs with carboxylate-terminated linkers, such as UiO-66[85] and NU-1000[86], are reported to show high thermal and chemical stability, due to highly oxophilic nature of Zr_6 nodes and their strong Coulomb interaction with negative charges of linkers.[87] Remarkable thermal stability up to 500 °C[85] as well as chemical stability in the range of pH 1-11[88] makes this family of materials promising for the application as catalysts. In the following, properties of NU-1000 are described in detail due to its relevance for this study.

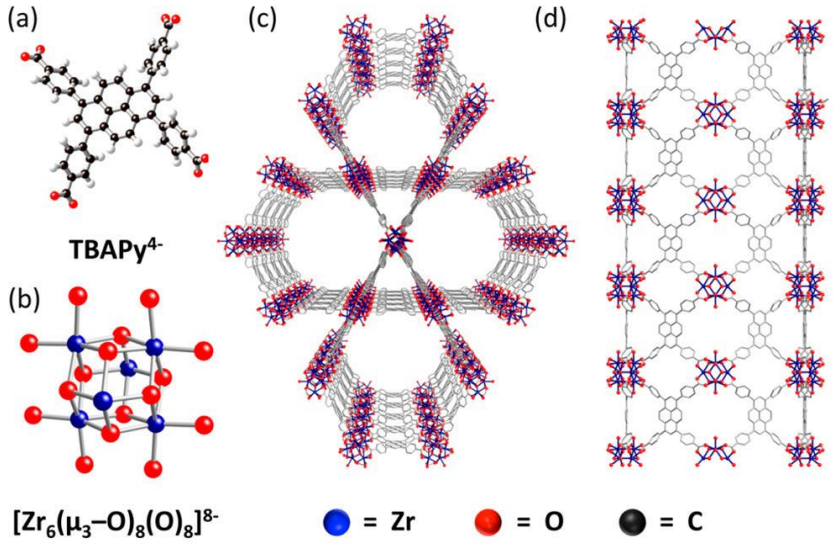

Figure 1-11. Structure of the $TBAPy^{4-}$ linker (a) and the $[Zr_6(\mu_3\text{-}O)_8(O)_8]^{8-}$ node (b) of NU-1000 (c, d). Hydrogen atoms are not shown for simplicity (adapted with permission from ref [86]).

NU-1000 consists of 1,3,6,8-tetrakis(*p*-benzoic acid)pyrene ($TBAPy^{4-}$) linkers interconnecting $[Zr_6(\mu_3\text{-}O)_8(O)_8]^{8-}$ nodes (Figure 1-11), and it possesses triangular microchannels (8 Å) and larger cylindrical mesopores (34 Å).[86] NU-1000 shows remarkable thermal stability up to 500 °C.[89] Though it is not resistant to capillary force-driven channel collapse, solvent exchange by acetone was found out to prevent the structural collapse during thermal activation.[87]

1.6.2. Catalytic Reactions on Metal-Loaded NU-1000

High thermal stability of NU-1000 as well as high accessibility of terminal –OH ligands on Zr_6 nodes through large mesopores enabled the post-synthetic introduction of metals and small metal oxide clusters by atomic layer deposition (ALD).[89] Zn- and Al-loaded NU-1000 successfully catalyzed Knoevenagel condensation between ethyl cyanoacetate and benzaldehyde, where Lewis acids are required to carry out the reaction.[89] Following the same strategy, single site Ni catalyst supported on NU-1000 was prepared for ethylene oligomerization.[90] While strong interaction between Ni cations with Zr_6 nodes enabled the formation of a single site, the organic linkers of NU-1000 prevented Ni from sintering, resulting in excellent activity, long-term stability and regenerability.[90]

1.7. Scope of This Study

Cu-based catalysts supported on microporous materials have been recently found to be able to selectively oxidize methane to methanol at moderate temperatures. Especially on Cu-MOR catalysts, high concentration of sites able to activate methane activation has been achieved, indicating the formation of tricopper- or dicopper-oxo clusters as single sites. However, activity of Cu-zeolites has shown to strongly depend on various factors in catalyst preparation and reaction conditions. As a result, essential factors and elementary steps governing the formation of such species under reaction conditions still need to be investigated.

In the first part, elementary steps of the formation of active Cu-oxo clusters, such as dehydration, oxidation and thermally-driven migration of Cu species, are investigated on a well-established Cu-MOR catalysts where the formation of single-site tricopper-oxo clusters has been proved by spectroscopy characterization.[77] Although it is known that activation has to be carried out at high temperature (450-500 °C), little is known on what is limiting the formation of active Cu-oxo clusters. Concentration of the active sites is quantified by three-stage oxidation of methane to methanol, where long enough time of CH_4 reaction assures the full coverage of active Cu species. In-situ X-ray absorption spectroscopy is employed to follow the structural change of coordination structure around Cu during activation step and to characterize the structure of Cu-oxo clusters formed. In-situ UV-Vis spectroscopy during activation of the catalyst and CH_4 reaction complement the structural information obtained by X-ray absorption spectroscopy.

In the second part, effect of Al sites in Cu-MOR on the formation of Cu-oxo clusters is studied. Although strong effect of framework Al site distribution in zeolites on the properties of ion-exchanged species has been reported, more understanding of this interaction and on the effect in the activity of ion-exchanged metals is necessary. Cu-MOR catalysts with different Cu concentrations and extra-framework Al distributions are prepared by ion-exchange of H- and NH_4-MOR under controlled conditions to avoid uncontrolled precipitation of CuO and $Cu(OH)_2$ clusters. Distribution of framework and extra-framework Al in H-MOR samples as well as Cu distribution in Cu-MOR catalysts are studied by infrared spectroscopy. Adsorption of probe molecules such as *n*-hexane and pyridine during infrared spectroscopy enables the quantification of Al sites at

different locations. Structural information of Al sites are obtained by X-ray absorption spectroscopies and solid-state nuclear magnetic resonance.

Finally, in the last chapter it is discussed the effect of the support on the properties of Cu species. Zeolites with different framework structures, i.e. MOR, FER, MFI, CHA and MEL, are employed to study the effect of zeolite pore structure on the activity of methane oxidation on Cu-exchanged zeolite catalysts. Presence of certain ring structure as well as pore dimension can affect the formation of Cu-oxo clusters upon Cu ion-exchange and thermal activation of the catalysts. In addition, NU-1000 metal-organic framework is also selected as a new class of support material for selective oxidation of methane to methanol. Stability of Cu-NU-1000 catalyst is studied by X-ray diffraction and thermogravimetric analysis combined with mass spectrometry.

1.8. Reference

1. Malakoff, D., The Gas Surge. *Science* **2014**, *344*, 1464.
2. Elvidge, C.; Zhizhin, M.; Baugh, K.; Hsu, F.-C.; Ghosh, T., Methods for Global Survey of Natural Gas Flaring from Visible Infrared Imaging Radiometer Suite Data. *Energies* **2016**, *9*, 14.
3. Golisz, S. R.; Brent Gunnoe, T.; Goddard, W. A.; Groves, J. T.; Periana, R. A., Chemistry in the Center for Catalytic Hydrocarbon Functionalization: An Energy Frontier Research Center. *Catal. Lett.* **2011**, *141*, 213.
4. Howarth, R. W.; Santoro, R.; Ingraffea, A., Methane and the Greenhouse-Gas Footprint of Natural Gas from Shale Formations. *Clim. Change* **2011**, *106*, 679.
5. Faramawy, S.; Zaki, T.; Sakr, A. A. E., Natural Gas Origin, Composition, and Processing: A Review. *J. Nat. Gas Sci. Eng.* **2016**, *34*, 34.
6. Muraza, O.; Galadima, A., A Review on Coke Management during Dry Reforming of Methane. *Int. J. Energ. Res.* **2015**, *39*, 1196.
7. Kroll, V. C. H.; Swaan, H. M.; Mirodatos, C., Methane Reforming Reaction with Carbon Dioxide Over Ni/SiO_2Catalyst: I. Deactivation Studies. *J. Catal.* **1996**, *161*, 409.
8. Montoya, J. A.; Romero-Pascual, E.; Gimon, C.; Del Angel, P.; Monzón, A., Methane Reforming with CO_2 over Ni/ZrO_2–CeO_2 Catalysts Prepared by Sol–Gel. *Catal. Today* **2000**, *63*, 71.
9. LeValley, T. L.; Richard, A. R.; Fan, M., The Progress in Water Gas Shift and Steam Reforming Hydrogen Production Technologies – A Review. *Int. J. Hydrogen Energy* **2014**, *39*, 16983.
10. Rhodes, C.; Hutchings, G. J.; Ward, A. M., Water-Gas Shift Reaction: Finding the Mechanistic Boundary. *Catal. Today* **1995**, *23*, 43.
11. Schubert, P. F.; Bayens, C. A.; Weick, L.; Haid, M. O., Expanding Markets for GTL Fuels and Specialty Products. In *Stud. Surf. Sci. Catal.*, Iglesia, E.; Spivey, J. J.; Fleisch, T. H., Eds. Elsevier: 2001; Vol. 136, pp 459.
12. Calvin H. Bartholomew, R. J. F., Hydrogen Production and Synthesis Gas Reactions. In *Fundamentals of Industrial Catalytic Processes*, 2010; pp 339.
13. Periana, R. A.; Taube, D. J.; Evitt, E. R.; Löffler, D. G.; Wentrcek, P. R.; Voss, G.; Masuda, T., A Mercury-Catalyzed, High-Yield System for the Oxidation of Methane to Methanol. *Science* **1993**, *259*, 340.
14. Periana, R. A.; Taube, D. J.; Gamble, S.; Taube, H.; Satoh, T.; Fujii, H., Platinum Catalysts for the High-Yield Oxidation of Methane to a Methanol Derivative. *Science* **1998**, *280*, 560.
15. Mironov, O. A.; Bischof, S. M.; Konnick, M. M.; Hashiguchi, B. G.; Ziatdinov, V. R.; Goddard, W. A.; Ahlquist, M.; Periana, R. A., Using Reduced Catalysts for Oxidation Reactions: Mechanistic Studies of the “Periana-Catalytica” System for CH_4 Oxidation. *J. Am. Chem. Soc.* **2013**, *135*, 14644.

16. Shilov, A. E.; Shul'pin, G. B., Activation of C−H Bonds by Metal Complexes. *Chem. Rev.* **1997**, *97*, 2879.

17. Labinger, J. A.; Bercaw, J. E., Understanding and Exploiting C–H Bond Activation. *Nature* **2002**, *417*, 507.

18. Wang, V. C. C.; Maji, S.; Chen, P. P. Y.; Lee, H. K.; Yu, S. S. F.; Chan, S. I., Alkane Oxidation: Methane Monooxygenases, Related Enzymes, and Their Biomimetics. *Chem. Rev.* **2017**.

19. Semrau, J. D.; DiSpirito, A. A.; Yoon, S., Methanotrophs and Copper. *FEMS Microbiol. Rev.* **2010**, *34*, 496.

20. Merkx, M.; Kopp, D. A.; Sazinsky, M. H.; Blazyk, J. L.; Müller, J.; Lippard, S. J., Dioxygen Activation and Methane Hydroxylation by Soluble Methane Monooxygenase: A Tale of Two Irons and Three Proteins. *Angew. Chem. Int. Ed.* **2001**, *40*, 2782.

21. Rosenzweig, A. C.; Frederick, C. A.; Lippard, S. J.; Nordlund, P.; auml, Crystal Structure of a Bacterial Non-Haem Iron Hydroxylase that Catalyses the Biological Oxidation of Methane. *Nature* **1993**, *366*, 537.

22. Sirajuddin, S.; Rosenzweig, A. C., Enzymatic Oxidation of Methane. *Biochemistry* **2015**, *54*, 2283.

23. Chan, S. I.; Yu, S. S. F., Controlled Oxidation of Hydrocarbons by the Membrane-Bound Methane Monooxygenase: The Case for a Tricopper Cluster. *Acc. Chem. Res.* **2008**, *41*, 969.

24. Balasubramanian, R.; Smith, S. M.; Rawat, S.; Yatsunyk, L. A.; Stemmler, T. L.; Rosenzweig, A. C., Oxidation of Methane by a Biological Dicopper Centre. *Nature* **2010**, *465*, 115.

25. Culpepper, M. A.; Rosenzweig, A. C., Architecture and Active Site of Particulate Methane Monooxygenase. *Crit. Rev. Biochem. Mol. Biol.* **2012**, *47*, 483.

26. Hung, S. C.; Chen, C. L.; Chen, K. H. C.; Yu, S. S. F.; Chan, S. I., The Catalytic Copper Clusters of the Particulate Methane Monooxygenase from Methanotrophic Bacteria: Electron Paramagnetic Resonance Spectral Simulations. *J. Chin. Chem. Soc.* **2004**, *51*, 1229.

27. Chen, P. P. Y.; Nagababu, P.; Yu, S. S. F.; Chan, S. I., Development of the Tricopper Cluster as a Catalyst for the Efficient Conversion of Methane into MeOH. *ChemCatChem* **2014**, *6*, 429.

28. Chan, S. I.; Lu, Y.-J.; Nagababu, P.; Maji, S.; Hung, M.-C.; Lee, M. M.; Hsu, I. J.; Minh, P. D.; Lai, J. C. H.; Ng, K. Y.; Ramalingam, S.; Yu, S. S. F.; Chan, M. K., Efficient Oxidation of Methane to Methanol by Dioxygen Mediated by Tricopper Clusters. *Angew. Chem. Int. Ed.* **2013**, *52*, 3731.

29. Blanchette, C. D.; Knipe, J. M.; Stolaroff, J. K.; DeOtte, J. R.; Oakdale, J. S.; Maiti, A.; Lenhardt, J. M.; Sirajuddin, S.; Rosenzweig, A. C.; Baker, S. E., Printable Enzyme-Embedded Materials for Methane to Methanol Conversion. *Nat. Commun.* **2016**, *7*, 11900.

30. Groothaert, M. H.; Smeets, P. J.; Sels, B. F.; Jacobs, P. A.; Schoonheydt, R. A., Selective Oxidation of Methane by the Bis(μ-oxo)dicopper Core Stabilized on ZSM-5 and Mordenite Zeolites. *J. Am. Chem. Soc.* **2005**, *127*, 1394.

31. Starokon, E. V.; Parfenov, M. V.; Pirutko, L. V.; Abornev, S. I.; Panov, G. I., Room-Temperature Oxidation of Methane by alpha-Oxygen and Extraction of Products from the FeZSM-5 Surface. *J. Phys. Chem. C* **2011**, *115*, 2155.

32. Mahyuddin, M. H.; Staykov, A.; Shiota, Y.; Yoshizawa, K., Direct Conversion of Methane to Methanol by Metal-Exchanged ZSM-5 Zeolite (Metal = Fe, Co, Ni, Cu). *ACS Catal.* **2016**, *6*, 8321.

33. Gabrienko, A. A.; Arzumanov, S. S.; Luzgin, M. V.; Stepanov, A. G.; Parmon, V. N., Methane Activation on Zn^{2+}-Exchanged ZSM-5 Zeolites. The Effect of Molecular Oxygen Addition. *J. Phys. Chem. C* **2015**, *119*, 24910.

34. Hammond, C.; Forde, M. M.; Ab Rahim, M. H.; Thetford, A.; He, Q.; Jenkins, R. L.; Dimitratos, N.; Lopez-Sanchez, J. A.; Dummer, N. F.; Murphy, D. M.; Carley, A. F.; Taylor, S. H.; Willock, D. J.; Stangland, E. E.; Kang, J.; Hagen, H.; Kiely, C. J.; Hutchings, G. J., Direct Catalytic Conversion of Methane to Methanol in an Aqueous Medium by using Copper-Promoted Fe-ZSM-5. *Angew. Chem. Int. Ed.* **2012**, *51*, 5129.

35. Beznis, N. V.; van Laak, A. N. C.; Weckhuysen, B. M.; Bitter, J. H., Oxidation of Methane to Methanol and Formaldehyde over Co-ZSM-5 Molecular Sieves: Tuning the Reactivity and Selectivity by Alkaline and Acid Treatments of the Zeolite ZSM-5 Agglomerates. *Microporous Mesoporous Mater.* **2011**, *138*, 176.

36. Smeets, P. J.; Groothaert, M. H.; Schoonheydt, R. A., Cu Based Zeolites: A UV–Vis Study of the Active Site in the Selective Methane Oxidation at Low Temperatures. *Catal. Today* **2005**, *110*, 303.

37. Kulkarni, A. R.; Zhao, Z.-J.; Siahrostami, S.; Nørskov, J. K.; Studt, F., Cation-Exchanged Zeolites for the Selective Oxidation of Methane to Methanol. *Catal. Sci. Technol.* **2017**.

38. Narsimhan, K.; Iyoki, K.; Dinh, K.; Román-Leshkov, Y., Catalytic Oxidation of Methane into Methanol over Copper-Exchanged Zeolites with Oxygen at Low Temperature. *ACS Cent. Sci.* **2016**.

39. Ipek, B.; Lobo, R. F., Catalytic Conversion of Methane to Methanol on Cu-SSZ-13 Using N_2O as Oxidant. *Chem. Commun.* **2016**, *52*, 13401.

40. Xu, J.; Armstrong, R. D.; Shaw, G.; Dummer, N. F.; Freakley, S. J.; Taylor, S. H.; Hutchings, G. J., Continuous Selective Oxidation of Methane to Methanol over Cu- and Fe-Modified ZSM-5 Catalysts in a Flow Reactor. *Catal. Today* **2016**, *270*, 93.

41. Baerlocher, C.; McCusker, L. B. Database of Zeolite Structures. http://www.iza-structure.org/databases/.

42. Schallmoser, S.; Ikuno, T.; Wagenhofer, M. F.; Kolvenbach, R.; Haller, G. L.; Sanchez-Sanchez, M.; Lercher, J. A., Impact of the Local Environment of Brønsted Acid Sites in ZSM-5 on the Catalytic Activity in n-Pentane Cracking. *J. Catal.* **2014**, *316*, 93.

43. Zhang, Y.; Zhao, R.; Sanchez-Sanchez, M.; Haller, G. L.; Hu, J.; Bermejo-Deval, R.; Liu, Y.; Lercher, J. A., Promotion of Protolytic Pentane Conversion on H-MFI Zeolite by

Proximity of Extra-Framework Aluminum Oxide and Brønsted Acid Sites. *J. Catal.* **2019**, *370*, 424.

44. Ahn, J. H.; Kolvenbach, R.; Gutiérrez, O. Y.; Al-Khattaf, S. S.; Jentys, A.; Lercher, J. A., Tailoring p-Xylene Selectivity in Toluene Methylation on Medium Pore-Size Zeolites. *Microporous Mesoporous Mater.* **2015**, *210*, 52.

45. Ahn, J. H.; Kolvenbach, R.; Al-Khattaf, S. S.; Jentys, A.; Lercher, J. A., Enhancing Shape Selectivity without Loss of Activity – Novel Mesostructured ZSM5 Catalysts for Methylation of Toluene to p-Xylene. *Chem. Commun.* **2013**, *49*, 10584.

46. Harrison, I. D.; Leach, H. F.; Whan, D. A., Comparison of the Shape Selective Properties of Ferrierite, ZSM-5 and ZSM-11. *Zeolites* **1987**, *7*, 21.

47. Domokos, L.; Lefferts, L.; Seshan, K.; Lercher, J. A., The Importance of Acid Site Locations for n-Butene Skeletal Isomerization on Ferrierite. *J. Mol. Catal. A: Chem.* **2000**, *162*, 147.

48. Hu, H.; Ke, M.; Zhang, K.; Liu, Q.; Yu, P.; Liu, Y.; Li, C.; Liu, W., Designing Ferrierite-Based Catalysts with Improved Properties for Skeletal Isomerization of n-Butene to Isobutene. *RSC Adv.* **2017**, *7*, 31535.

49. Liu, Y.; Zhao, J.; Lee, J. M., Conventional and New Materials for Selective Catalytic Reduction (SCR) of NO_x. *ChemCatChem* **2018**, *10*, 1499.

50. Beale, A. M.; Gao, F.; Lezcano-Gonzalez, I.; Peden, C. H. F.; Szanyi, J., Recent Advances in Automotive Catalysis for NO_x Emission Control by Small-Pore Microporous Materials. *Chem. Soc. Rev.* **2015**, *44*, 7371.

51. Mortier, W. J.; Sauer, J.; Lercher, J. A.; Noller, H., Bridging and Terminal Hydroxyls. A Structural Chemical and Quantum Chemical Discussion. *J. Phys. Chem.* **1984**, *88*, 905.

52. Ehrmaier, A.; Liu, Y.; Peitz, S.; Jentys, A.; Chin, Y.-H. C.; Sanchez-Sanchez, M.; Bermejo-Deval, R.; Lercher, J., Dimerization of Linear Butenes on Zeolite-Supported Ni^{2+}. *ACS Catal.* **2019**, *9*, 315.

53. Jabłońska, M.; Delahay, G.; Kruczała, K.; Błachowski, A.; Tarach, K. A.; Brylewska, K.; Petitto, C.; Góra-Marek, K., Standard and Fast Selective Catalytic Reduction of NO with NH_3 on Zeolites Fe-BEA. *J. Phys. Chem. C* **2016**, *120*, 16831.

54. Moreau, F.; Ayrault, P.; Gnep, N. S.; Lacombe, S.; Merlen, E.; Guisnet, M., Influence of Na Exchange on the Acidic and Catalytic Properties of an HMOR Zeolite. *Microporous Mesoporous Mater.* **2002**, *51*, 211.

55. Yokoi, T.; Mochizuki, H.; Namba, S.; Kondo, J. N.; Tatsumi, T., Control of the Al Distribution in the Framework of ZSM-5 Zeolite and Its Evaluation by Solid-State NMR Technique and Catalytic Properties. *J. Phys. Chem. C* **2015**, *119*, 15303.

56. Dědeček, J.; Sobalík, Z.; Wichterlová, B., Siting and Distribution of Framework Aluminium Atoms in Silicon-Rich Zeolites and Impact on Catalysis. *Catal. Rev.* **2012**, *54*, 135.

57. Dedecek, J.; Kaucky, D.; Wichterlova, B.; Gonsiorova, O., Co^{2+} Ions as Probes of Al Distribution in the Framework of Zeolites. ZSM-5 Study. *Phys. Chem. Chem. Phys.* **2002**, *4*, 5406.

58. Dědeček, J.; Kaucký, D.; Wichterlová, B., Al Distribution in ZSM-5 Zeolites: an Experimental Study. *Chem. Commun.* **2001**, 970.

59. Mortier, W. J., *Compilation of Extra-framework Sites in Zeolites*; Butterworth Scientific Ltd., Guildford, UK, , 1982.

60. Dědeček, J.; Wichterlová, B., Co^{2+} Ion Siting in Pentasil-Containing Zeolites. I. Co^{2+} Ion Sites and Their Occupation in Mordenite. A Vis−NIR Diffuse Reflectance Spectroscopy Study. *J. Phys. Chem. B* **1999**, *103*, 1462.

61. Beznis, N. V.; Weckhuysen, B. M.; Bitter, J. H., Partial Oxidation of Methane Over Co-ZSM-5: Tuning the Oxygenate Selectivity by Altering the Preparation Route. *Catal. Lett.* **2010**, *136*, 52.

62. Dedecek, J.; Sobalik, Z.; Tvaruazkova, Z.; Kaucky, D.; Wichterlova, B., Coordination of Cu Ions in High-Silica Zeolite Matrixes. Cu^{+} Photoluminescence, IR of NO Adsorbed on Cu^{2+}, and Cu^{2+} ESR Study. *J. Phys. Chem.* **1995**, *99*, 16327.

63. Eder, F.; Stockenhuber, M.; Lercher, J. A., Brønsted Acid Site and Pore Controlled Siting of Alkane Sorption in Acidic Molecular Sieves. *J. Phys. Chem. B* **1997**, *101*, 5414.

64. Iwamoto, M.; Yokoo, S.; Sakai, K.; Kagawa, S., Catalytic Decomposition of Nitric Oxide over copPer(II)-Exchanged, Y-Type Zeolites. *J. Chem. Soc., Faraday Trans. 1* **1981**, *77*, 1629.

65. Iwamoto, M.; Yahiro, H.; Tanda, K.; Mizuno, N.; Mine, Y.; Kagawa, S., Removal of Nitrogen Monoxide through a Novel Catalytic Process. 1. Decomposition on Excessively Copper-Ion-Exchanged ZSM-5 Zeolites. *J. Phys. Chem.* **1991**, *95*, 3727.

66. Beutel, T.; Sárkány, J.; Lei, G. D.; Yan, J. Y.; Sachtler, W. M. H., Redox Chemistry of Cu/ZSM-5. *J. Phys. Chem.* **1996**, *100*, 845.

67. Lei, G. D.; Adelman, B. J.; Sárkány, J.; Sachtler, W. M. H., Identification of Copper(II) and Copper(I) and Their Interconversion in Cu/ZSM-5 De-NO_x Catalysts. *Appl. Catal. B* **1995**, *5*, 245.

68. Sárkány, J.; d'Itri, J. L.; Sachtler, W. M. H., Redox Chemistry in Excessively Ion-Exchanged Cu/Na-ZSM-5. *Catal. Lett.* **1992**, *16*, 241.

69. Gao, F.; Peden, H. C., Recent Progress in Atomic-Level Understanding of Cu/SSZ-13 Selective Catalytic Reduction Catalysts. *Catalysts* **2018**, *8*.

70. Lomachenko, K. A.; Borfecchia, E.; Negri, C.; Berlier, G.; Lamberti, C.; Beato, P.; Falsig, H.; Bordiga, S., The Cu-CHA deNO_x Catalyst in Action: Temperature-Dependent NH_3-Assisted Selective Catalytic Reduction Monitored by Operando XAS and XES. *J. Am. Chem. Soc.* **2016**, *138*, 12025.

71. Gao, F.; Washton, N. M.; Wang, Y.; Kollár, M.; Szanyi, J.; Peden, C. H. F., Effects of Si/Al Ratio on Cu/SSZ-13 NH_3-SCR Catalysts: Implications for the Active Cu Species and the Roles of Brønsted Acidity. *J. Catal.* **2015**, *331*, 25.

72. Sushkevich, V. L.; Palagin, D.; van Bokhoven, J. A., Effect of Active Sites Structure on Activity of Copper Mordenite in Aerobic and Anaerobic Conversion of Methane to Methanol. *Angew. Chem. Int. Ed.* **2018**, *57*, 8906.

73. Sushkevich, V. L.; Palagin, D.; Ranocchiari, M.; van Bokhoven, J. A., Selective Anaerobic Oxidation of Methane Enables Direct Synthesis of Methanol. *Science* **2017**, *356*, 523.

74. Woertink, J. S.; Smeets, P. J.; Groothaert, M. H.; Vance, M. A.; Sels, B. F.; Schoonheydt, R. A.; Solomon, E. I., A $[Cu_2O]^{2+}$ Core in Cu-ZSM-5, the Active Site in the oxidATION of Methane to Methanol. *Proc. Natl. Acad. Sci.* **2009**, *106*, 18908.

75. Vanelderen, P.; Snyder, B. E. R.; Tsai, M.-L.; Hadt, R. G.; Vancauwenbergh, J.; Coussens, O.; Schoonheydt, R. A.; Sels, B. F.; Solomon, E. I., Spectroscopic Definition of the Copper Active Sites in Mordenite: Selective Methane Oxidation. *J. Am. Chem. Soc.* **2015**, *137*, 6383.

76. Alayon, E. M. C.; Nachtegaal, M.; Bodi, A.; Ranocchiari, M.; van Bokhoven, J. A., Bis(μ-oxo) Versus Mono(μ-oxo)dicopper Cores in a Zeolite for Converting Methane to Methanol: an in Situ XAS and DFT Investigation. *Phys. Chem. Chem. Phys.* **2015**, *17*, 7681.

77. Grundner, S.; Markovits, M. A. C.; Li, G.; Tromp, M.; Pidko, E. A.; Hensen, E. J. M.; Jentys, A.; Sanchez-Sanchez, M.; Lercher, J. A., Single-Site Trinuclear Copper Oxygen Clusters in Mordenite for Selective Conversion of Methane to Methanol. *Nat. Commun.* **2015**, *6*, 7546.

78. Grundner, S.; Luo, W.; Sanchez-Sanchez, M.; Lercher, J. A., Synthesis of Single-Site Copper Catalysts for Methane Partial Oxidation. *Chem. Commun.* **2016**, *52*, 2553.

79. Pappas, D. K.; Borfecchia, E.; Dyballa, M.; Pankin, I. A.; Lomachenko, K. A.; Martini, A.; Signorile, M.; Teketel, S.; Arstad, B.; Berlier, G.; Lamberti, C.; Bordiga, S.; Olsbye, U.; Lillerud, K. P.; Svelle, S.; Beato, P., Methane to Methanol: Structure–Activity Relationships for Cu-CHA. *J. Am. Chem. Soc.* **2017**, *139*, 14961.

80. Wulfers, M. J.; Teketel, S.; Ipek, B.; Lobo, R. F., Conversion of Methane to Methanol on Copper-Containing Small-Pore Zeolites and Zeotypes. *Chem. Commun.* **2015**, *51*, 4447.

81. Sheppard, T.; Hamill, C. D.; Goguet, A.; Rooney, D. W.; Thompson, J. M., A Low Temperature, Isothermal Gas-Phase System for Conversion of Methane to Methanol over Cu-ZSM-5. *Chem. Commun.* **2014**, *50*, 11053.

82. Kim, Y.; Kim, T. Y.; Lee, H.; Yi, J., Distinct Activation of Cu-MOR for Direct Oxidation of Methane to Methanol. *Chem. Commun.* **2017**, *53*, 4116.

83. Tomkins, P.; Mansouri, A.; Bozbag, S. E.; Krumeich, F.; Park, M. B.; Alayon, E. M.; Ranocchiari, M.; van Bokhoven, J. A., Isothermal Cyclic Conversion of Methane into Methanol over Copper-Exchanged Zeolite at Low Temperature. *Angew. Chem. Int. Ed.* **2016**, *55*, 5467.

84. Furukawa, H.; Cordova, K. E.; O'Keeffe, M.; Yaghi, O. M., The Chemistry and Applications of Metal-Organic Frameworks. *Science* **2013**, *341*, 974.

85. Cavka, J. H.; Jakobsen, S.; Olsbye, U.; Guillou, N.; Lamberti, C.; Bordiga, S.; Lillerud, K. P., A New Zirconium Inorganic Building Brick Forming Metal Organic Frameworks with Exceptional Stability. *J. Am. Chem. Soc.* **2008**, *130*, 13850.

86. Planas, N.; Mondloch, J. E.; Tussupbayev, S.; Borycz, J.; Gagliardi, L.; Hupp, J. T.; Farha, O. K.; Cramer, C. J., Defining the Proton Topology of the Zr_6-Based Metal–Organic Framework NU-1000. *J. Phys. Chem. Lett.* **2014**, *5*, 3716.

87. Mondloch, J. E.; Katz, M. J.; Planas, N.; Semrouni, D.; Gagliardi, L.; Hupp, J. T.; Farha, O. K., Are Zr_6-Based MOFs Water Stable? Linker Hydrolysis vs. Capillary-force-Driven Channel Collapse. *Chem. Commun.* **2014**, *50*, 8944.

88. Jiang, H.-L.; Feng, D.; Wang, K.; Gu, Z.-Y.; Wei, Z.; Chen, Y.-P.; Zhou, H.-C., An Exceptionally Stable, Porphyrinic Zr Metal–Organic Framework Exhibiting pH-Dependent Fluorescence. *J. Am. Chem. Soc.* **2013**, *135*, 13934.

89. Mondloch, J. E.; Bury, W.; Fairen-Jimenez, D.; Kwon, S.; DeMarco, E. J.; Weston, M. H.; Sarjeant, A. A.; Nguyen, S. T.; Stair, P. C.; Snurr, R. Q.; Farha, O. K.; Hupp, J. T., Vapor-Phase Metalation by Atomic Layer Deposition in a Metal–Organic Framework. *J. Am. Chem. Soc.* **2013**, *135*, 10294.

90. Li, Z.; Schweitzer, N. M.; League, A. B.; Bernales, V.; Peters, A. W.; Getsoian, A.; Wang, T. C.; Miller, J. T.; Vjunov, A.; Fulton, J. L.; Lercher, J. A.; Cramer, C. J.; Gagliardi, L.; Hupp, J. T.; Farha, O. K., Sintering-Resistant Single-Site Nickel Catalyst Supported by Metal Organic Framework. *J. Am. Chem. Soc.* **2016**, *138*, 1977.

2. Formation of Cu-Oxo Clusters Active for Methane Oxidation in Cu-Exchanged Mordenite

Abstract

Cu-exchanged zeolites are known to be active in the selective oxidation of methane to methanol at moderate temperatures. Among them, Cu-exchanged MOR is the system that has shown so far the highest methanol yield per Cu atom. This high efficiency is attributed to the ability of MOR to selectively stabilize an active tricopper cluster with structure $[Cu_3(\mu\text{-}O)_3]^{2+}$ when activated in the presence of O_2 at high temperatures. In this chapter,[1,2] we investigate the elementary steps in the formation of $[Cu_3(\mu\text{-}O)_3]^{2+}$ by *in-situ* spectroscopies such as X-ray absorption spectroscopy (XAS) and ultraviolet-visible (UV-Vis) spectroscopy. We demonstrate that the Cu cations undergo a series of thermally driven steps during activation that precede the formation of active oxidizing species. We hypothesize that the thermal formation of highly mobile Cu^+ species by auto-reduction of Cu^{2+} in inert gas is essential to enable the reorganization of Cu ions in MOR, necessary for the formation of a reduced precursor of $[Cu_3(\mu\text{-}O)_3]^{2+}$. Such precursor can be oxidized in the presence of strong oxidants - such as O_2 and N_2O - to form active $[Cu_3(\mu\text{-}O)_3]^{2+}$ at temperatures as low as 50 °C.

[1] This chapter is adapted with permission from the publication of the same title as appeared in the Journal of Physical Chemistry C: Ikuno, T.; Grundner, S.; Jentys, A.; Li, G.; Pidko, E. A.; Fulton, J. L.; Sanchez-Sanchez, M.; Lercher, J. A. *J. Phys. Chem. C* **2019**, *123*, 8759. Copyright 2019 American Chemical Society.

[2] All results on density functional theory calculation were provided by Guanna Li and Evgeny A. Pidko from Delft University of Technology.

2.1. Introduction

In nature, *methane monooxygenases* (MMOs) enzymes in methanotrophic bacteria are able to convert methane to methanol under aerobic conditions at Cu and Fe active centers.[1-3] Inspired by these enzymes, Cu-[4-8] and Fe-exchanged zeolites[4, 9-11] have been studied extensively as inorganic biomimetic catalysts. Studies on Fe-zeolites have shown that the active site precursor in the catalyst has to be oxidized using N_2O in order to form Fe(III)–$O^{\bullet-}$ species, which are concluded to be able to activate methane via highly active radical oxygen species.[9, 11] However, methane oxidation with molecular O_2, which is more economical than N_2O, has not been achieved on Fe-zeolites. Conversely, Cu-exchanged zeolites have shown activity in the partial oxidation of methane to methanol with small concentrations of O_2[5, 7-8, 12-17] as well as with N_2O[13, 15] or NO[17].

Selective oxidation of methane to methanol on Cu-zeolites has to be carried out in three separated stages. First, the catalyst has to be activated at high temperatures (450-600 °C) to form active Cu-oxo species. Then, at lower temperatures, typically 150-250 °C, CH_4 reacts on the activated material via hydrogen abstraction, resulting in an intermediate that is strongly adsorbed on the active sites.[18] In order to desorb the oxidized product as methanol, it is necessary to aid desorption by adding H_2O or by extraction in polar solvents. Once methanol is extracted, the catalyst must undergo thermal activation again at 450-600 °C in order to regenerate the active Cu species. The highest temperature of the three-stage methane oxidation process is typically needed for the oxidative activation of the catalysts, rather than for methane reaction or methanol extraction steps. In general, activation temperatures lower than 450 °C seem to lead consistently to a significant reduction of the activity of the catalysts.[7, 13, 15, 17, 19] Therefore, it seems highly important to understand the formation and regeneration of Cu active species in zeolite frameworks in order to achieve higher methanol yields.

The chemical processes during the synthesis of Cu-zeolite catalysts, ranging from the Cu ion exchange step to the thermal activation, determine the final speciation of Cu species in a particular framework.[6, 13, 15, 20-26] Water ligands coordinated to Cu^{2+} ions - located in the zeolite cavities after the ion exchange step- are removed during thermal treatment. During this process, Cu^{2+} ions move towards their final exchange positions in the zeolite, which are closer to the negative charges at Al-substituted T-sites.[22, 24, 27] The generation of monovalent $[Cu\text{-}OH]^+$ species attached to framework Al sites has

also been proposed to occur in this step.[13, 25-26, 28] Such species have the potential to generate multinuclear Cu-oxo clusters via condensation with adjacent $[Cu\text{-}OH]^+$ and formation of a μ-oxo bridge between Cu^{2+} cations.[29-31] The activation of methane at low temperatures is attributed to this μ-oxo species bridging two Cu^{2+}.[6, 12, 32-34] Therefore, the processes of formation and decomposition of this moiety are relevant to the synthesis of efficient Cu-zeolite catalysts. Aside of the removal of water ligands during the thermal treatment performed at temperatures above 350 °C in inert atmosphere, auto-reduction of Cu^{2+} to Cu^+ has been observed.[12, 24, 30, 35] This auto-reduction process is supposed to occur via recombination and desorption of the bridging O of μ-oxo bridged Cu species as O_2.[26, 31, 36-37]

Pappas et al. studied the dehydration and oxidation of Cu species in CHA framework and their effect on Cu speciation and activity in methane oxidation.[13] They attributed the lower activity of Cu-SSZ-13 oxidized at mild temperatures to differences in the Cu-O coordination structure formed during the activation at different conditions. Differences in the activity of O_2- and N_2O-activated Cu-MOR catalysts were reported by Kim et al.[15] They attributed the higher activity obtained with N_2O to the lower negative change in entropy during activation in N_2O compared to O_2 and, in addition, to the necessary O-O cleavage of an intermediate species when O_2 is used as oxidant. Recent theoretical studies have also tackled both the generation and activity of $[CuOCu]^{2+}$ and $[Cu_3(\mu\text{-}O)_3]^{2+}$ species in MOR.[38-39]

Despite all these studies, it is still unclear why is it necessary to activate the catalyst at temperatures above 400 °C to achieve the full activity. A better understanding of the formation of active Cu-oxo clusters and its kinetically or thermodynamically limiting steps is required in order to develop more efficient methane oxidation catalysts.

In this chapter, we investigate the formation of Cu-oxo species in a highly active Cu-MOR catalyst that was developed in our laboratories.[7] This material has been shown to contain only a tricopper-oxo cluster as active species when activated in O_2 at 450-500 °C.[7] The processes of dehydration, auto-reduction and oxidation of Cu species in MOR were monitored in detail by *in situ* spectroscopies and the activity in methane oxidation was correspondingly tested under various conditions. The mobility of auto-reduced Cu^+ species at high temperature was found to be crucial factor in the formation of active Cu-oxo clusters.

2.2. Experimental Methods

2.2.1. Preparation of the Cu-MOR Catalyst

Parent H-MOR was obtained by the calcination of a commercial NH_4-MOR (Clariant, Si/Al = 11) in synthetic air (100 mL/min) at 550 °C for 6 hours. The Cu-MOR catalyst was prepared by ion-exchange of H-MOR in an aqueous solution of $Cu(CH_3COO)_2$ at ambient temperature using 60mL/$g_{zeolite}$ of the 0.01 M precursor solution. The pH of the solution was adjusted to 5.7 by adding HNO_3 prior to the addition of H-MOR. After the exchange, the solid phase was collected by centrifugation, rinsed by re-dispersion in water (50 mL/$g_{zeolite}$) and subsequent centrifugation. The rinsing step was repeated four times, and the sample was dried at 100 °C for 24 h. Under these well-controlled Cu-exchange conditions, formation of CuO and $Cu(OH)_2$ nanoparticles can be excluded.[40] Concentrations of Cu, Al and Si of the catalysts were measured by atomic absorption spectroscopy (AAS) on a UNICAM 939 AA spectrometer after dissolution of the samples in boiling hydrofluoric acid.

2.2.2. Selective Oxidation of Methane to Methanol

CH_4 oxidation activity of the Cu-MOR catalyst (50 mg) was tested under ambient pressure in a stainless steel plug flow reactor with 4 mm inner diameter. The catalyst was pressed and sieved to the particle size of 250-400 µm. In the typical reaction testing, the catalyst was first activated in pure O_2 (16 mL/min) at 500 °C for 1 h. After cooling down to 200 °C in O_2, the catalyst was purged in He and CH_4 loading was performed for 4 h in 90% CH_4 in He (16 mL/min). The catalyst was subsequently cooled down to 135 °C in He, and H_2O steam-assisted product desorption was performed for 30 min in 50% H_2O in He (20 mL/min). The reaction products were identified and quantified by online mass spectrometry (m/z 31, 44 and 46 for CH_3OH, CO_2 and $(CH_3)_2O$, respectively). $(CH_3)_2O$ was regarded as a product that stems from the condensation of two CH_3OH molecules, therefore considered as a CH_3OH equivalent. The sum of all detected product was defined as the total yield of methane oxidation products.

2.2.3. In-Situ X-Ray Absorption Spectroscopy

X-ray absorption spectra were recorded on beamline P65 at PETRA III of DESY in Hamburg, Germany. The electron energy was 6 GeV with a beam current of 100 mA. The beam size at the sample was 200 × 300 µm. Around 10 mg of the sample was sandwiched between quartz wools and packed in a quartz capillary reactor (1 mm outer diameter, 0.02 mm wall thickness), and placed on top of a gas-blower for controlled heating. Double-crystal Si(111) monochromator was used to control the incident photon energy and the spectra were recorded with ionization chamber detectors in a transmission mode. To suppress higher harmonics in the incident beam the monochromator was detuned to 70 % of the maximum peak intensity. Thermal activation of the samples was performed in a flow of 10% O_2 in He as well as in He at 5 mL/min at 450 °C for 1 h with the 10 °C/min heating rate. After the thermal activation of the sample in He at 450 °C, the sample was cooled down to 200 °C in He flow, and treated in a flow of 10%O_2 in He for 30 min. The gas flows over the samples was controlled by mass-flow controllers. A moisture/oxygen trap and a moisture trap were employed on He and O_2 gases respectively to avoid unwanted contamination of the gas stream on the catalyst. XANES and EXAFS data processing and EXAFS fitting were performed on Athena and Artemis softwares from the Demeter package.[41]

2.2.4. In-Situ Ultraviolet-Visible Spectroscopy

Measurements of Ultraviolet-Visible (UV-vis) spectra of the Cu-MOR catalyst were carried out on an Avantes Avaspec 2048 spectrometer equipped with high temperature optical fiber (Avantes FCR-7UV400-2ME-HTX). The sample (250-400 µm particle size) was placed in a quartz flow reactor with square optical-grade quartz windows. The intensity of the diffuse reflectance UV-vis is shown as the Kubelka-Munk function, defined as $F(R) = (1-R)^2/2R$, where $R = R_s/R_r$. R_s and R_r refer to the signal intensity of the sample and reference, respectively. Parent H-MOR was used as a reference. The catalyst was first treated in N_2 flow (16 mL/min) at 450 °C for 1 h, and then cooled down to 200 °C. Then the catalyst was contacted with O_2 flow (16 mL/min) for 30 min at 200 °C, followed by flushing in N_2 and subsequent contact with CH_4 flow (16 mL/min) for 1 h.

2.2.5. In-Situ Infrared Spectroscopy

Infrared (IR) spectra of the Cu-MOR catalyst were recorded on a Nicolet iS50 FT-IR spectrometer equipped with auxilary experiment module detector (Thermo Scientific). The sample was first pressed to a self-standing wafer with a denstiy of ca. 10 mg/cm^2. The sample was heated up to a target temperature (100, 200 and 500 °C) at a heating rate of 10 °C in a flow of synthetic air (20 mL/min) and equilibrated for 1 h prior to measurements of the spectra.

2.2.6. Density Functional Theory Calculation

Spin- polarized density functional theory (DFT) calculations were performed using VASP 5.3.5.[42-43] The Perdew−Burke−Ernzerhof functional based on the generalized gradient approximation was chosen to account for the exchange−correlation energy.[44] A plane-wave basis set in combination with the projected augmented wave method was used to describe the valence electrons and the valence−core interactions, respectively.[42] The kinetic energy cutoff of the plane-wave basis set was 400 eV. Gaussian smearing of the population of partial occupancies with a width of 0.05 eV was used. The threshold for energy convergence for each iteration was set to 10−5 eV. Geometries were assumed to be converged when forces on each atom were less than 0.05 eV/Å. Considering the large unit cell, Brillouin zone-sampling was restricted to the gamma point. The supercell of the all-silica MOR framework was constructed by doubling the monoclinic primary unit cell along the c-axis.[45] The positive charge of the extra framework Cu-containing clusters is compensated by the Al pair located in the 12-membered ring at the mouth of the side pocket.

2.3. Results and Discussion

2.3.1. Effect of Activation Temperature and Oxidant on the Selective Oxidation of Methane on the Cu-MOR Catalyst

Methane oxidation activity of the Cu-MOR catalyst (Table 2-1) after activation under different conditions were performed in a typical three-stage reaction, as described elsewhere[6] and in the methods section. Methane is allowed to react for 4 h in all experiments performed in this work. The long reaction time allows for a complete titration of all sites active for methane activation. In this way, quantification of the methane oxidation products yields quantitative information of the active site concentration in Cu-MOR.[6]

Table 2-1. Compositions of the parent H-MOR and the Cu-MOR catalyst.

Cu conc. (μmol/g)	Si/Al (-)	Brønsted acid sites conc. (μmol/g)
0	11	1090
420	11	840

To study the impact of activation temperature on methane oxidation activity, the freshly prepared sample was activated in pure O_2 for 1 h at different temperatures, subsequently cooled to 200 °C in O_2 and then flushed with He at the reaction temperature, before it was contacted with methane. A significant increase in activity with increasing temperature of activation was observed from 200 to 450 °C before it leveled off at 450-500 °C (Figure 2-1 (a)). The structure of Cu active sites for the sample treated at 450-500 °C is a tricopper-oxo cluster (Cu_3O_3).[6] We would like to mention that Cu spectators did not exist when activation was performed at 450-500 °C.[6] Thus, the high activity of Cu-MOR activated at 450-500 °C is attributed to the high concentration of Cu species forming active sites. It should be noted, however, that for activation temperatures as low as 200 °C, about 30 % of the maximum methane yield is reached. This lower activity is hypothesized to result from an incomplete formation of $(Cu_3O_3)^{2+}$ active sites or from the formation of different active species such as water-stable Cu^{II}-oxide species.[20] However, the constant selectivity over the whole temperature range strongly points to a gradual increase of the concentration of one structurally well-defined type of active Cu species with activation temperature. Ab initio calculations have shown that $[Cu_3(\mu\text{-}O)_3]^{2+}$ is thermodynamically the most stable

species at low H_2O partial pressures.[6] IR spectra of the Cu-MOR sample were recorded at different temperatures in O_2 flow (Figure 2-2). The spectra show a band at 3610 cm^{-1}, attributed to Brønsted acid sites of the zeolite, already at 200 °C. This indicates that, although dehydration of zeolite is not complete, local H_2O concentration in at least some regions is low enough to allow the formation of $[Cu_3(\mu\text{-}O)_3]^{2+}$ species. Hence, it is hypothesized that the formation of active sites is either kinetically or thermodynamically limited at temperatures below 450 °C and only a fraction of Cu reaches the configuration able to activate methane.

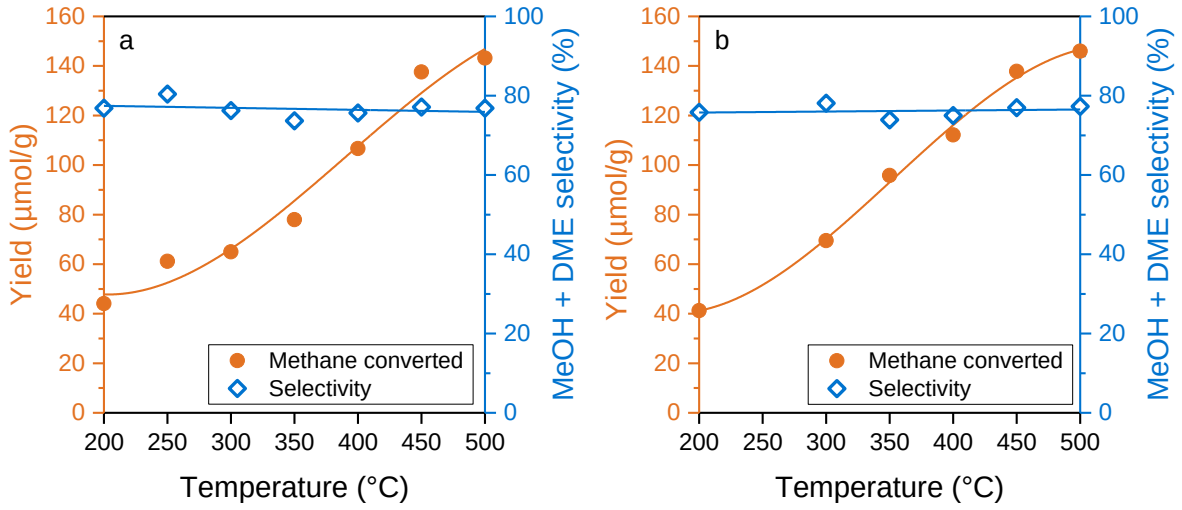

Figure 2-1. Comparison of activity and selectivity of Cu-MOR with a Cu loading of 420 µmol/g after activation in (a) pure O_2 and (b) N_2O at various temperatures.

Prolonging the duration of the activation step in pure O_2 from 1 h to 3 h at 350 °C and 500 °C resulted in the increment of the activity of only 6.5% and 3.3%, respectively, while the selectivity to methanol was maintained in the range 70-77% (Figure A 2-1 (a)). Thus, we conclude that the formation of active Cu species is mostly thermodynamically controlled in the temperature range of 350-500 °C, and the increase in the activity observed in Figure 2-1 is mainly due to increasing concentrations of the active sites, with the maximum concentration achieved at 450 °C. It should be noted that in the case of Cu-CHA catalyst, it has been reported that prolonging the activation time from 1 h to 2 h and 8 h at 450 °C increased the activity of the catalyst by ca. 25% and ca. 100%, respectively.[13] This different behavior is a first indication of the strong impact of the zeolite framework structure on the processes leading to Cu speciation in the micropores.

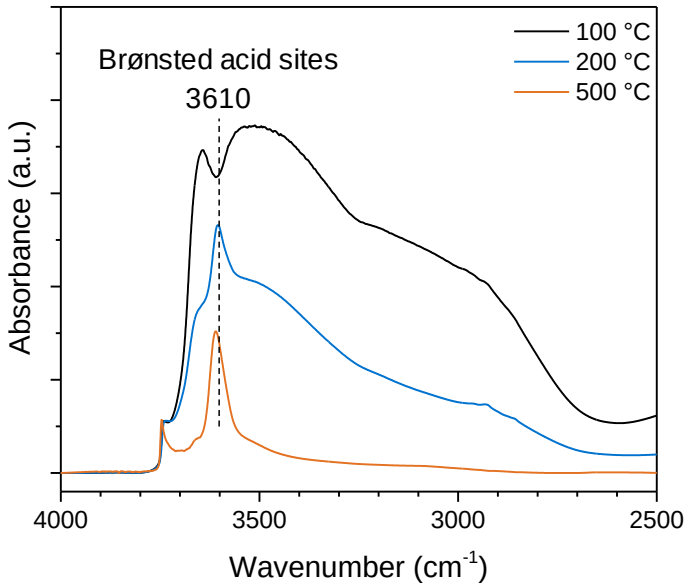

Figure 2-2. In-situ IR spectra of Cu-MOR measured during heating in O_2 flow.

In the next step, oxidative activation of Cu-MOR was studied using two different types of oxidants: O_2 and N_2O. It is widely accepted that μ-oxo bridges connecting Cu ions activate methane.[6, 34] In O_2, the formation of μ-oxo bridges (as well as the subsequent insertion of an O atom in methane to produced methanol) requires O-O bond cleavage. This implies the migration of the second O atom in the zeolite pores and its subsequent recombination to O_2 or, alternatively, the formation of another μ-oxo bridge between available Cu ions. Conversely, N_2O can readily provide one oxygen atom to a Cu site, releasing N_2. Thus, differences between activity after O_2 and N_2O activation would allow to detect if the oxidative activation is a limiting process for Cu-MOR.

Methane activation was performed on the same Cu-MOR catalyst activated at different temperatures in O_2 and N_2O (Figure 2-1). Both activity and selectivity of Cu-MOR after activation at 200-500 °C in O_2 and N_2O were similar, even though small differences can be noticed in the activation temperature range of 300-400 °C. The identical maximum yield of ca. 140 μmol/g of converted methane was achieved with both oxidants at temperatures of activation of 450-500 °C. This maximum yield corresponds to a stoichiometry of approximately 1 CH_4 molecule activated per 3 Cu atoms. Thus, we conclude that the formation of active Cu-oxo species - in particular tricopper oxo clusters - is complete after activation at 450-500 °C both in O_2 and in N_2O. The nearly identical activity and selectivity when activated either in O_2 or N_2O (Figure 2-1), shows

also that the O-O bond cleavage in the oxidation by O_2 is not limiting the formation of active Cu species in the zeolite under the conditions studied here.

It should be noted that a similar study by Kim et al. reported significantly higher activities (2-3 times higher) for Cu-MOR activated at 300-350 °C in N_2O in comparison to activation in O_2.[15] They attributed this behavior to the higher enthalpy release of the formation of Cu(II) oxide with N_2O (82 kJ/mol more exothermic than with O_2 under standard conditions). However, the oxidation of Cu^+ to Cu^{2+} in N_2O and O_2 are both thermodynamically favored under the conditions studied here, therefore, we do not expect that this enthalpy difference would have an remarkable impact on the formation of active Cu-oxo species. Kim et al.[15] also suggested that the lower activity of O_2-activated catalyst when treated at 500-600 °C is because the formation of an intermediate species is hampered at high temperatures.[46] On the contrary, we did not observe difference in CH_4 oxidation activity between N_2O- and O_2-activated catalysts.

2.3.2. Elementary Steps in the Activation of Cu-MOR Catalysts

To obtain deeper insight in the elementary steps involved in the oxidative activation of Cu species in MOR, it is necessary to decouple the (re-)oxidation of Cu from other thermally driven processes taking place during the high temperature activation, such as dehydration of the zeolite. Thus, we activated Cu-MOR, first in a He flow at 500 °C for 1 h, and then in 5% O_2/He for 10 min at temperatures ranging from 50 to 200 °C. Even though oxidation conditions in terms of oxidant concentration and temperature were much milder than in the standard procedure, Cu-MOR converted a similar amount of CH_4 (Figure 2-3). Thermal activation of Cu-MOR in He and subsequent low temperature oxidation in N_2O also led to similar conversion and selectivity (Figure A 2-1 (b)). As a reference, a Cu-MOR was activated in He at 500 °C without subsequent O_2/N_2O step and this catalyst showed only 10% of the full activity. This indicates that (re-)oxidation of the Cu species is required for developing activity in methane conversion to methanol. On the other hand, when the Cu-MOR catalyst was activated in He at moderate temperatures (350 °C) and subsequently oxidized in O_2 at 200 °C, it showed only 23% of the full activity obtained by thermal activation in O_2 at 500 °C (Figure 2-3). Therefore, we conclude that the maximum concentration of active sites in Cu-MOR are produced upon contact with O_2 (or N_2O) as long as the material has been previously thermally treated at 450-500 °C.

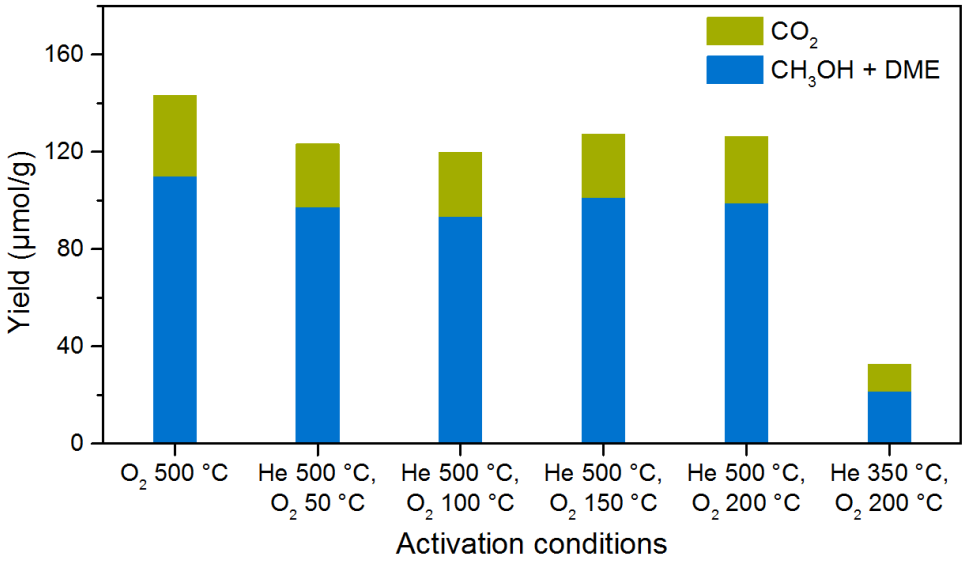

Figure 2-3. Yield of CH_4 oxidation on the Cu-MOR catalyst after activation in O_2 at 500 °C and after activation in He for 1 h followed by oxidation in 5% O_2 for 10 min at lower temperatures.

It should be noted that similar experiments performed on Cu-SSZ-13 catalysts (i.e., oxidation in O_2 at 200 °C after thermal activation in He at 500 °C) resulted in 45% lower activity compared to thermal activation in O_2 at 500 °C.[13] This was attributed to a different speciation of Cu. The difference between zeolites convincingly shows that the nature of the framework plays an important role in the type of active Cu species stabilized at different conditions.

Our activity results suggest that the temperature dependence of the activation step is related to the formation of a Cu cluster precursor, which requires the high temperatures. Such precursor can be easily oxidized (even at low temperatures) by both N_2O and O_2 and it rapidly forms the active species responsible for methane activation.

2.3.3. In-Situ Spectroscopic Study of Cu-MOR Activation

The redox chemistry of Cu embedded in zeolites during activation was monitored by in situ XAS and UV-vis spectroscopy.

First, oxidative activation under standard conditions (pure O_2 atmosphere, 450 °C, 1 h) was studied by *in situ* XAS. Figure 2-4 shows the Cu K-edge X-ray absorption near edge structure (XANES) of Cu-MOR during the heating stage and after the activation treatment. The presence of a weak pre-edge feature at 8978 eV, due to 1s → 3d

transition of Cu^{2+}, indicates the dominant Cu^{2+} character of all spectra taken along the activation process. The rising edge feature at 8987 eV, assigned to 1s → 4p transition of Cu^{2+}, is attributed to a change of the coordination geometry of Cu^{2+} due to the loss of ligated water and an increasing interaction with the zeolite framework during thermal treatment.[33] The loss in intensity of the maximum absorption feature at 8997 eV with increasing temperature is indicative of the removal of water ligands,[20] and indicates that the dehydration of the octahedral Cu^{2+} complexes in the pores leads to framework-coordinated Cu^{2+} species. The white line intensity at 8997 eV did not change at temperatures above 350 °C, revealing that dehydration of the Cu^{2+} centers is already complete at this temperature.

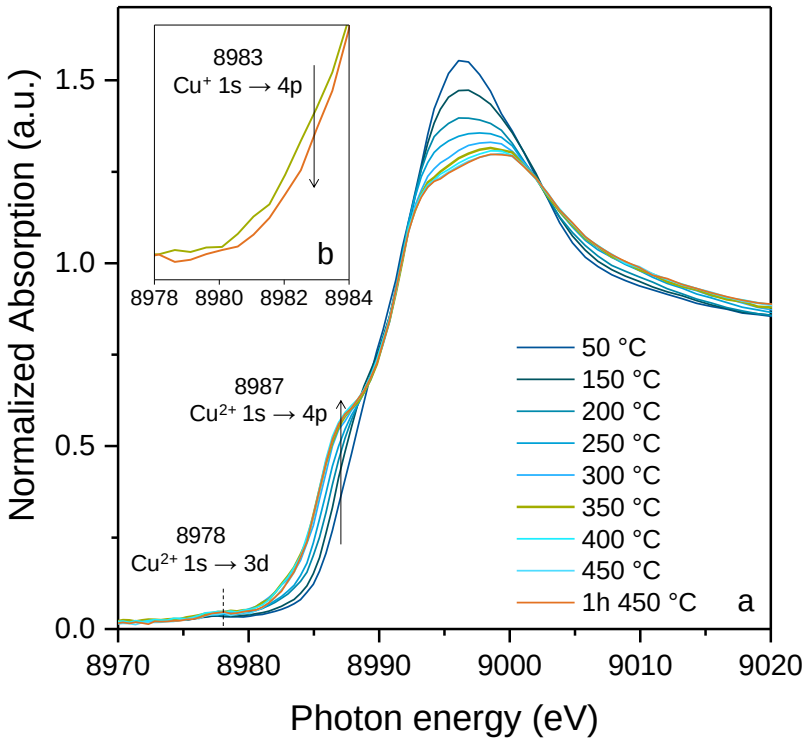

Figure 2-4. Cu K-edge XANES of Cu-MOR during thermal activation in O_2 flow and comparison of the Cu(I) feature at 8983-8984 eV at 350 and 450 °C.

Comparison of the XANES recorded during activation at 350 °C with the spectra after activation at 450 °C for 1 h (Figure 2-4 (b)) showed a feature at 8983 eV attributed to a 1s → 4p transition of Cu^+ at 350 °C, which disappears with increasing temperature to 450 °C. Hence, we hypothesize that a small fraction of Cu (ca. 5%) is reduced to Cu^+ during the heating ramp even in the presence of O_2.

The state of Cu during thermal activation of Cu-MOR in inert atmosphere was followed by XANES. Figure 2-5 shows XANES recorded during heating the fresh sample in He to 450 °C. Similar to activation in O_2, the intensity of the peak at 8997 eV decreased with increasing temperature and reached an almost constant intensity at 350 °C, indicating that dehydration of Cu^{2+} species is largely complete at 350 °C. The most characteristic change during activation in He was the emergence of a pronounced absorption at 8984 eV, which is attributed to a 1s → 4p transition of Cu^{+}. At 350 °C, this feature corresponded to approximately 60% of the total reducible Cu, i.e., the Cu population that underwent auto-reduction in He at 450 °C. Since dehydration was completed at 350 °C, the $Cu^{2+} \rightarrow Cu^{+}$ reduction was the dominant reaction in the range 350-450 °C.

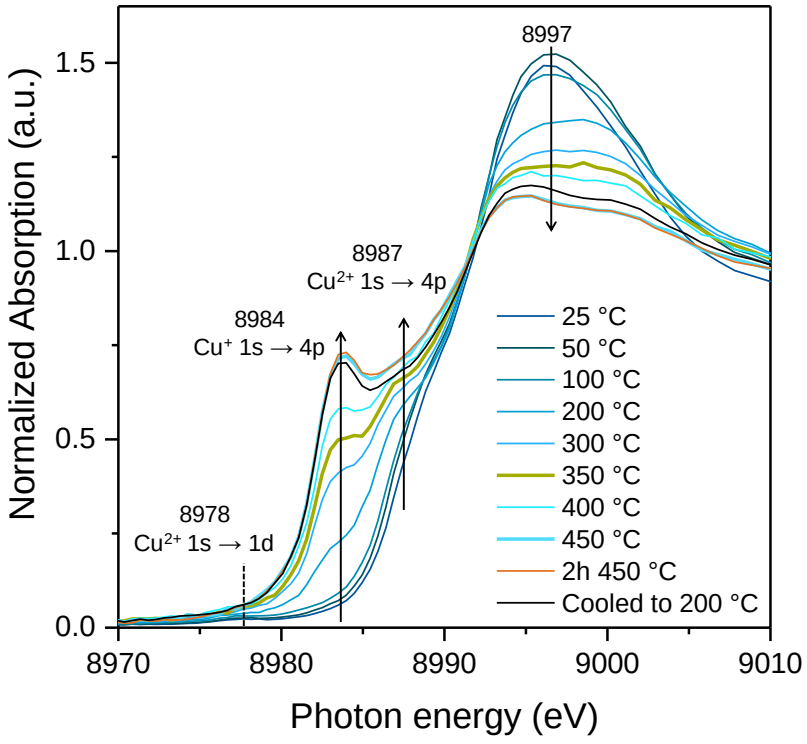

Figure 2-5. Cu K-edge XANES of Cu-MOR during thermal activation in He flow.

The auto-reduction of Cu^{2+} to Cu^{+} during thermal treatment in inert atmosphere has been widely reported.[21, 25-26, 30, 36, 47-51] The most widely proposed mechanism is the desorption of an O radical from μ-oxo bridged Cu^{2+} followed by subsequent recombination to O_2.[21, 28-29, 31] It has been also suggested that Cu^{+} is formed via the loss of a -OH ligand from $[CuOH]^{+}$ exchanged species, resulting in a Cu^{+} species

coordinated to an Al-site.[25, 30] The different pathways are hypothesized to be caused by different Cu species, i.e., a single Cu^{2+} coordinated to two Al tetrahedra cannot be auto-reduced by oxygen desorption under the described conditions.[13]

The auto-reduction of exchanged Cu^{2+} appears to be favored[52], because even in the presence of O_2, reduction of a fraction of Cu^{2+} to Cu^{+} was detected by XANES (Figure 2-4), which is in good agreement with the literature.[15, 52]

The radial distribution function (rdf) of the coordination structure around Cu during activation probed by EXAFS is compiled in Figure 2-6 (a). The most prominent peak was observed below 2 Å in *R*-space and is associated with backscattering from oxygen directly linked to Cu. The features above 2.0 Å are assigned to Cu-Cu and second shell Cu-O single-scattering paths.[53] The appearance of these features is attributed to the formation of the active tricopper-oxo cluster.[6] EXAFS fitting analysis of the Cu-MOR sample after activation in O_2 at 450 °C including Cu-Al scattering showed that the intensity of the Cu-Al path is lower compared to that of Cu-Cu (see details in section 2.6.4 in Appendix). Therefore, although we cannot rule out a small contribution of Cu-Al scattering to the feature at ca. 2.3 Å, we attribute the observed intensity to Cu-Cu single scattering. The decrease of the first shell intensity with increasing temperature is attributed to a decrement of the number of O atoms coordinated to Cu^{2+}. These results indicate a change in the coordination structure of Cu with increasing temperature, in good agreement with XANES (Figure 2-4) that is attributed to the dehydration of the Cu^{2+}-aquo complex and the formation of tricopper-oxo clusters.

The radial distribution functions of Cu-MOR (Figure 2-6 (b)) measured in situ during thermal activation in He shows the most prominent peak to be caused by Cu-O back scattering, observed below 2 Å in *R*-space. With increasing temperature, a distinct peak appears at large interatomic distances (R ~ 2.3 Å - not phase corrected), corresponding to the second coordination shell of Cu, which is assigned to a Cu-Cu path.[6, 54] This feature can be observed at 100 °C and is attributed to the formation of μ-oxo bridges between Cu^{2+} species. We conclude that it is the result of condensation of two adjacent $[CuOH]^{+}$ species. This feature remains largely unchanged in intensity up to 300 °C. The intensity of the first shell feature decreased with increasing temperature, indicating a decrease in the number of O atoms coordinated to Cu^{2+}. Both observations are attributed to the dehydration of Cu^{2+} exchanged species. However, above 300 °C, the intensity of the Cu-Cu path decreased, and it disappeared

completely at 400 °C. In the temperature range 300-450 °C, further decrease of the Cu-O first shell intensity is observed, leading to a final Cu-O coordination number of approximately 2.

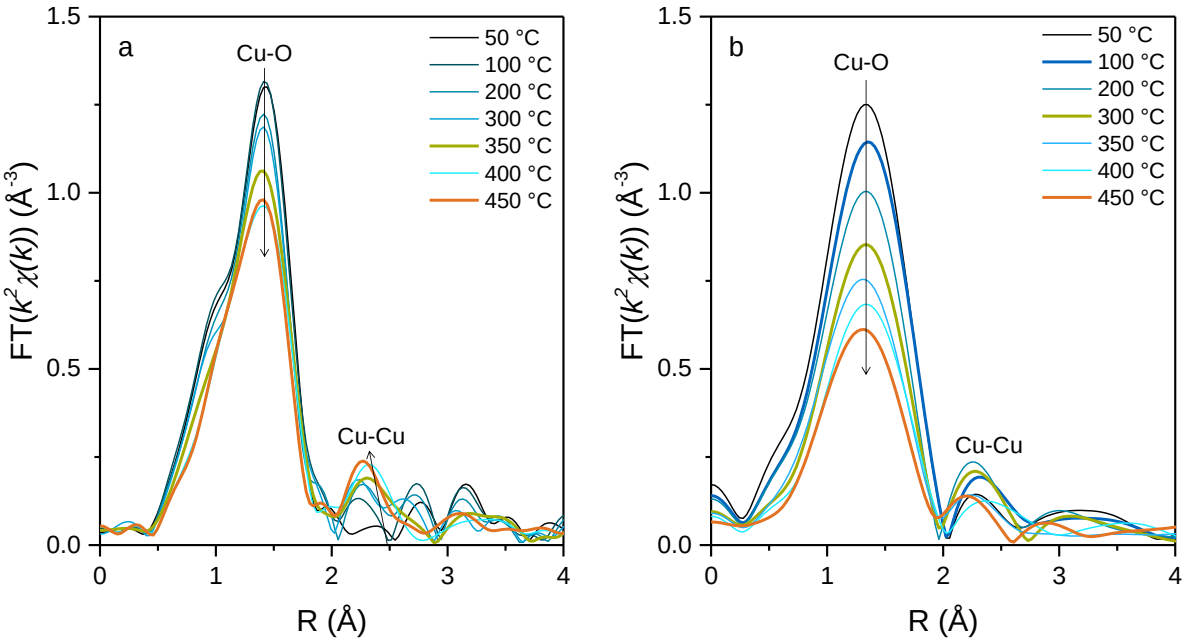

Figure 2-6. k^2-weighted Fourier-transformed (FT)-EXAFS of the Cu-MOR during thermal activation in O_2 flow (a) and in He flow (b). FT was performed in the range of 1.9-2.2 to 10.0 Å^{-1} and 1.9-2.2 to 7.9 Å^{-1} in the case of O_2 and He, respectively.

In situ XANES showed that dehydration of Cu-MOR is largely complete at 350 °C (Figure 2-4). Taking into account that significant fraction of Cu^{2+} is still present at this temperature, it is reasonable to assume the presence of $[Cu\text{-}O\text{-}Cu]^{2+}$ species formed via condensation of two $[CuOH]^+$ species. It is reported that the auto-reduction of such O-bridged Cu species proceeds by desorption and recombination of the bridging oxygen atoms.[21, 28-29, 31] Therefore, the further decrease in O coordination in the range of 300-450 °C together with complete reduction of Cu^{2+} to Cu^+ as observed in XANES is attributed to auto-reduction via elimination of O_2 from μ-oxo bridges. Thus, the lower intensity of the Cu-Cu path at temperatures above 300 °C (Figure 2-6 (b)) is likely due to the formation of Cu^+ □ Cu^+ species that is either stabilized by an Al pair or re-dispersed across the framework.[22]

Finally, the XANES and EXAFS of Cu-MOR activated in O_2 (1 h) are compared with Cu-MOR activated in He at 450 °C (1 h) followed by oxidation at 200 °C for 15 min (Figure 2-7 and Figure A 2-10). Both activation treatments have yielded equally active

catalysts, as seen in Figure 2. The Cu^+ feature at 8984 eV emerged after activation in He and disappeared completely after exposure to O_2 at 200 °C as well as 450°C. The XANES obtained after treatment of Cu-MOR at 200 °C for 15 min in O_2 was identical to the one obtained for a sample activated in O_2 at 450 °C for 1 h. Overlapping EXAFS of the Cu-MOR also indicate that the structure of Cu species obtained by both activation treatments can be regarded as identical. Thus, we conclude that a precursor of the trinuclear copper-oxo cluster is formed during treatment at high temperatures (450-500 °C). Given the auto-reduction process observed in thermal treatment under inert atmosphere, such precursor seems to consist of Cu^+ or a mixture of Cu^+/Cu^{2+} species. The identical structure (Figure 2-7) and activity in methane oxidation (Figure 2-3) of Cu species in Cu-MOR samples oxidized at 200 °C and 450 °C indicate that the trimer precursor is fully re-oxidized when contacted with O_2, regardless of the oxidation temperature applied.

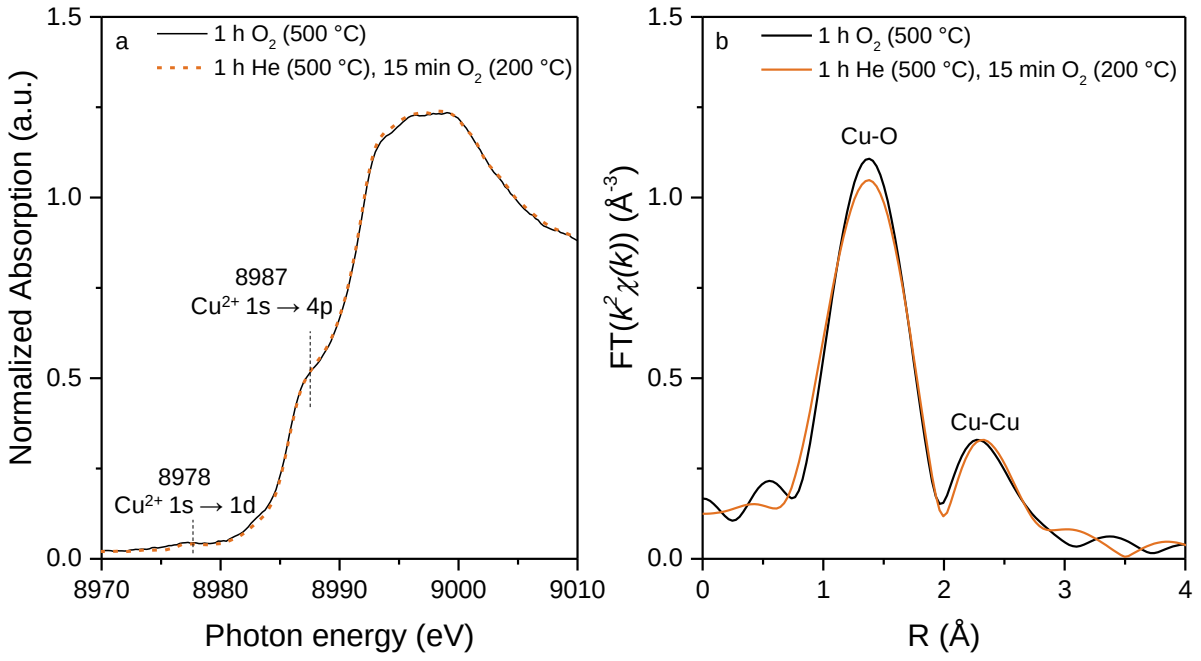

Figure 2-7. Comparison of Cu K-edge XANES (a) and k^2-weighted FT-EXAFS (b) of Cu-MOR treated at 450 °C in O_2 and Cu-MOR oxidized at 200 °C in O_2 after treatment in He at 450 °C.

The formation of active trinuclear copper-oxo clusters upon contacting the cluster precursor with O_2 has been associated with specific bands in the UV-vis spectra.[6] The in situ UV-vis spectra of Cu-MOR during oxidation of the cluster precursor at 200 °C after activation at 450 °C in N_2 atmosphere are shown in Figure 2-8. The band

observed at ca. 13,000 cm^{-1} and the weak shoulder at ca. 16,500 cm^{-1} are attributed to the d-d transition of Cu^{2+} in square-pyramidal or pyramidal and square-planar coordination structure, respectively.[55-56] Previously, we tentatively associated the trinuclear copper-oxo cluster in activated Cu-MOR with a contribution to a broad band at ca. 31,000 cm^{-1} in the UV-vis spectrum, because this band was the only one that decreased upon reaction with methane.[6] We have observed that this characteristic band at ca. 30,000 cm^{-1} is weakly present in a N_2 activated Cu-MOR sample and its intensity increased after contact with O_2 at 200 °C. Inspection of the difference spectra showed a shoulder at 24,000 cm^{-1}, which also increases upon contact with O_2. The low resolution of the spectra, however, does not allow for an assignment of this shoulder to a particular electronic transition.

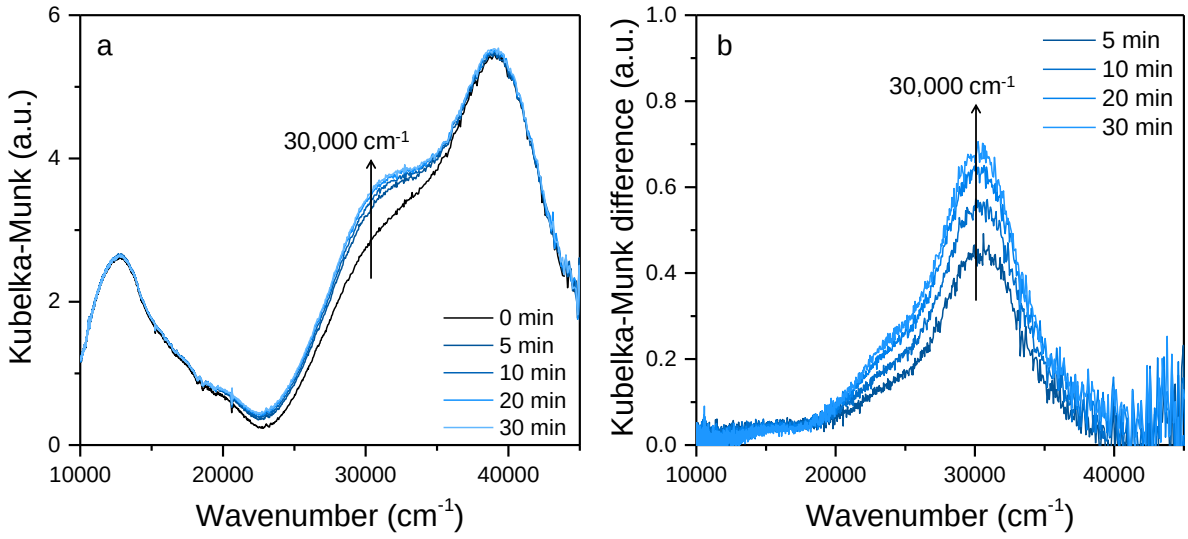

Figure 2-8. In-situ UV-Vis spectra of Cu-MOR recorded during oxidation in O_2 at 200 °C after thermal treatment in N_2 at 450 °C (a) and the corresponding difference spectra obtained by subtracting the spectrum measured at 0 min (b).

Upon reaction of CH_4 on the oxidized catalyst, increase in the intensity of the bands at 13,300 cm^{-1}, 16,400 cm^{-1} and 19,600 cm^{-1} were observed. Increasing intensity of the bands in d-d transition regions of Cu^{2+} during CH_4 reaction was also observed by Narshiman et al.[5] Recent study on Cu-SSZ-13 has shown that dinuclear Cu clusters can show bands at these positions.[57] Even though it is tempting to speculate the formation of dimeric Cu species upon reaction of $[Cu_3(\mu\text{-}O)_3]^{2+}$ with CH_4, no further experimental proof was obtained. On the other hand, decreasing intensity of the UV-vis absorption at ca. 30,000 cm^{-1} and 38,000 cm^{-1} (Figure A 2-11) are both assigned to

$Cu^{2+} \leftarrow O^{2-}$ charge transfer. While the band at 30,000 cm^{-1} is associated with $[Cu_3(\mu\text{-}O)_3]^{2+}$, we hypothesize that the band at 38,000 cm^{-1} is also due to this Cu species, since the tricopper-oxo cluster contains Cu and O atoms with different electron spin densities.[6, 39] This indicates an active species consistent with a Cu-oxo trimer[6] is formed under oxidative activation of Cu-MOR at low temperatures (200 °C), as long as the material is subjected to a thermal pretreatment in inert at 500 °C.

These results, together with the lack of dependence of the methanol selectivity with temperature or nature of the oxidant (Figure 2-3 and Figure A 2-1 (b)), support the conclusion that the cluster precursor formed at high temperatures can be oxidized in the presence of O_2 or N_2O at lower temperatures (at least 200 °C) to form the active tricopper-oxo cluster.

2.3.4. On the Formation of Active Tricopper-Oxo Cluster

Having established that thermal activation of Cu-MOR is essential for the generation of copper-µ-oxo species active in methane oxidation to methanol, we address the pathway for this chemistry. Several mechanisms for the formation of active Cu species during the activation of Cu zeolites has been previously proposed for Cu-ZSM-5[21], Cu-SSZ-13[13] and Cu-MOR.[15] Smeets et al. proposed that the active sites in Cu-ZSM-5 are $[Cu(\mu\text{-}O)Cu]^{2+}$ species, with fingerprint UV-vis band at 22,700 cm^{-1}.[21] According to these authors, a different formation mechanism of active $[Cu(\mu\text{-}O)Cu]^{2+}$ species is verified depending on the nature of the oxidant.

In the present work, differences between oxidation in O_2 and N_2O were not observed neither in the yield of CH_4 oxidation nor in the selectivity to methanol, as long as the oxidation is preceded by high temperature pretreatment (Figure 2-3 and Figure A 2-1 (b)). Thus, we conclude that the cleavage of the O-O bond in molecular O_2 is not kinetically or thermodynamically limiting and occurs close to ambient temperature to form active $[Cu_3(\mu\text{-}O)_3]^{2+}$ clusters in MOR. This conclusion, however, may not necessarily be transferable to other zeolite frameworks in view of the different behavior reported for Cu-ZSM-5 and Cu-SSZ-13 by other authors.[13, 21] Differences in Cu speciation with zeolite framework have been widely reported before[6, 13, 21] and it is therefore not surprising that the processes involved here in the formation of Cu-oxo species active in methane oxidation also follow different mechanisms.

Our results indicate that the necessity of high temperature treatment (in either inert or oxidant atmosphere) to achieve high catalytic activity in Cu-MOR must be related to steps preceding the (re-)oxidation of the precursor of the Cu active species. In situ XAS (Figure 2-4) showed that the transformation of the octahedral Cu^{2+} complexes in the zeolite pores into dehydrated and framework-coordinated Cu^{2+} was largely complete at 350 °C. However, when Cu-MOR was activated at 350 °C in O_2 it only reached 54 % of the full activity (achieved at 500 °C in O_2). Hence, we hypothesize that dehydration is not the sole reason for high temperature activation. Above 350 °C in inert atmosphere, the majority of Cu^{2+} was concluded to be reduced to Cu^{+} (Figure 2-5), partly even during activation in O_2 (Figure 2-4). We hypothesize that the appearance of Cu^{+} in samples treated at high temperatures is due to the reversible emission of O from μ-oxo bridges between Cu^{2+}. Such reaction equilibrium would be shifted towards the desorption of O as O_2 at increasing temperatures. Small concentrations of Cu^{+} were observed during activation in O_2, which indicates that the autoreduction reaction is feasible in presence of oxygen, even though the equilibrium is shifted towards higher concentrations of Cu^{2+} species. The stabilization of Cu^{+} species provided by the localized negative charges of the zeolite[58-59] could explain the presence of Cu^{+} in spite of being thermodynamically not favored.

Studies on Cu speciation in Cu-SSZ-13 have shown a higher mobility of Cu^{+} compared to Cu^{2+}, due to the weaker ionic interactions of monovalent Cu^{+} with the negatively charged zeolite framework.[27] In line with this conclusion, Li and Hall hypothesized that the reduction of Cu^{2+} to Cu^{+} facilitated redistribution of Cu and, therefore, enhanced the formation of active sites in Cu-ZSM-5.[60] It was also recently observed for Cu-SSZ-13 both the reduction of Cu^{2+} to Cu^{+} and the migration of Cu cations to 6R of CHA structure at temperatures above 375 °C.[24] Thus, the formation of a mobile Cu^{+} species is hypothesized to facilitate the redistribution and the migration of Cu in MOR. The lower concentration of active sites in Cu-MOR activated in He at 350 °C and subsequently oxidized at 200 °C in O_2 (Figure 2-3) is attributed to limited mobility or a limited concentration of Cu^{+}. Conversely, activation at 450-500 °C provides the conditions for a larger concentration of Cu^{+} to form the precursor of active Cu-oxo clusters.

Based on the results obtained here, we propose that formation of the active Cu-μ-oxo cluster occurs via the series of elementary steps shown in Scheme 2-1. The scheme is valid for the formation of the active cluster from fresh and spent Cu-MOR samples

in hydrated form. First, the exchange of Cu^{2+} species in aqueous solution can take place either in Al pairs or in one isolated Al T-site of the zeolite. At the moderate pH used in this study, partial dissociation of water ligands takes place and ion exchange occurs also via the Hirschler-Plank-Mechanism in the zeolite pores leading to $(Cu\text{-}OH)^+$ (Reaction 2.1).[47, 61] Then, as seen by XAS (Figure 4 and 6), Cu^{2+} species is dehydrated when the temperature is increased, resulting in a change of coordination from octahedral to framework-coordinated $[Cu^{II}OH]^+$ species (Reaction 2.2). The formation of μ-oxo bridges occurs via condensation of 2 adjacent $[Cu^{II}OH]^+$ species (Reaction 2.3)[26] in the temperature range 50-300 °C (Figure 6). At 450 °C, significant concentrations of Cu^{2+} have been auto-reduced to Cu^+ (although formation of first Cu^+ species can be detected already at 200 °C). This auto-reduction is hypothesized to involve the emission of O_2 from the Cu-O-Cu μ-oxo bridges (Reaction 2.4a).[26] The auto-reduction of $[Cu^{II}OH]^+$ has been also proposed to take place by the formation of a OH radical from the OH ligand[25, 30], leading to Cu^+ species coordinated to isolated Al-sites (Reaction 2.4b).

Larsen et al. proposed that the OH radical species generated in Reaction 2.4b decompose by reaction with a second $[CuOH]^+$, releasing H_2O and forming a $Cu^{2+}O^-$ species.[30] Such scheme implies the mobilization of OH radicals to a second Cu ion in the framework. However, if Cu^+ formed in Reaction 4.4b is mobilized above 400 °C, the local negative charge of the zeolite framework left behind needs to be compensated. We speculate that OH radical species may decompose into a H^+ - compensating a negative charge at the Al T-site - and an O^- species. In the next step, Cu^+ mobile species reacts with Cu pairs located at Al pairs, and are re-oxidized to Cu^{2+} by a combination of O_2 (or N_2O) and the generated O^- species leading to the active $[Cu^{II}_3(\mu\text{-}O)_3]^{2+}$ cluster. Taking into account the Al distribution for the present MOR under study, with high concentration of Al sites in 8-MR positions[6], it is to be expected that Cu pairs are located in 8-MR while Cu^+ mobile species originates in isolated exchanged sites in the 12-MR channels.

Two possible pathways for the overall reaction of formation of the oxidized cluster are shown in Reactions 2.5 a and b. As mentioned above, previous characterization of Cu-MOR has shown that Cu-oxo species are preferentially located at the pore mouth of 8 MR side pockets of MOR, because such framework positions are often multiple Al-substituted.[6] Therefore, it is reasonable to expect the presence of species like those

proposed in reaction 2.5a, $[Cu^{II}\text{-}O\text{-}Cu^{II}]^{2+}\text{-}2Al_F$ species, or in reaction 2.5b, Cu^{+} □ Cu^{+} (which is the reduced analog of $[Cu^{II}\text{-}O\text{-}Cu^{II}]^{2+}$) at the 8 MR side pocket of MOR.

Scheme 2-1. Proposed elementary steps for the formation of $[Cu_3(\mu\text{-}O)_3]^{2+}$ clusters in MOR. "Z⁻" stands for a negatively charged framework Al site in MOR. "AlF" refers to the cationic species anchored to the negatively charged framework Al site. "mig" indicates migrated cationic species.

$$(Z^-)_2[Cu^{II}(H_2O)_n]^{2+} \rightleftharpoons Z^-[Cu^{II}(H_2O)_{n-1}OH]^+ + Z^-H^+ \quad (2.1)$$

$$Z^-[Cu(H_2O)_{n-1}OH]^+ \rightleftharpoons Z^-[Cu^{II}OH]^+_{AlF} + (n\text{-}2)\ H_2O \quad (2.2)$$

$$2Z^-[Cu\text{-}OH]^+_{AlF} \longrightarrow (Z^-)_2[Cu^{II}\text{-}O\text{-}Cu^{II}]^{2+}_{2AlF} + H_2O \quad (2.3)$$

$$(Z^-)_2[Cu^{II}\text{-}O\text{-}Cu^{II}]^{2+}_{2AlF} \rightleftharpoons 2(Z^-Cu^+_{AlF}) + 1/2\ O_2 \quad (2.4a)$$

$$Z^-[Cu^{II}OH]_{AlF} \rightleftharpoons Z^-Cu^+_{AlF} + \bullet OH \quad (2.4b)$$

$$2(Z^-Cu^+_{AlF}) + Z^-Cu^+ + O_2 + \bullet OH \longrightarrow (Z^-)_2[Cu^{II}{}_3(\mu\text{-}O)_3]_{2AlF} + Z^-H^+ \quad (2.5a)$$

$$(Z^-)_2[Cu^{II}\text{-}O\text{-}Cu^{II}]^{2+}_{2AlF} + Z^-Cu^+ + 1/2\ O_2 + \bullet OH \longrightarrow (Z^-)_2[Cu^{II}{}_3(\mu\text{-}O)_3]^{2+}_{2AlF} + Z^-H^+ \quad (2.5b)$$

The experiments emphasize the necessity of a thermal treatment inducing the formation of mobile species via Reaction 2.4. Nearly full activity of Cu-MOR was reached after oxidation at low temperatures of a He-activated sample (Figure 2-3). Thus, the last step in the mechanism of formation of the active Cu-oxo cluster (any of the alternative Reactions 2.5) has a high driving force in presence of O_2 or N_2O and occurs to near completion already at 50 °C. This is confirmed by the observation that the radial distribution function and XANES (Figure 2-7) of Cu species after high-temperature and low-temperature oxidation were identical. Conversely, we attribute the partial activity registered when Cu-MOR is treated at temperatures in the range of 200 to 400 °C (Figure 2-1) to the formation of active clusters in locally Al-rich regions of the zeolite. In these regions, availability of Cu species is enough to ensure the formation of a trimer without the mobilization of distant Cu exchanged species.

2.4. Conclusions

The formation of Cu-μ-oxo species in Cu^{2+} exchanged MOR was shown to occur through a combination of thermal activation of the cationic species followed by an oxidation step. XAS demonstrated that dehydration of the octahedral Cu^{2+} complexes leads to μ-oxo bridged Cu^{2+} species coordinated to framework Al sites in the temperature range 50-300 °C. Formation of Cu^{+} occurs by auto-reduction via thermally driven emission of the Cu-O-Cu bridging oxygen and/or by the generation of OH radicals from $[CuOH]^{+}$. The auto-reduction starts at 200 °C in inert but only reached its maximum at 450-500 °C. It is unclear at present to which extent this reduction is required to induce cation mobility. We hypothesize that the high mobility of Cu^{+} is essential to enable the reorganization of Cu ions to form a precursor of the active multi-copper cluster. The last step is the oxidation of this precursor to form the active (tri)nuclear copper-oxo cluster, which takes place under mild conditions (50-200 °C) in the presence of strong oxidants such as O_2 or N_2O. The fact that Cu speciation in MOR micropores seems to be significantly different from Cu in ZSM-5 or SSZ-13 highlights the critical role of a specific zeolite lattice. The high efficiency of MOR in forming active Cu-oxo clusters even at low oxidation temperatures is attributed to a high concentration of Al pairs at the pore mouth of 8MR side pocket of MOR, which is a position structurally accessible for the formation of Cu-oxo clusters. While the present study highlights the importance of individual steps in the formation of the active species, more work is needed to understand how aluminum siting and structural aspects of zeolite lattice can be used to direct and maximize the concentration of the active sites.

2.5. Acknowledgement

The financial support from the Deutsche Forschungsgemeinschaft DFG under project LE1187/13-1 is acknowledged. Part of the research was supported by the TUM International Graduate School of Science and Engineering (IGSSE) and the Max-Buchner Forschungsstiftung from DECHEMA (Grant number 3568). We acknowledge DESY (Hamburg, Germany), a member of the Helmholtz Association HGF, for the provision of experimental facilities. Parts of this research were carried out at PETRA III and we would like to thank Edmund Welter for assistance in using beamline P 65.

2.6. Appendix

2.6.1. Effect of Activation Conditions on the Formation of Active Cu-oxo Clusters

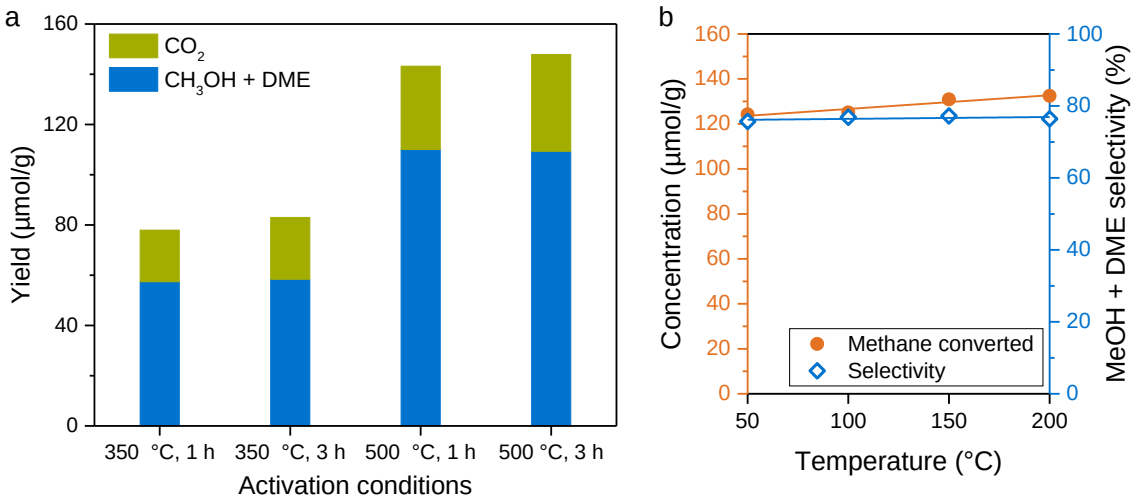

Figure A 2-1. Yields of CH_4 oxidation on the Cu-MOR catalyst after thermal activation in O_2 at various temperatures and duration (a). CH_4 oxidation yields and selectivities to methanol and DME on the Cu-MOR catalyst after thermal activation in He at 500 °C for 1 h and subsequent oxidation in 5% N_2O at lower temperatures for 10 min (b).

2.6.2. XAS Analysis of Cu-MOR during Thermal Activation

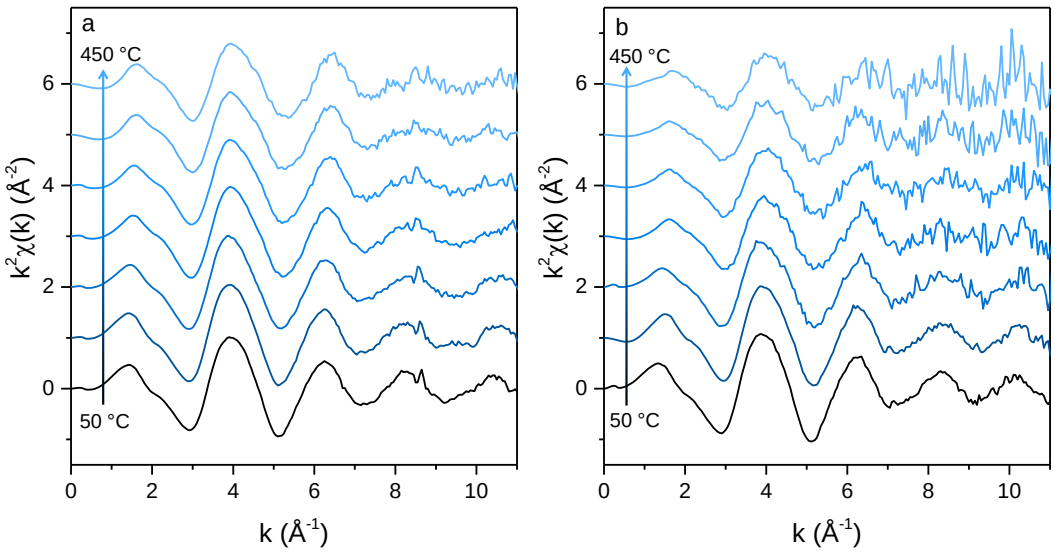

Figure A 2-2. k^2-weighted EXAFS of Cu-MOR while heating up in O_2 (a) and in He (b). FT was performed in the range from 1.9-2.2 to 10.0 $Å^{-1}$ and from 1.9-2.2 to 7.9 $Å^{-1}$ in the case of O_2 and He, respectively.

2.6.3. EXAFS Fitting Analysis of Cu-MOR after Activation in O_2 at 450 °C

EXAFS fitting of the spectrum recorded after activation of the Cu-MOR sample in O_2 at 450 °C was performed to confirm if the feature seen at ca. 2.3 Å in FT-EXAFS actually stems from Cu-Cu single scattering. EXAFS fitting was performed in R-space in the range of ΔR = 1.0 – 4.0 Å on the FT of k^2-weighted EXAFS in the k range of 2.2-10.0 $Å^{-1}$.

First, the model structure of $[Cu_3(\mu\text{-}O)_3]^{2+}$ (Figure A 2-3 (a)) was used to perform EXAFS fitting with and without Cu-Al single scattering paths. Coordination numbers (CNs) were derived from the DFT-optimized structural model, and were averaged for the three Cu scatterers. Throughout the fitting procedure, CNs were fixed to the values obtained from the structural model to decrease the number of fitting variables.

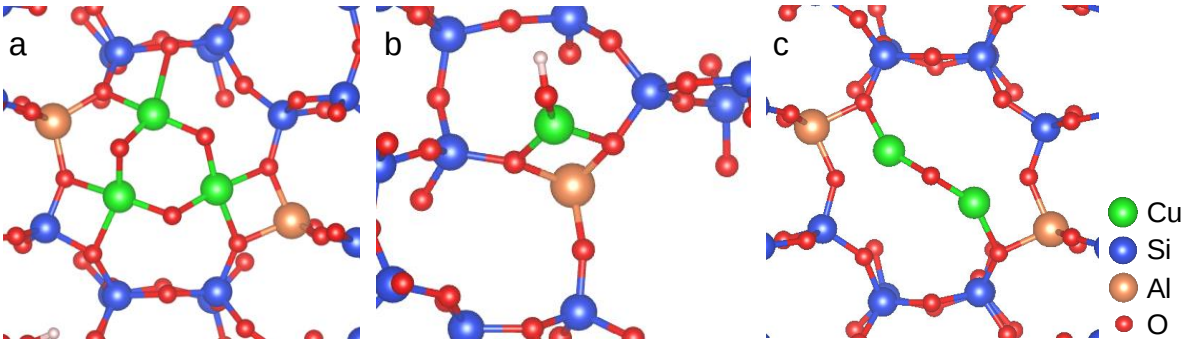

Figure A 2-3. DFT-optimized structures of $[Cu_3(\mu\text{-}O)_3]^{2+}$ (a), $[Cu(\mu\text{-}O)Cu]^{2+}$ (b) and $[CuOH]^{+}$ (c) located at the pore mouth of 8MR side pocket in MOR.

EXAFS fitting results obtained without including the Cu-Al scattering paths are reported in the Table A 2-1 and Figure A 2-4. Energy shift of 7.53 (± 3.69) eV and *R*-factor of 0.011 were obtained. Scattering paths that appear at ca. 2.3 Å are plotted together with the experimental and fit RDF. It can be seen that the feature at ca. 2.3 Å is well reproduced by two single scattering paths of Cu-Cu.

Table A 2-1. EXAFS fitting results of Cu-MOR using DFT-optimized model structure of $[Cu_3(\mu\text{-}O)_3]^{2+}$ without including Cu-Al single scattering paths.

Path	CN	R (Å)	Debye-Waller factor (Å^2)
Cu-O_{EF}	2	1.84 (± 0.04)	0.004 (± 0.003)
Cu-O_{FW} (short)	1.66	1.97 (± 0.05)	0.002 (± 0.005)
Cu-O_{FW} (long)	0.33	2.36 (set)	0.003 (set)
Cu-Cu (short)	0.66	2.86 (± 0.08)	0.009 (± 0.007)
Cu-Cu (long)	1.33	2.94 (± 0.11)	0.021 (± 0.011)
Cu-O_{EF}	1	3.33 (± 0.13)	0.010 (set)

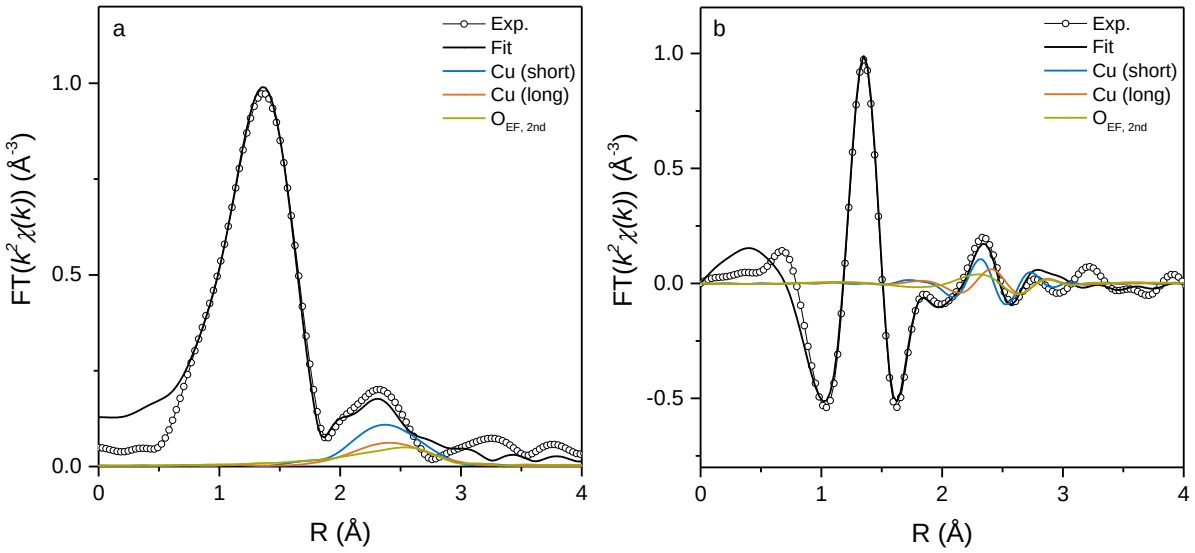

Figure A 2-4. Magnitude (a) and imaginary part (b) of the fitting results of FT-EXAFS of Cu-MOR after activation in O_2 at 450 °C using $[Cu_3(\mu\text{-}O)_3]^{2+}$ model structure, without including Cu-Al single scattering paths.

Next, EXAFS fitting was performed with including Cu-Al single scattering paths. Again, since there are largely two different Cu-Al distances (2.7 Å and 3.2 Å in the DFT-optimized structure model), Cu-Al coordination number for the each path was averaged among three Cu scatterers. Cu-Si single scattering was not included in the fit, since each Cu-Si single scattering paths have different distances and therefore they cancel out. As a result, obtained energy shift and *R*-factor were -8.77 (± 1.21) eV and 0.012, respectively. Fitting results are shown in Table A 2-2 and Figure A 2-5. The feature at

2.3 Å is well reproduced with including Cu-Al single scattering paths. However, it is reproduced as the convolution of Cu-Cu and Cu-Al single scattering paths, suggesting that the presence of Cu-Al single scattering cannot be excluded.

Table A 2-2. EXAFS fitting results of Cu-MOR using DFT-optimized model structure of $[Cu_3(\mu\text{-}O)_3]^{2+}$ with including Cu-Al single scattering paths.

Path	CN	R (Å)	DW factor
$Cu\text{-}O_{EF}$	2	1.83 (set)	0.005 (± 0.003)
$Cu\text{-}O_{FW}$ (short)	1.66	1.94 (± 0.03)	0.003 (set)
$Cu\text{-}O_{FW}$ (long)	0.33	3.12 (set)	0.003 (set)
Cu-Cu (short)	0.66	2.80 (± 0.05)	0.009 (± 0.020)
Cu-Cu (long)	1.33	3.11 (± 0.26)	0.018 (± 0.024)
$Cu\text{-}O_{EF}$	1	3.29 (± 0.20)	0.005 (set)
Cu-Al (short)	0.33	2.75 (± 0.25)	0.003 (set)
Cu-Al (long)	0.66	3.17 (± 0.16)	0.003 (set)

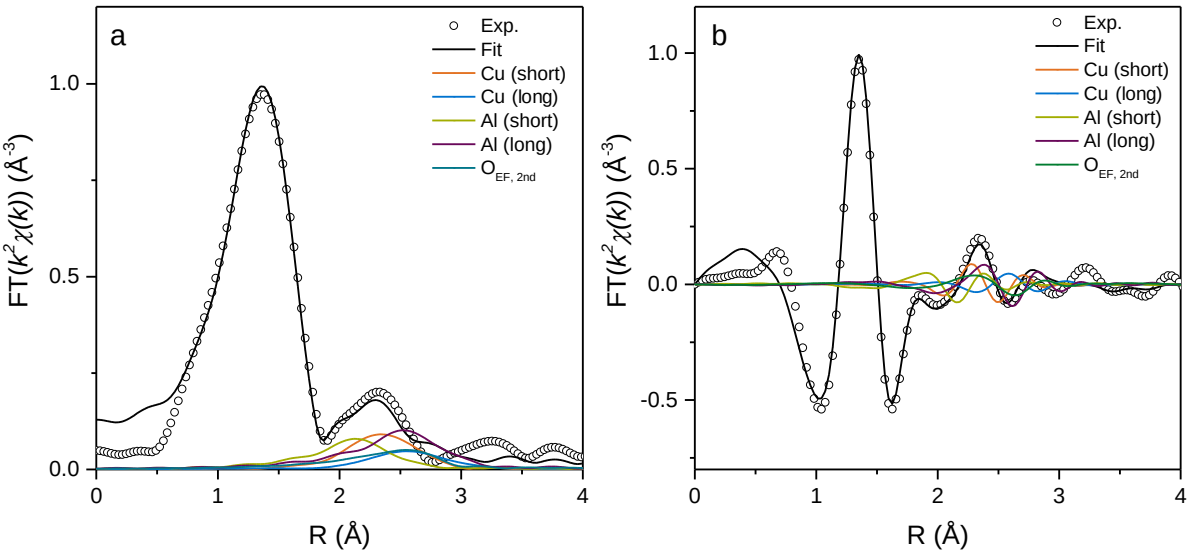

Figure A 2-5. Magnitude (a) and imaginary part (b) of the fitting results of FT-EXAFS of Cu-MOR after activation in O_2 at 450 °C using $[Cu_3(\mu\text{-}O)_3]^{2+}$ model structure, with including Cu-Al single scattering paths.

In order to see Cu-Al scattering alone better, EXAFS fitting of Cu-MOR was also performed using the DFT-optimized structural model of $[Cu\text{-}OH]^+$ monomer (Figure A

2-3 (b)). Since the Cu-H scattering is very weak and invisible in the EXAFS, it was excluded from the fitting procedure. Energy shift and *R*-factor obtained from the fitting were -4.18 (± 3.00) eV and 0.044, respectively. Fitting results are presented in Table A 2-3 and Figure A 2-6. As rather high *R*-factor and the plot in Figure A2-6 show, Cu-Al single scattering only cannot fully reproduce the feature at ca. 2.3 Å. It is also worth noting that Cu-Al single scattering alone shows rather weak scattering intensity, contrary to what is observed experimentally (Figure 2-5 and 2-6). Therefore, we conclude that, although the feature at 2.3 Å may indeed arise partially from Cu-Al scattering, Cu-Cu scattering is stronger. Therefore, the experimentally observed feature at the position is better attributed to Cu-Cu single scattering, without ruling out a small contribution of Cu-Al scattering.

Table A 2-3. EXAFS fitting results of Cu-MOR using DFT-optimized model structure of [Cu-OH]$^+$ with including Cu-Al single scattering paths.

Path	CN	R (Å)	DW factor
Cu-O_{EF}	1	1.86 +/- 0.14	0.003 (set)
Cu-O_{FW}	2	1.94 +/- 0.03	0.005 +/- 0.007
Cu-Al	1	2.68 +/- 0.06	0.013 +/- 0.010

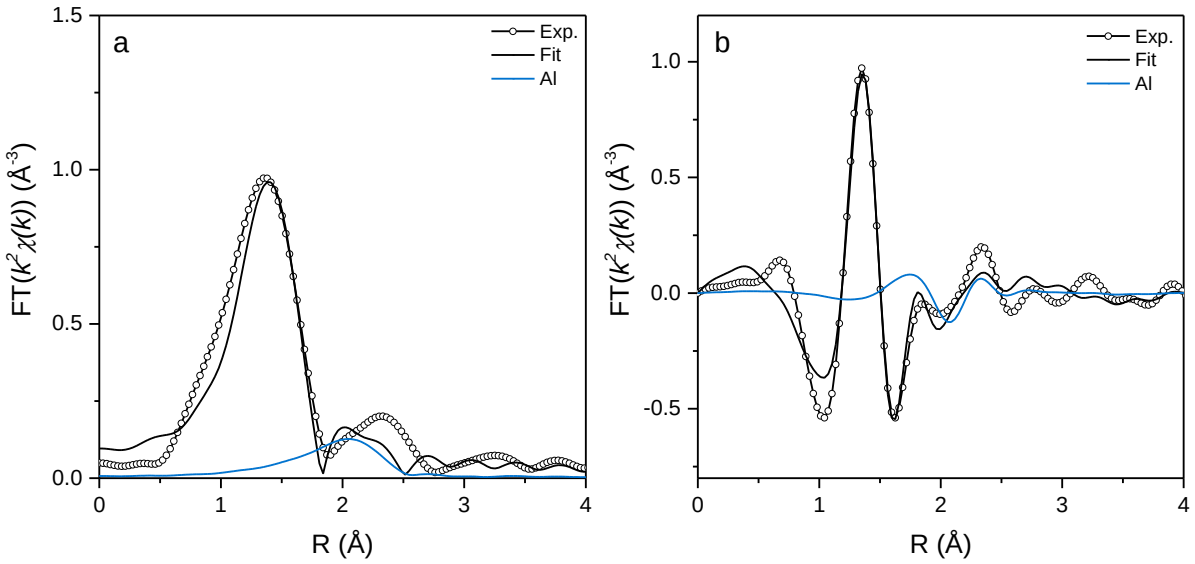

Figure A 2-6. Magnitude (a) and imaginary part (b) of the fitting results of FT-EXAFS of Cu-MOR after activation in O_2 at 450 °C using [Cu-OH]$^+$ model structure, with including Cu-Al single scattering paths.

Additionally, fitting of the EXAFS of Cu-MOR using the model structure of Cu dimer $[Cu\text{-}O\text{-}Cu]^{2+}$ (Figure A2-3 (c)) was also performed. Identical fitting procedure shown in SI was employed.

EXAFS fitting was first performed with only Cu-O and Cu-Cu single scattering paths, excluding Cu-Al and Cu-Si scatterings. Fitting results are shown in Table A 2-4 and Figure A 2-7. An energy shift of -6.32 (± 2.57) eV and *R*-factor of 0.025 were obtained. As suggested by the high *R*-factor and as it can be seen in Figure A 2-7, experimentally obtained EXAFS, especially the feature at 2.3 Å, is poorly reproduced.

Table A 2-4. EXAFS fitting results of Cu-MOR using DFT-optimized structure of $[Cu(\mu\text{-}O)Cu]^{2+}$ with Cu-O and Cu-Cu single scattering paths.

Path	CN	R (Å)	Debye-Waller factor (Å^2)
$Cu\text{-}O_{EF}$	1	1.84 (± 0.09)	0.003 (set)
$Cu\text{-}O_{FW}$	2	1.93 (± 0.01)	0.004 (± 0.006)
Cu-Cu	1	2.88 (± 0.03)	0.012 (± 0.004)

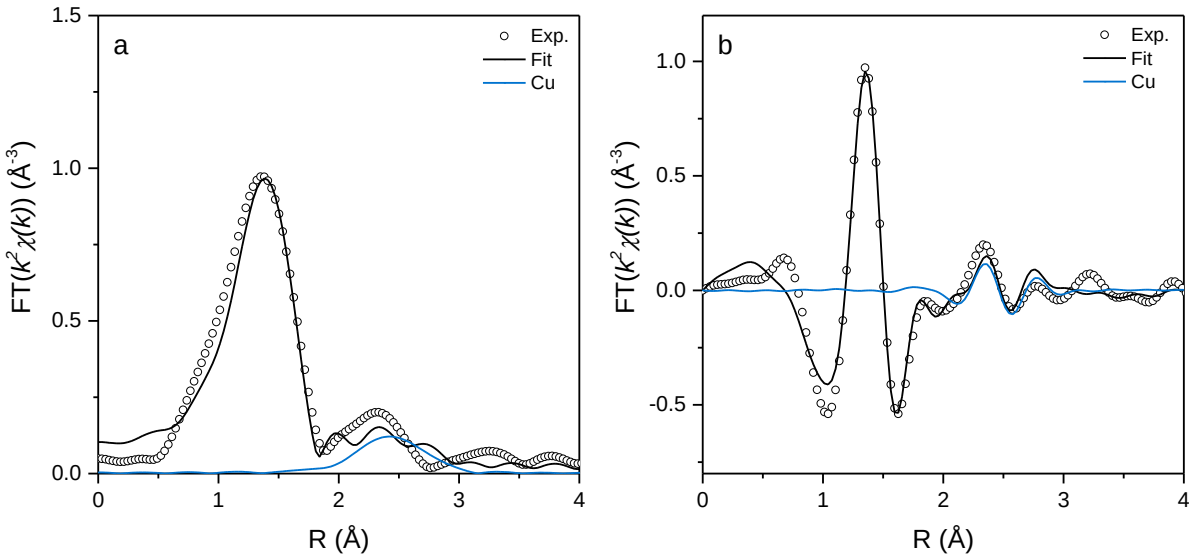

Figure A 2-7. Magnitude (a) and imaginary part (b) of the fitting results of FT-EXAFS of Cu-MOR after activation in O_2 at 450 °C using $[Cu(\mu\text{-}O)Cu]^{2+}$ model structure with Cu-O and Cu-Cu single scattering paths.

Next, EXAFS fitting was performed with including Cu-Al single scattering, in addition to what was occluded in the former fitting. An energy shift of -9.90 (± 3.91) eV and *R*-

factor of 0.019 were obtained, and the fitting results are shown in Table A 2-5 and Figure A 2-8. Again, the feature at 2.3 Å could not be well reproduced. Moreover, the Cu-Al distance obtained by fitting is far below reported value of 2.7-2.8 Å for Cu-CHA (ref.25, Pappas *et al.*), making those fitting results unreasonable.

Table A 2-5. EXAFS fitting results of Cu-MOR using DFT-optimized structure of $[Cu(\mu\text{-}O)Cu]^{2+}$ with Cu-O, Cu-Al and Cu-Cu single scattering paths.

Path	CN	R (Å)	Debye-Waller factor (Å^2)
Cu-O_{EF}	1	1.81 (± 0.09)	0.003 (set)
Cu-O_{FW}	2	1.91 (± 0.03)	0.003 (± 0.005)
Cu-Al	1	2.29 (± 0.05)	0.020 (± 0.014)
Cu-Cu	1	2.85 (± 0.04)	0.011 (± 0.004)

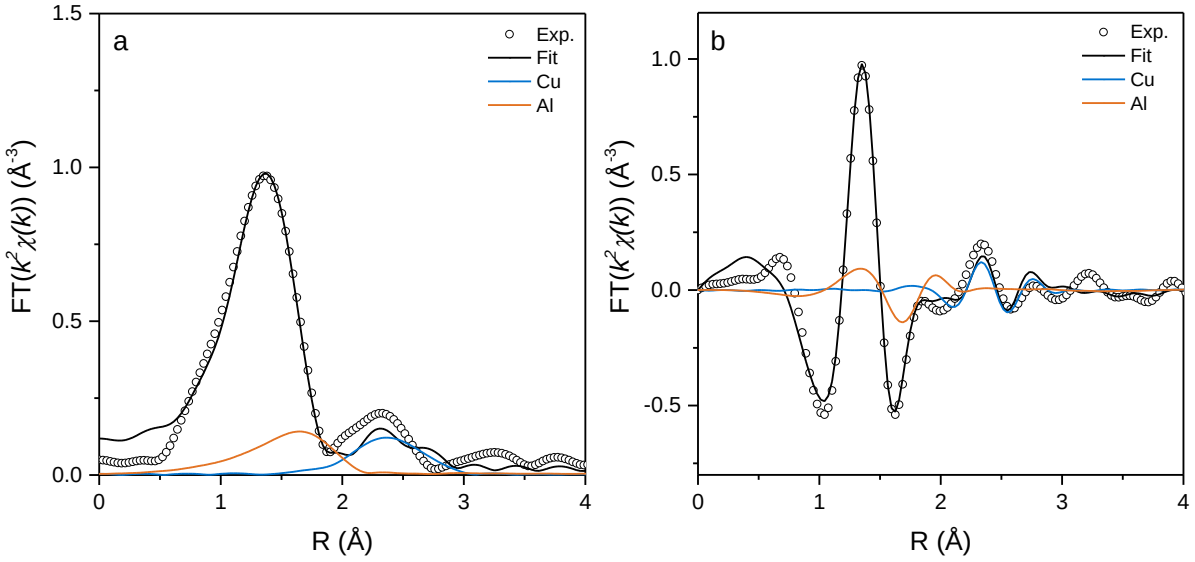

Figure A 2-8. Magnitude (a) and imaginary part (b) of the fitting results of FT-EXAFS of Cu-MOR after activation in O_2 at 450 °C using $[Cu(\mu\text{-}O)Cu]^{2+}$ model structure with Cu-O, Cu-Al and Cu-Cu single scattering paths.

At last, Cu-Si single scattering paths were included in the fitting. An energy shift of -10.27 (± 1.88) eV and *R*-factor of 0.009 were obtained. The fitting results are shown in Table A 2-6 and Figure A 2-9. As seen from relatively low *R*-factor and the Figure A 2-9, the fitted EXAFS reproduce the experimentally recorded data of Cu-MOR. However,

the very short Cu-Al distance of makes it unlikely that the obtained results are chemically reasonable.

In summary, the best and most reasonable results during fitting the EXAFS were obtained with $[Cu_3(\mu\text{-}O)_3]^{2+}$ structure. These EXAFS fitting results are also in line with ref.6, underlining the reproducibility of EXAFS analysis of the Cu-MOR sample.

Table A 2-6. EXAFS fitting results of Cu-MOR using DFT-optimized structure of $[Cu(\mu\text{-}O)Cu]^{2+}$ with Cu-O, Cu-Al, Cu-Cu and Cu-Si single scattering paths.

Path	CN	R (Å)	Debye-Waller factor (Å^2)
$Cu\text{-}O_{EF}$	1	1.83 (± 0.13)	0.003 (set)
$Cu\text{-}O_{FW}$	2	1.91 (± 0.05)	0.007 (± 0.014)
Cu-Al	1	2.23 (± 0.03)	0.010 (± 0.006)
Cu-Cu	1	3.05 (± 0.23)	0.021 (± 0.041)
Cu-Si	2	3.06 (± 0.06)	0.010 (± 0.010)

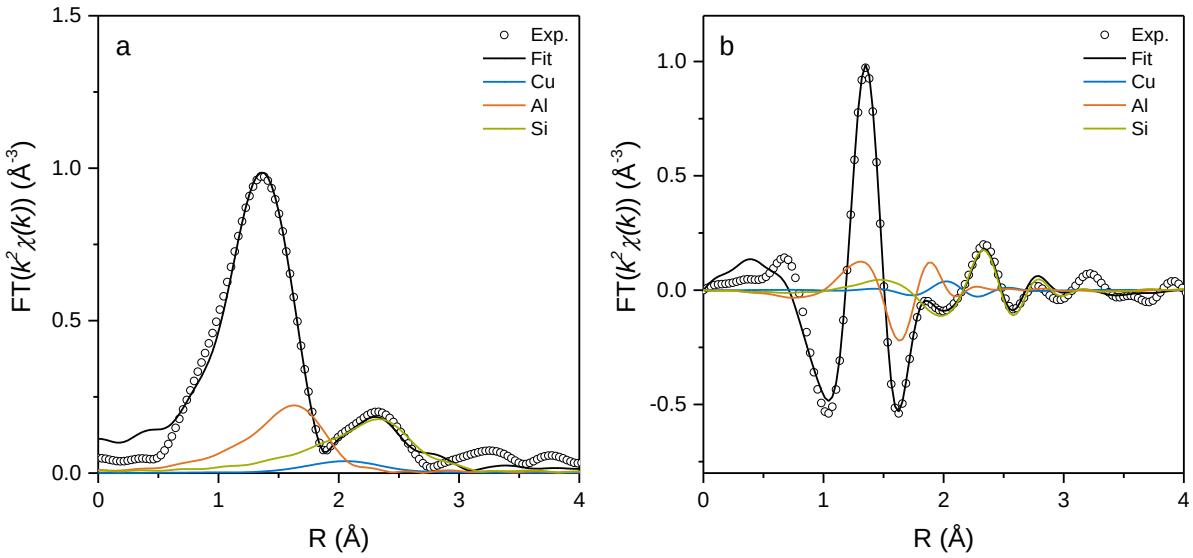

Figure A 2-9. Magnitude (a) and imaginary part (b) of the fitting results of FT-EXAFS of Cu-MOR after activation in O_2 at 450 °C using $[Cu(\mu\text{-}O)Cu]^{2+}$ model structure with Cu-O, Cu-Al, Cu-Cu and Cu-Si single scattering paths.

2.6.4. EXAFS Analysis of Cu-MOR after Activation under Different Conditions

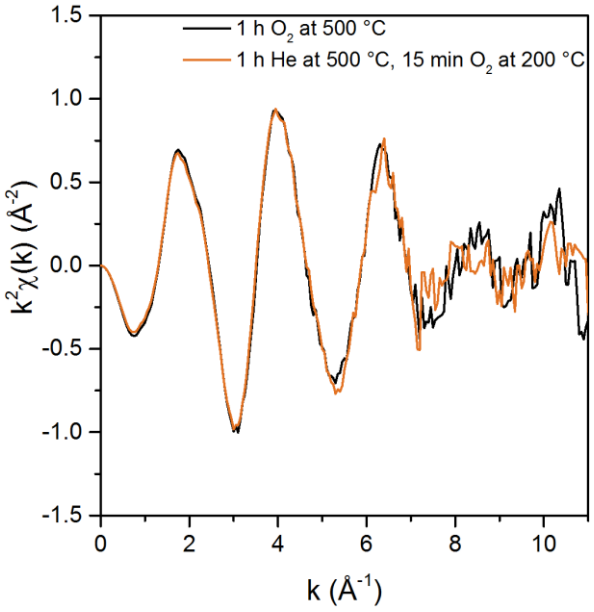

Figure A 2-10. k^2-weighted EXAFS of Cu-MOR after activation in O_2 at 500 °C and thermal treatment in He at 500 °C and subsequent oxidation in O_2 at 200 °C. Fourier-Transformation was performed in the range from 2.2 to 8.0 Å^{-1}.

2.6.5. In-Situ UV-Vis Study of Cu-MOR during Reaction with CH_4

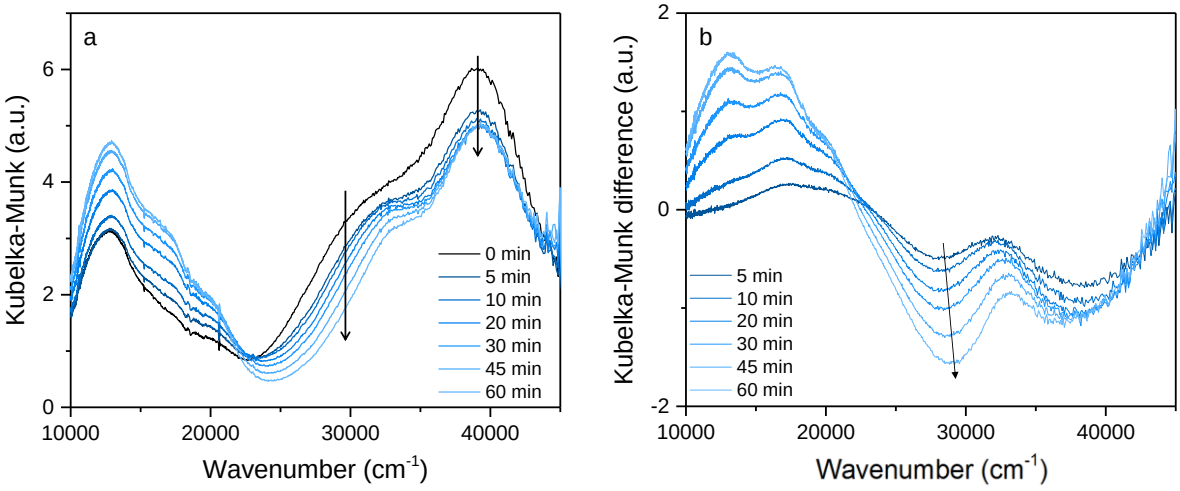

Figure A 2-11. In-situ diffuse-reflectance UV-Vis spectra (a) and difference spectra (b) while contacting the Cu-MOR catalyst with CH_4 flow after thermal treatment of the catalyst in N_2 at 450 °C and subsequent oxidation in O_2 at 200 °C.

2.7. Reference

1. Wang, V. C. C.; Maji, S.; Chen, P. P. Y.; Lee, H. K.; Yu, S. S. F.; Chan, S. I., Alkane Oxidation: Methane Monooxygenases, Related Enzymes, and Their Biomimetics. *Chem. Rev.* **2017**.
2. Lieberman, R. L.; Rosenzweig, A. C., Crystal Structure of a membrane-Bound Metalloenzyme that Catalyses the Biological Oxidation of Methane. *Nature* **2005**, *434*, 177.
3. Merkx, M.; Kopp, D. A.; Sazinsky, M. H.; Blazyk, J. L.; Müller, J.; Lippard, S. J., Dioxygen Activation and Methane Hydroxylation by Soluble Methane Monooxygenase: A Tale of Two Irons and Three Proteins. *Angew. Chem. Int. Ed.* **2001**, *40*, 2782.
4. Mahyuddin, M. H.; Staykov, A.; Shiota, Y.; Yoshizawa, K., Direct Conversion of Methane to Methanol by Metal-Exchanged ZSM-5 Zeolite (Metal = Fe, Co, Ni, Cu). *ACS Catal.* **2016**, *6*, 8321.
5. Narsimhan, K.; Michaelis, V. K.; Mathies, G.; Gunther, W. R.; Griffin, R. G.; Román-Leshkov, Y., Methane to Acetic Acid over Cu-Exchanged Zeolites: Mechanistic Insights from a Site-Specific Carbonylation Reaction. *J. Am. Chem. Soc.* **2015**, *137*, 1825.
6. Grundner, S.; Markovits, M. A. C.; Li, G.; Tromp, M.; Pidko, E. A.; Hensen, E. J. M.; Jentys, A.; Sanchez-Sanchez, M.; Lercher, J. A., Single-Site Trinuclear Copper Oxygen Clusters in Mordenite for Selective Conversion of Methane to Methanol. *Nat. Commun.* **2015**, *6*, 7546.
7. Alayon, E. M.; Nachtegaal, M.; Ranocchiari, M.; van Bokhoven, J. A., Catalytic Conversion of Methane to Methanol over Cu-Mordenite. *Chem. Commun.* **2012**, *48*, 404.
8. Groothaert, M. H.; Smeets, P. J.; Sels, B. F.; Jacobs, P. A.; Schoonheydt, R. A., Selective Oxidation of Methane by the Bis(μ-oxo)dicopper Core Stabilized on ZSM-5 and Mordenite Zeolites. *J. Am. Chem. Soc.* **2005**, *127*, 1394.
9. Snyder, B. E. R.; Vanelderen, P.; Bols, M. L.; Hallaert, S. D.; Bottger, L. H.; Ungur, L.; Pierloot, K.; Schoonheydt, R. A.; Sels, B. F.; Solomon, E. I., The Active Site of Low-Temperature Methane Hydroxylation in Iron-Containing Zeolites. *Nature* **2016**, *536*, 317.
10. Göltl, F.; Michel, C.; Andrikopoulos, P. C.; Love, A. M.; Hafner, J.; Hermans, I.; Sautet, P., Computationally Exploring Confinement Effects in the Methane-to-Methanol Conversion Over Iron-Oxo Centers in Zeolites. *ACS Catal.* **2016**, *6*, 8404.
11. Starokon, E. V.; Parfenov, M. V.; Pirutko, L. V.; Abornev, S. I.; Panov, G. I., Room-Temperature Oxidation of Methane by alpha-Oxygen and Extraction of Products from the FeZSM-5 Surface. *J. Phys. Chem. C* **2011**, *115*, 2155.
12. Pappas, D. K.; Martini, A.; Dyballa, M.; Kvande, K.; Teketel, S.; Lomachenko, K. A.; Baran, R.; Glatzel, P.; Arstad, B.; Berlier, G.; Lamberti, C.; Bordiga, S.; Olsbye, U.; Svelle, S.; Beato, P.; Borfecchia, E., The Nuclearity of the Active Site for Methane to Methanol Conversion in Cu-Mordenite: A Quantitative Assessment. *J. Am. Chem. Soc.* **2018**, *140*, 15270.

13. Pappas, D. K.; Borfecchia, E.; Dyballa, M.; Pankin, I. A.; Lomachenko, K. A.; Martini, A.; Signorile, M.; Teketel, S.; Arstad, B.; Berlier, G.; Lamberti, C.; Bordiga, S.; Olsbye, U.; Lillerud, K. P.; Svelle, S.; Beato, P., Methane to Methanol: Structure–Activity Relationships for Cu-CHA. *J. Am. Chem. Soc.* **2017**, *139*, 14961.

14. Le, H. V.; Parishan, S.; Sagaltchik, A.; Göbel, C.; Schlesiger, C.; Malzer, W.; Trunschke, A.; Schomäcker, R.; Thomas, A., Solid-State Ion-Exchanged Cu/Mordenite Catalysts for the Direct Conversion of Methane to Methanol. *ACS Catal.* **2017**, 1403.

15. Kim, Y.; Kim, T. Y.; Lee, H.; Yi, J., Distinct Activation of Cu-MOR for Direct Oxidation of Methane to Methanol. *Chem. Commun.* **2017**, *53*, 4116.

16. Wulfers, M. J.; Teketel, S.; Ipek, B.; Lobo, R. F., Conversion of Methane to Methanol on Copper-Containing Small-Pore Zeolites and Zeotypes. *Chem. Commun.* **2015**, *51*, 4447.

17. Sheppard, T.; Hamill, C. D.; Goguet, A.; Rooney, D. W.; Thompson, J. M., A Low Temperature, Isothermal Gas-Phase System for Conversion of Methane to Methanol over Cu-ZSM-5. *Chem. Commun.* **2014**, *50*, 11053.

18. Li, G.; Vassilev, P.; Sanchez-Sanchez, M.; Lercher, J. A.; Hensen, E. J. M.; Pidko, E. A., Stability and Reactivity of Copper Oxo-Clusters in ZSM-5 Zeolite for selective Methane Oxidation to Methanol. *J. Catal.* **2016**, *338*, 305.

19. Tomkins, P.; Mansouri, A.; Bozbag, S. E.; Krumeich, F.; Park, M. B.; Alayon, E. M.; Ranocchiari, M.; van Bokhoven, J. A., Isothermal Cyclic Conversion of Methane into Methanol over Copper-Exchanged Zeolite at Low Temperature. *Angew. Chem. Int. Ed.* **2016**, *55*, 5467.

20. Alayon, E. M. C.; Nachtegaal, M.; Bodi, A.; van Bokhoven, J. A., Reaction Conditions of Methane-to-Methanol Conversion Affect the Structure of Active Copper Sites. *ACS Catal.* **2014**, *4*, 16.

21. Smeets, P. J.; Hadt, R. G.; Woertink, J. S.; Vanelderen, P.; Schoonheydt, R. A.; Sels, B. F.; Solomon, E. I., Oxygen Precursor to the Reactive Intermediate in Methanol Synthesis by Cu-ZSM-5. *J. Am. Chem. Soc.* **2010**, *132*, 14736.

22. Dědeček, J.; Wichterlová, B., Role of Hydrated Cu Ion Complexes and Aluminum Distribution in the Framework on the Cu Ion Siting in ZSM-5. *J. Phys. Chem. B* **1997**, *101*, 10233.

23. Dedecek, J.; Sobalik, Z.; Tvaruazkova, Z.; Kaucky, D.; Wichterlova, B., Coordination of Cu Ions in High-Silica Zeolite Matrixes. Cu^{+} Photoluminescence, IR of NO Adsorbed on Cu^{2+}, and Cu^{2+} ESR Study. *J. Phys. Chem.* **1995**, *99*, 16327.

24. Andersen, C. W.; Borfecchia, E.; Bremholm, M.; Jørgensen, M. R. V.; Vennestrøm, P. N. R.; Lamberti, C.; Lundegaard, L. F.; Iversen, B. B., Redox-Driven Migration of Copper Ions in the Cu-CHA Zeolite as Shown by the In Situ PXRD/XANES Technique. *Angew. Chem. Int. Ed.* **2017**, *56*, 10367.

25. Borfecchia, E.; Lomachenko, K. A.; Giordanino, F.; Falsig, H.; Beato, P.; Soldatov, A. V.; Bordiga, S.; Lamberti, C., Revisiting the Nature of Cu Sites in the Activated Cu-SSZ-13 Catalyst for SCR Reaction. *Chem. Sci.* **2015**, *6*, 548.

26. Llabrés i Xamena, F. X.; Fisicaro, P.; Berlier, G.; Zecchina, A.; Palomino, G. T.; Prestipino, C.; Bordiga, S.; Giamello, E.; Lamberti, C., Thermal Reduction of

Cu^{2+}−Mordenite and Re-oxidation upon Interaction with H_2O, O_2, and NO. *J. Phys. Chem. B* **2003**, *107*, 7036.

27. Kwak, J. H.; Varga, T.; Peden, C. H. F.; Gao, F.; Hanson, J. C.; Szanyi, J., Following the Movement of Cu Ions in a SSZ-13 Zeolite during Dehydration, Reduction and Adsorption: A Combined in Situ TP-XRD, XANES/DRIFTS study. *J. Catal.* **2014**, *314*, 83.

28. Iwamoto, M.; Yahiro, H.; Tanda, K.; Mizuno, N.; Mine, Y.; Kagawa, S., Removal of Nitrogen Monoxide through a Novel Catalytic Process. 1. Decomposition on Excessively Copper-Ion-Exchanged ZSM-5 Zeolites. *J. Phys. Chem.* **1991**, *95*, 3727.

29. Valyon, J.; Hall, W. K., Effects of Reduction and Reoxidation on the Infrared Spectra from Cu-Y and Cu-ZSM-5 Zeolites. *J. Phys. Chem.* **1993**, *97*, 7054.

30. Larsen, S. C.; Aylor, A.; Bell, A. T.; Reimer, J. A., Electron Paramagnetic Resonance Studies of Copper Ion-Exchanged ZSM-5. *J. Phys. Chem.* **1994**, *98*, 11533.

31. Sárkány, J.; d'Itri, J. L.; Sachtler, W. M. H., Redox Chemistry in Excessively Ion-Exchanged Cu/Na-ZSM-5. *Catal. Lett.* **1992**, *16*, 241.

32. Alayon, E. M. C.; Nachtegaal, M.; Bodi, A.; Ranocchiari, M.; van Bokhoven, J. A., Bis(μ-oxo) versus Mono(μ-oxo)dicopper Cores in a Zeolite for Converting Methane to Methanol: an in Situ XAS and DFT Investigation. *Phys. Chem. Chem. Phys.* **2015**, *17*, 7681.

33. Alayon, E. M. C.; Nachtegaal, M.; Kleymenov, E.; van Bokhoven, J. A., Determination of the Electronic and Geometric Structure of Cu Sites during Methane Conversion over Cu-MOR with X-Ray Absorption Spectroscopy. *Microporous Mesoporous Mater.* **2013**, *166*, 131.

34. Woertink, J. S.; Smeets, P. J.; Groothaert, M. H.; Vance, M. A.; Sels, B. F.; Schoonheydt, R. A.; Solomon, E. I., A $[Cu_2O]^{2+}$ Core in Cu-ZSM-5, the Active Site in the Oxidation of Methane to Methanol. *Proc. Natl. Acad. Sci.* **2009**, *106*, 18908.

35. Jacobs, P. A.; de Wilde, W.; Schoonheydt, R. A.; Uytterhoeven, J. B.; Beyer, H., Redox Behaviour of Transition Metal Ions in Zeolites. Part 3.—Auto-Reduction of Cupric Ions in Y Zeolites. *J. Chem. Soc., Faraday Trans. 1* **1976**, *72*, 1221.

36. Palomino, G. T.; Fisicaro, P.; Bordiga, S.; Zecchina, A.; Giamello, E.; Lamberti, C., Oxidation States of Copper Ions in ZSM-5 Zeolites. A Multitechnique Investigation. *J. Phys. Chem. B* **2000**, *104*, 4064.

37. Lei, G. D.; Adelman, B. J.; Sárkány, J.; Sachtler, W. M. H., Identification of Copper(II) and Copper(I) and their Interconversion in Cu/ZSM-5 De-NO_x Catalysts. *Appl. Catal. B* **1995**, *5*, 245.

38. Mahyuddin, M. H.; Tanaka, T.; Shiota, Y.; Staykov, A.; Yoshizawa, K., Methane Partial Oxidation over $[Cu_2(\mu\text{-}O)]^{2+}$ and $[Cu_3(\mu\text{-}O)_3]^{2+}$ Active Species in Large-Pore Zeolites. *ACS Catal.* **2018**, *8*, 1500.

39. Vogiatzis, K. D.; Li, G.; Hensen, E. J. M.; Gagliardi, L.; Pidko, E. A., Electronic Structure of the $[Cu_3(\mu\text{-}O)_3]^{2+}$ Cluster in Mordenite Zeolite and Its Effects on the Methane to Methanol Oxidation. *J. Phys. Chem. C* **2017**, *121*, 22295.

40. Grundner, S.; Luo, W.; Sanchez-Sanchez, M.; Lercher, J. A., Synthesis of Single-Site Copper Catalysts for Methane Partial Oxidation. *Chem. Commun.* **2016**, *52*, 2553.

41. Ravel, B.; Newville, M., ATHENA, ARTEMIS, HEPHAESTUS: Data Analysis for X-Ray Absorption Spectroscopy using IFEFFIT. *J. Synchrotron Rad.* **2005**, *12*, 537.

42. Perdew, J. P.; Burke, K.; Ernzerhof, M., Generalized Gradient Approximation Made Simple. *Phys. Rev. Lett.* **1996**, *77*, 3865.

43. Kresse, G.; Furthmüller, J., Efficient Iterative Schemes for Ab Initio Total-Energy Calculations using a Plane-Wave Basis Set. *Phys. Rev. B* **1996**, *54*, 11169.

44. Blöchl, P. E., Projector Augmented-Wave Method. *Phys. Rev. B* **1994**, *50*, 17953.

45. Pidko, E. A.; van Santen, R. A.; Hensen, E. J. M., Multinuclear Gallium-Oxide Cations in High-Silica Zeolites. *Phys. Chem. Chem. Phys.* **2009**, *11*, 2893.

46. Samira, S.; Hanne, F.; Pablo, B.; Georg, M. P.; K., N. J.; Felix, S., Exploring Scaling Relations for Chemisorption Energies on Transition-Metal-Exchanged Zeolites ZSM-22 and ZSM-5. *ChemCatChem* **2016**, *8*, 767.

47. Lo Jacono, M.; Fierro, G.; Dragone, R.; Feng, X.; d'Itr, J.; Hall, W. K., Zeolite Chemistry of CuZSM-5 Revisited. *J. Phys. Chem. B* **1997**, *101*, 1979.

48. Fanning, P. E.; Vannice, M. A., A DRIFTS Study of Cu–ZSM-5 Prior to and during Its Use for N_2O Decomposition. *J. Catal.* **2002**, *207*, 166.

49. Da Costa, P.; Moden, B.; Meitzner, G. D.; Lee, D. K.; Iglesia, E., Spectroscopic and Chemical Characterization of Active and Inactive Cu Species in NO Decomposition Catalysts based on Cu-ZSM5. *Phys. Chem. Chem. Phys.* **2002**, *4*, 4590.

50. Jang, H. J.; Hall, W. K.; d'Itri, J. L., Redox Behavior of CuZSM-5 Catalysts: FTIR Investigations of Reactions of Adsorbed NO and CO. *J. Phys. Chem.* **1996**, *100*, 9416.

51. Kuroda, Y.; Yoshikawa, Y.; Konno, S.-i.; Hamano, H.; Maeda, H.; Kumashiro, R.; Nagao, M., Specific Feature of Copper Ion-Exchanged Mordenite for Dinitrogen Adsorption at Room Temperature. *J. Phys. Chem.* **1995**, *99*, 10621.

52. Nachtigallová, D.; Nachtigall, P.; Sauer, J., Coordination of Cu^+ and Cu^{2+} Ions in ZSM-5 in the Vicinity of Two Framework Al Atoms. *Phys. Chem. Chem. Phys.* **2001**, *3*, 1552.

53. Tromp, M.; van Bokhoven, J. A.; Arink, A. M.; Bitter, J. H.; van Koten, G.; Koningsberger, D. C., Cu K-Edge EXAFS Characterisation of Copper(I) Arenethiolate Complexes in both the Solid and Liquid State: Detection of Cu-Cu Coordination. *Chem. Eur. J.* **2002**, *8*, 5667.

54. Groothaert, M. H.; van Bokhoven, J. A.; Battiston, A. A.; Weckhuysen, B. M.; Schoonheydt, R. A., Bis(μ-oxo)dicopper in Cu-ZSM-5 and Its Role in the Decomposition of NO: A Combined in Situ XAFS, UV-Vis-Near-IR, and Kinetic Study. *J. Am. Chem. Soc.* **2003**, *125*, 7629.

55. Vanelderen, P.; Vancauwenbergh, J.; Tsai, M.-L.; Hadt, R. G.; Solomon, E. I.; Schoonheydt, R. A.; Sels, B. F., Spectroscopy and Redox Chemistry of Copper in Mordenite. *ChemPhysChem* **2014**, *15*, 91.

56. Delabie, A.; Pierloot, K.; Groothaert, M. H.; Weckhuysen, B. M.; Schoonheydt, R. A., The Siting of Cu(II) in Mordenite: a Theoretical Spectroscopic Study. *Phys. Chem. Chem. Phys.* **2002**, *4*, 134.

57. Li, H.; Paolucci, C.; Khurana, I.; Wilcox, Laura N.; Göltl, F.; Albarracin-Caballero, J. D.; Shih, A. J.; Ribeiro, F. H.; Gounder, R.; Schneider, W. F., Consequences of Exchange-Site Heterogeneity and Dynamics on the UV-Visible Spectrum of Cu-Exchanged SSZ-13. *Chem. Sci.* **2019**.

58. Kefirov, R.; Penkova, A.; Hadjiivanov, K.; Dzwigaj, S.; Che, M., Stabilization of Cu^{+} Ions in BEA Zeolite: Study by FTIR Spectroscopy of Adsorbed CO and TPR. *Microporous Mesoporous Mater.* **2008**, *116*, 180.

59. Schoonheydt, R. A., Transition Metal Ions in Zeolites: Siting and Energetics of Cu^{2+}. *Catal. Rev.* **1993**, *35*, 129.

60. Li, Y. J.; Hall, W. K., Catalytic Decomposition of Nitric-Oxide over Cu-Zeolites. *J. Catal.* **1991**, *129*, 202.

61. Hirschler, A. E., The Measurement of Catalyst Acidity Using Indicators Forming Stable Surface Carbonium Ions. *J. Catal.* **1963**, *2*, 428.

3. Effect of Extra-Framework Al on the Activity of Cu-Oxo Clusters in Mordenite for the Selective Oxidation of Methane to Methanol

Abstract

Cu-exchanged zeolites are of great interest due to their ability to selectively oxidize methane into methanol at moderate temperatures. Among them, Cu-exchanged mordenite (MOR) catalysts have shown the highest yield of CH_4 oxidation per Cu atom. The active sites of the Cu-MOR catalysts have been proposed to be trimeric and dimeric Cu-oxo clusters, which are able to oxidize one CH_4 molecule per three and two Cu atoms, respectively. However, in this study, we have prepared a new series of Cu-MOR catalysts, which are able to oxidize CH_4 with the stoichiometry of up to two CH_4 molecules per three Cu atoms. We used X-ray absorption spectroscopy, infrared spectroscopy and ^{27}Al magic angle-spinning nuclear magnetic resonance to demonstrate that such high reactivity of the Cu species is due to their interaction with extra-framework Al species located inside the 8 MR side pockets of MOR. Interaction of Cu species with extra-framework Al induces the change in the electronic structures or geometric confinement of the Cu-oxo clusters located at the pore mouth of 8 MR side pockets. We hypothesize that this affects accessibility and/or electronic structure of the Cu-oxo active sites, allowing reaction of two CH_4 molecules per cluster in one cycle.

3.1. Introduction

Due to increasing abundance of methane and its local geographic dispersion as well as importance of methanol as energy source and chemical feedstock,[1] direct conversion of methane to methanol is a desired pathway. However, it is challenging to selectively transform CH_4 into CH_3OH due to high symmetry and stability of CH_4, as well as lower C-H bond dissociation energy of methanol.

Methanotrophic bacteria are able to selectively oxidize methane into methanol utilizing enzymes called *methane monooxygenases* (MMOs) at Cu- and Fe-centers under ambient temperature and pressure using O_2.[2-4] Zeolites, possessing crystalline microporous structure and negatively-charged framework, are shown to be able to host small Cu- and Fe-oxo clusters, mimicking active centers in MMOs.[5-15] While Fe-exchanged zeolites need to be activated in N_2O,[5, 8] active centers for methane oxidation can be formed on Cu-zeolites using more economical O_2 as an oxidant.[9-10, 14, 16-20] Selective oxidation of methane to methanol on Cu-zeolites is typically carried out under three-stage reaction conditions: (i) thermal activation (450-600 °C) in the presence of strong oxidant for the formation of active Cu-oxo clusters, (ii) reaction of CH_4 on the activated catalyst, forming strongly adsorbed products and (iii) H_2O steam-assisted product desorption as methanol or liquid-phase extraction in polar solvents. Sufficient time of CH_4 reaction enables the complete coverage of the active Cu-oxo clusters. Under these conditions, CH_4 oxidation yield can be used to quantify the active species formed in the catalyst. Cu efficiency defined as [activated CH_4]/[Cu] provides information on the nuclearity of Cu-oxo clusters and possible formation of spectator species in Cu-zeolite catalysts.

While initial studies of Cu-zeolites gave modest Cu efficiencies, major improvements have been achieved especially on Cu-MOR catalysts.[10, 17, 21] Grundner et al. have proposed that the formation of single-site $[Cu_3(\mu\text{-}O)_3]^{2+}$ without the presence of spectator species results in the average Cu efficiency of 0.31.[10] Such Cu-oxo species have been shown to be located at the pore mouth of 8 membered-ring (MR) side pocket of MOR.[10] While Cu-exchange of H-type of MOR resulted in Cu efficiency of 0.33, attributed to the formation of the tricopper-oxo clusters, presence of co-cations such as Na^+, K^+, Mg^{2+} and Ca^{2+} was found to lead to lower Cu-efficiency.[22] More recently, Pappas et al. have reported a series of Cu-MOR catalysts where one Cu loading showed a Cu efficiency of 0.5, which is the highest value reported to date.[21] H-MOR

was used as a parent sample for Cu-exchange. They proposed that dimeric Cu species, such as mono(μ-oxo) dicopper species and/or trans-(μ-1,2-peroxo) dicopper clusters, are responsible for the selective CH_4 oxidation.[21]

Cu efficiencies of Cu-zeolites are believed to strongly depend framework Al, which is determined by zeolite synthesis conditions and Si/Al ratio.[14, 21, 23] Indeed, Dedecek et al. have shown that different Al distribution in zeolites leads to different reducibility of Cu^{2+} to Cu^{+} due to different locations and coordination environment around Cu^{2+}.[24-25] The degree of Cu loading can also affect the siting of Cu species in the framework, thus affecting reactivity of Cu and overall efficiency of the catalyst.[10, 13, 21, 23]

Structures and nature of Cu-oxo clusters supported on zeolites have been discussed in terms of interaction of exchanged Cu^{2+} with negatively charged framework Al (FAl) sites in zeolites. Effect of distribution of Lewis acid sites (LAS) or extra-framework Al (EFAl) in zeolites was not considered to date. However, recent study of Dyballa et al. has suggested a possible dependence of Cu efficiency of Cu-MOR catalysts on the concentration of octahedral EFAl,[26] although it is still unclear if EFAl species actually affect the nature of Cu-oxo clusters supported on zeolites. The effect of EFAl species on the activity of Brønsted acid sites (BAS) in zeolites for acid catalyzed hydrocarbon conversions has been widely reported.[27-29] Rate enhancement of catalytic reactions at BAS in the vicinity of EFAl is attributed to the stabilization of transition states by spatial constraints[27-28] or perturbation of BAS by EFAl.[29]

In this study, Cu-MOR catalysts are prepared via ion exchange of parent H-MOR samples with different EFAl distribution but similar Al siting in the framework. This subtle difference in the EFAl composition has doubled the Cu efficiency of Cu-MOR catalysts. Distribution of Cu and Al in MOR, as well as change in the coordination structures around Al upon Cu loading, are investigated by in-situ spectroscopies. Results point to the interaction of EFAl in the vicinity of the Cu-oxo clusters as origin for their high reactivity in some MOR samples. Location of EFAl species in the 8 MR side pockets of MOR is proposed to induce changes in electronic structures or geometric confinement of the Cu species.

3.2. Experimental Methods

3.2.1. Aqueous Ion-Exchange of H-MOR

Parent H-MOR samples were obtained by the calcination of commercial NH_4-MOR (Clariant, Si/Al = 10 and 11) in a flow of synthetic air (100 mL/min) at 550 °C for 6 h. For clarity, the H-MOR samples with Si/Al = 11 and 10 were named H-MOR-*A* and H-MOR-*B*, respectively.

Cu-exchange was performed under well-controlled conditions to exclude the formation of CuO and $Cu(OH)_2$ nanoparticles. A parent H-MOR sample was exchanged in aqueous solution of $Cu(CH_3COO)_2$ (0.001-0.01 M, 60 mL/$g_{zeolite}$) at ambient temperature for 20 h. The pH of the solution was adjusted to 5.7 by the addition of aqueous HNO_3 before the addition of H-MOR. After the exchange, the solid phase was collected by centrifugation, rinsed by re-dispersion in water (50 mL/$g_{zeolite}$) and subsequent centrifugation. The rinsing step was repeated four times, and the sample was dried at 100 °C for 24 h. NH_4-MOR-*B* sample was also used as a parent zeolite instead of H-MOR-*B*, and the resulting catalysts were named Cu(NH_4)-MOR-*B*-*x*, where *x* denotes the resulting Cu loading (µmol/g).

Na-exchange of H-MOR was performed in an aqueous solution of $NaNO_3$ (0.5 M, 100 mL/$g_{zeolite}$) at 60 °C for 24 h. Excess amount of Na^+ in aqueous phase ensures the total exchange of H^+ in H-MOR. Na back-exchange was performed under the same conditions on Cu-MOR catalysts after calcination in the flow of synthetic air (100 mL/min) at 500 °C for 2 h.

Co-exchange of Na-MOR was carried out in an aqueous solution of $Co(NO_3)_2$ (0.05 M, 150 mL/$g_{zeolite}$) at ambient temperature for 24 h, following the procedure reported by Dedecek et al.[30] Under these conditions, controlled exchange of Co^{2+} cations at paired Al sites are achieved.

Concentrations of framework Si and Al as well as exchanged cations were determined by atomic absorption spectroscopy (AAS) on a UNICAM 939 AA spectrometer after dissolution in boiling hydrofluoric acid.

3.2.2. Selective Oxidation of Methane to Methanol

CH_4 oxidation activity of Cu-MOR catalysts were measured in a stainless steel plug-flow reactor (4 mm inner diameter) using 50 mg of a catalyst (pressed and sieved into a particles size of 250-400 µm). The catalyst was first activated in the presence of O_2 (10-100% in He, 16 mL/min) at 500 °C for 1 h at a heating rate of 10 °C/min. After cooling down to 200 °C, the catalyst was purged in He (50 mL/min) for 30 min and CH_4 reaction was carried out in 100% CH_4 (16 mL/min) for 4 h. The catalyst was subsequently cooled down to 135 °C in He to perform H_2O steam-assisted product desorption in 10% H_2O/90% He (20 mL/min) for 1 h. The reaction products were detected and analyzed by online mass spectrometry. CH_3OH, $(CH_3)_2O$ and CO_2 were detected as the products, and signals of m/z 31, 44 and 46 were used for quantification, respectively. $(CH_3)_2O$ was regarded as a product that stems from condensation of two CH_3OH molecules, thus regarded as a methanol equivalent. The sum of all detected products was defined as total yield of CH_4 oxidation.

3.2.3. Infrared Spectroscopy

Samples were pressed into self-standing wafers of a density of ca. 10 mg/cm^2, and activated in-situ in vacuum (10^{-7} mbar) at 450 °C for 1 h at a heating rate of 10 °C/min. Infrared spectra with the adsorption of *n*-hexane were recorded on a Vertex 70 spectrometer (Bruker Optics) at a resolution of 4 cm^{-1}. After the thermal activation, measurements were performed at 30 °C upon adsorption of *n*-hexane (0.1-5 mbar). After reaching a target pressure of *n*-hexane, the sample was equilibrated for at least 15 min until no spectral change is observed. Infrared spectroscopy of adsorbed pyridine was carried out on a Nicolet 5700 FT-IR spectrometer (Thermo Scientific) with a resolution of 4 cm^{-1}. Following the thermal activation of the sample, adsorption of pyridine was performed at 150 °C at 0.1 mbar for 1 h and subsequently evacuated for 30 min to desorb any physisorbed pyridine. Measurements were performed before and after adsorption of pyridine at 150 °C.

3.2.4. Nuclear Magnetic Resonance

^{27}Al magic-angle spinning (MAS) nuclear magnetic resonance (NMR) spectra were recorded on Bruker Avance 500 Ultrashield NMR spectrometer with a magnetic field of 11.75 T, corresponding to the Larmor frequency of 130.3 MHz. Samples were hydrated in 42 mbar H_2O for at least 48 h before packed into ZrO_2 rotors, and the rotor was spun at 12 kHz. For 1D single-pulse experiments, 2400 scans were accumulated with the pulse width of 1.16 µs and the relaxation delay of 2 s. ^{27}Al 3QMAS NMR spectra were acquired using *z*-filtered split-t_1 pulse sequence.[31-32] 1344 scans were measured with the relaxation delay of 0.25 s. The optimized pulse widths of 3Q excitation pulse p_1 and 3Q–1Q conversion pulse p_2 were 9 µs and 5.5 µs, respectively. The pulse width of the following 90 degree selective pulses p_3 was 57.3 µs, and *z*-filter delay time was 20 µs. The acquired spectra were processed with Bruker Topspin.

The ultrahigh field ^{27}Al MAS NMR experiments were performed on a Varian-Agilent Inova 63 mm wide-bore 900 MHz NMR spectrometer. The main magnetic field was 21.1 T, and the corresponding ^{27}Al Larmor frequency was 234.56 MHz. Experiments were performed using a 3.2 mm pencil type MAS probe with a MAS rate of 20 kHz. A single pulse sequence with a pulse length of 2.0 µs was selected for acquiring each spectrum with a recycle time of 1 s and total accumulation of 5000 scans. The spectra were referenced to 1.5 M $Al(NO_3)_3$ in H_2O (0 ppm) using the center of the octahedral peak of solid γ-Al_2O_3 (at 13.8 ppm) as a secondary reference.

3.2.5. Al K-edge X-ray Absorption Spectroscopy

X-ray absorption spectra at Al K-edge (1559.6 eV) were measured on PHOENIX II, an elliptical undulator beamline at the Swiss Light Source of Paul-Scherrer Institut (Villigen, Switzerland). The electron energy was 2.4 GeV with a beam current of 400 mA. The PHOENIX II end station is located at the exit port of the X-Treme beamline. Photons were provided from an elliptical undulator and monochromatic light was generated using a planer grating monochromator. Energy calibration was performed by setting an inflection point of a measured spectrum of Al-foil to 1559.6 eV.

Zeolite samples were pressed into self-standing pellets with ca. 0.5 mm thickness and placed into a pellet holder made from Cu, which can hold up to 8 pellets. The pellet holder was then mounted on a Cu heating block in a vacuum chamber. The samples

were first activated in 1% O_2 in Ar at 800 mbar at 450 °C for 1 h at a heating rate of 10 °C/min, and then cooled down to 200 °C. After evacuation of O_2 at 200 °C, the chamber was filled with 10% CH_4/90% He up to 800 mbar and reacted for 1 h. Measurements were performed in vacuum (10^{-4} mbar) before thermal activation and after each treatment.

Incoming photon I_0 was measured as total electron yield signal taken from a 0.5 μm thin polyester foil, which was coated with 50 nm of Ni. This I_0 detector was held about 1 m upstream of the sample in the beamline vacuum (ca. 10^{-6} mbar). The X-ray fluorescence of the samples was detected using a single-element Ketec Si-drift diode detector. XANES and EXAFS data processing was performed on Athena software from the Demeter package.

3.2.6. High Energy Resolution Fluorescence Detected X-ray Absorption Near Edge Structure

Measurements of High Energy Resolution Fluorescence Detected (HERFD) X-ray Absorption Near Edge Structure (XANES) at Cu K-edge (8979 eV) were performed at beamline P64 at PETRA III of DESY (Hamburg, Germany). The electron energy was 6 GeV with a beam current of 100 mA. Around 10 mg of the sample was sandwiched between quartz wools and packed in a quartz capillary reactor (1 mm outer diameter, 0.02 mm wall thickness), and placed on top of a gas-blower for controlled heating. Double-crystal Si(111) monochromator was used to control the incident photon energy and von Hamos-type x-ray emission spectrometer[33-34] with eight Si(444) mirrors was used to record the spectra. Energy calibration was performed by recording elastic scattering at 8015, 8027, 8047, 8060 eV. Thermal activation of the samples was performed in a flow of 10% O_2 in He at 5 mL/min at 450 °C for 1 h with the 10 °C/min heating rate. After the thermal activation of the sample, the sample was cooled down to 200 °C, and purged in He for 30 min, followed by reaction in 10% CH_4 in He for 2 h at a flow rate of 5 mL/min. The gas flows over the samples was controlled by mass-flow controllers. A moisture/oxygen trap and a moisture trap were employed on He and CH_4, and O_2 gases respectively to avoid unwanted contamination of the gas stream on the catalyst.

3.2.7. In-situ Ultraviolet-Visible spectroscopy

Ultraviolet–visible (UV-Vis) spectra of Cu-MOR samples were recorded in-situs on an Avaspec 2048 spectrometer (Avantes) with a light source AvaLight-DH-S-BAL (Avantes) in the diffuse reflectance mode. The samples were pressed and sieved into a size of 250-400 µm and placed in a quartz flow reactor (6 mm inner diameter) with square optical-grade quartz windows, sandwiched between quartz wool. The reactor was placed horizontally in a lab-made heating chamber with an 8-mm diameter hole at the bottom, where a high-temperature optical fiber (Avantes FCR-7UV400 2ME-HTX) can be vertically directed to the reactor. The sample was first activated in pure O_2 flow (16 mL/min) at 450 °C for 1 h with a heating rate of 10 °C/min. After the thermal activation step, the catalyst was cooled down to 200 °C and purged with He for 30 min, and then CH_4 reaction was performed for 30 min in pure CH_4 (16 mL/min). Spectra were measured periodically throughout the experimental procedure (every 5 min during thermal activation, every minute during CH_4 reaction). The spectra are presented as Kubelka-Munk function, defined as $F(R) = (1-R)^2/2R$, where $R = R_s/R_r$. R_s and R_r refer to the signal intensity of the sample and reference, respectively. Parent H-MOR sample was used as reference.

3.3. Results and Discussion

3.3.1. Activity of Cu-MOR Catalysts

In order to examine if the Cu-exchange was successful without undesired precipitation of CuO or $Cu(OH)_2$ nanoparticles, Na^+ back-exchange of Cu-MOR samples was performed. Prior to Na^+ back-exchange, Cu-MOR samples were calcined in the presence of O_2 at 500 °C for 2 h to re-distribute the exchanged Cu cations and to form active Cu-oxo clusters.[16] While cationic Cu and Cu clusters can be re-hydrolyzed and back-exchanged by Na^+, CuO and $Cu(OH)_2$ clusters precipitated in MOR pores during Cu-exchange cannot be back-exchanged by Na^+.[22] For all the samples reported in this study, it was found out that more than 90% of the introduced Cu were back-exchanged by Na^+ (Table A 3-1 in appendix), indicating that most of the introduced Cu are present as cationic species.

Activities of Cu-MOR catalysts in CH_4 oxidation were measured in the typical three-stage reaction conditions, as described in the experimental section. Thermal activation of a catalyst was performed at 500 °C for 1 h in the presence of O_2 to complete the formation of active Cu-oxo clusters.[16] The long reaction time of CH_4 ensures the complete reaction of the formed Cu-oxo clusters with CH_4, which enables the titration of all the active site.[10]

Activities of the catalysts in CH_4 oxidation and selectivities to methanol are presented in Figure 3-1 (a), and Cu efficiency of each catalyst is plotted in Figure 3-1 (b). Assuming the absence of spectator species, CH_4 molecule activated by a single-site Cu dimer and trimer results in the Cu efficiency of 0.33 and 0.5, respectively. It has been previously shown that Cu-MOR catalysts prepared via aqueous ion-exchange under well-controlled conditions show a CH_4/Cu of ca. 0.3.[10, 17, 21, 35] Indeed, a series of Cu-MOR-*A* catalysts, prepared under the same ion-exchange conditions from a H-type of MOR (H-MOR-*A*),[10] show an average Cu efficiency of 0.33 as represented by the slope of the linear regression (Figure 3-1 (a)).

We have now prepared another series of Cu-MOR catalysts (Cu-MOR-*B*) under the same conditions, using H-MOR-*B* as a parent sample. Cu-MOR-*B* catalysts show linear increase of CH_4 oxidation yield up to 283 µmol/g Cu loading, while it levels off at higher Cu loadings. Surprisingly, average Cu efficiency of 0.58 was obtained at Cu loadings below 283 µmol/g, and the maximum Cu efficiency of 0.63 was observed at

156 µmol/g Cu loading. These values are larger than any reported values for Cu-zeolite catalysts on the selective oxidation of methane to methanol. Moreover, this stoichiometry is larger than expected values for dimers such as mono(µ-oxo) dicopper or trans-(µ-1,2-peroxo) dicopper species (0.5) or trimers such as $[Cu_3(\mu\text{-}O)_3]^{2+}$ clusters (0.33), assuming that one CH_4 molecule is activated by one active Cu cluster.

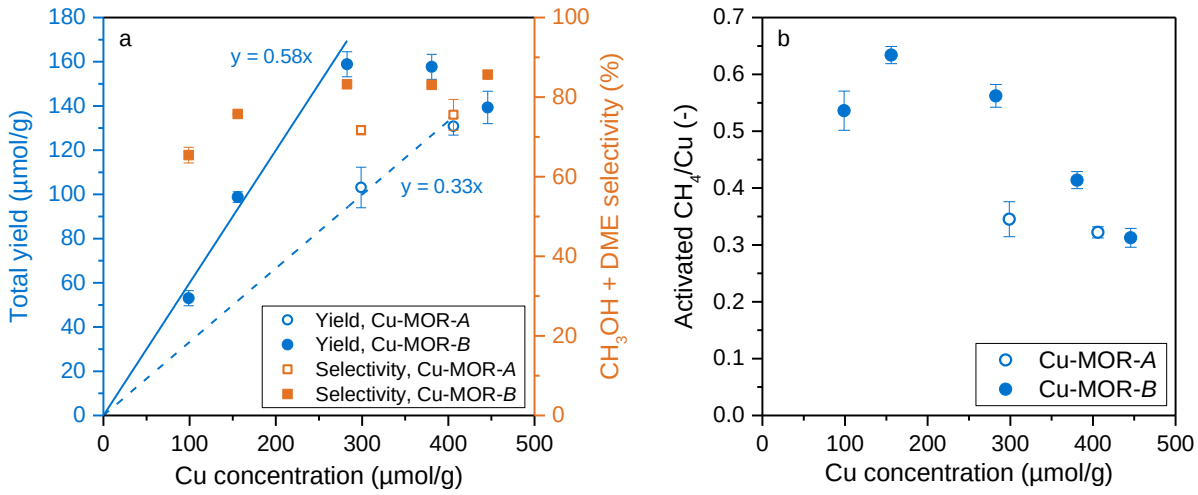

Figure 3-1. Yield of CH_4 oxidation and selectivity to CH_3OH and $(CH_3)_2O$ on the Cu-MOR catalysts prepared from different parent H-MOR samples with different Cu loading (a) and their Cu efficiency (b). Activity tests were repeated 3 times on each catalyst and averaged values are reported.

While flattening of CH_4 oxidation yield at high Cu loadings was also observed on Cu-MOR catalysts by Grundner *et al*., it was attributed to the formation of unexchanged CuO or $Cu(OH)_2$ nanoparticles, which do not take part in the CH_4 oxidation reaction.[10] On the other hand, Na back-exchange of Cu-MOR-*B* catalysts has shown that 90% of the Cu are exchanged as cationic species. Therefore, the flattening of CH_4 oxidation yield on these catalysts can be attributed to the formation of cationic spectator species which does not take part in the CH_4 oxidation or the change in the nature of Cu-oxo clusters, such as transformation of active Cu-oxo clusters to those with higher nuclearity of Cu.

Having observed unusually high Cu efficiencies of Cu-MOR-*B* catalysts in the selective oxidation of CH_4, it is important to investigate the distribution of Al and Cu atoms in the

Cu-MOR catalysts in order to understand the factors that are responsible for the formation of high activity catalysts.

3.3.2. Distribution of Framework and Extra-Framework Al in Parent MOR Samples

It is well known that Al distribution in zeolites strongly affects the locations and the nature of exchanged cations.[30, 36] Therefore, distributions of FAl sites in the parent H-MOR samples used for Cu ion exchanged were investigated.

Al sites that are separated by one or two SiO_4 tetrahedra (so called Al pairs) can be probed by Co^{2+}-exchange in aqueous phase under controlled conditions[30, 37] Formation of multinuclear Cu-oxo clusters, including dimeric and trimeric Cu species, is proposed to occur on such paired Al sites.[10, 21, 23] The population of the paired FAl sites were determined to be 63% and 60% of the total Al on parent H-MOR-*A* and H-MOR-*B* samples, respectively.

Table 3-1. Compositions and FAl distribution in the parent H-MOR samples determined by IR spectroscopy.

Sample	Si/Al (-)	$FAl_{main\ channel}$[a] (µmol/g)	$FAl_{SP\ bottom}$[b] (µmol/g)	$FAl_{SP\ pore\ mouth}$[b] (µmol/g)	Total FAl[c] (µmol/g)
H-MOR-*A*	10.7	400	251	439	1090
H-MOR-*B*	9.6	419	220	486	1130

[a]Concentration of FAl located in 12 MR main channel was determined by deconvolution of the IR band at 3600 cm^{-1}. [b]Concentrations of FAl located at the pore mouth and the bottom of 8 MR side pocket were determined by combination of IR spectroscopy with pyridine and *n*-hexane adsorption. [c]Total FAl concentration was determined by Na-exchange of a H-MOR sample.

Locations of FAl sites, which function as BAS, in the parent H-MOR samples were investigated by IR spectroscopy with the aid of probe molecules, such as *n*-hexane and pyridine. BAS located in 12 MR main channel, giving a band at 3612 cm^{-1}, are accessible to *n*-hexane molecules, while BAS located inside 8 MR side pocket, showing a band at 3590 cm^{-1}, remain unperturbed (Figure A 3-1 in Appendix).[38] On the other hand, pyridine can interact with the sites located in 12 MR main channel and at

the pore mouth of 8 MR side pockets.[39] As seen in Table 3-1, significant difference in the distribution of FAl is not observed in the H-MOR samples.

In the next step, distribution of EFAl species, which function as LAS in parent H-MOR samples, was studied. Dyballa *et al.* has suggested that EFAl in MOR might affect the CH_4 oxidation activity of Cu-MOR catalysts.[26] Concentrations of LAS located in 12 MR main channel and at the pore mouth of 8 MR side pockets in H-MOR-*A* and H-MOR-*B* samples are analyzed by IR spectroscopy with pyridine adsorption, while significant difference was not observed (Table 3-2, Figure A 3-2 in Appendix). We assume that every Al atom in the H-MOR samples is associated to a BAS or to a LAS. Then, by combining LAS concentration in H-MOR samples accessible by pyridine with the total Al concentration and BAS distribution, it is possible to estimate the distribution of LAS in the parent H-MOR samples. The concentration of LAS in 12 MR main channel and at the pore mouth of 8 MR side pocket, which is accessible by pyridine, is similar between H-MOR-*A* and H-MOR-*B*. However, significant difference is observed in the concentration of LAS located at the bottom of 8 MR side pocket, which is inaccessible to bulky pyridine molecules. While H-MOR-*A* possesses only 90 µmol/g of LAS inside 8 MR side pocket, H-MOR-*B* has much larger amount of LAS (260 µmol/g) inside the 8 MR side pocket.

Table 3-2. Comparison of Al distribution in the parent H-MOR samples.

	H-MOR-*A*	H-MOR-*B*
Total Al (µmol/g)[a]	1440	1620
Total FAl (µmol/g)[b]	1090	1130
Total EFAl (µmol/g)[c]	350	490
$EFAl_{main\ channel\ +\ SP\ pore\ mouth}$ (µmol/g)[d]	260	230
$EFAl_{SP\ bottom}$ (µmol/g)[e]	90	260

[a]Total Al concentration was determined by elemental analysis (AAS). [b]Total FAl concentration was determined by Na-exchange of a H-MOR sample. [c]Total EFAl concentration was determined as [Total Al] - [Total FAl]. [d]Concentration of EFAl located at 12 MR main channel and the pore mouth of 8 MR side pocket (SP) was analyzed by IR spectroscopy with pyridine adsorption. [e]Concentration of EFAl located at the bottom of 8 MR side pocket (SP) was determined as [Total EFAl] – [$EFAl_{main\ channel\ +\ SP\ pore\ mouth}$].

Coordination of Al in H-MOR samples was investigated by ^{27}Al MAS NMR spectroscopy at the high magnetic field of up to 19.9 T (850 MHz spectrometer). While it is known that some Al species cannot be detected by NMR, it has been shown that such NMR-silent Al species can be detected by high magnetic field-NMR due to restrained second-order quadrupole interactions and enhanced resoution.[40-41] Figure 3-2 shows the ^{27}Al MAS NMR spectra of the parent H-MOR samples, recorded on an 850 MHz instrument. Both H-MOR-*A* and H-MOR-*B* samples show two sharp peaks at ca. 58 and 0 ppm, corresponding to tetrahedral and octahedral Al species, respectively. While tetrahedral Al is typically regarded as framework Al species, octahedral Al is attributed to EFAl which creates Lewis acidity in zeolites.[26] Fractions of octahedral Al in both H-MOR-*A* and H-MOR-*B* samples are ca. 20% of the total Al population. However, in both samples, concentration of octahedral Al species determined by ^{27}Al MAS NMR is smaller compared to the concentration of total LAS (Table 3-2), suggesting that some LAS have tetrahedral coordination structures. The presence of tetrahedrally coordinated EFAl in zeolites has been also reported before.[42]

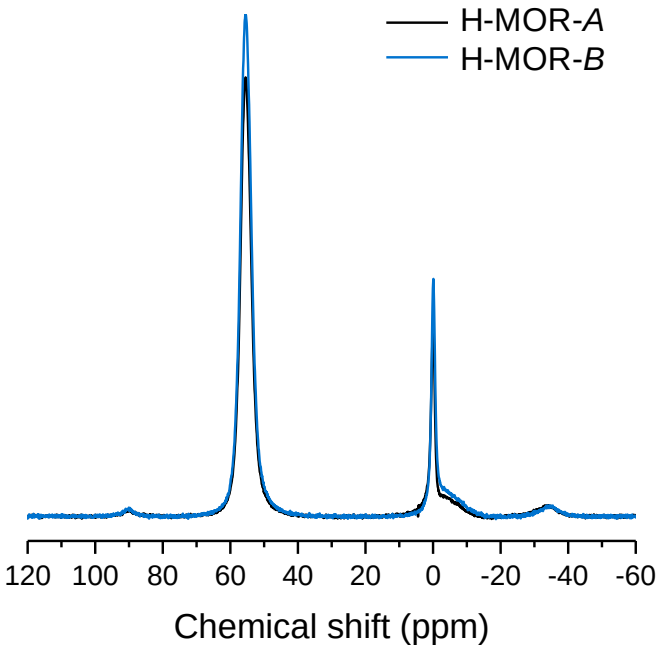

Figure 3-2. Weight-normalized ^{27}Al MAS NMR spectra of the parent H-MOR samples (850 MHz instrument).

Table 3-3. Concentrations of Al in tetrahedral and octahedral coordination structures determined by ^{27}Al MAS NMR.

	H-MOR-*A*	H-MOR-*B*
Total Al_{EA} (μmol/g)[a]	1440	1620
$Al_{tetrahedral}$ (μmol/g)[b]	1150	1290
$Al_{octahedral}$ (μmol/g)[b]	290	330

[a]Concentration of total Al_{EA} was determined by elemental analysis (EA). [b]Areas of the peaks at 58 ppm and 0 ppm of weight-normalized NMR spectra were analyzed for the determination of the concentrations of tetrahedral and octahedral Al, respectively.

^{27}Al 3QMAS NMR measurements were performed on the parent H-MOR samples to study the coordination environment around Al more in detail. Two types of line broadening effects can be distinguished by 3QMAS NMR experiments.[28-29] One is the horizontal broadening (to the direction of F2) due to quadrupolar coupling to local electric field gradients caused by the nearby cationic species or distortion in the coordination geometry. On the other hand, vertical broadening (to the direction of F1) is caused by chemical heterogeneity. It is known that second-order quadrupolar interaction of Al with local electric field gradients can lead to line broadening of ^{27}Al MAS NMR spectra beyond detection.[29] Both H-MOR-*A* and H-MOR-*B* samples show similar spectra with the peaks of tetrahedrally and octahedrally coordinated Al species (Figure 3-3). The peaks of the both samples are vertically elongated, indicating the high chemical heterogeneity within the Al species. These observations are in line with our hypothesis that a part of LAS is present as tetrahedrally coordinated species. Line broadening towards F2 direction, on the other hand, is relatively small compared to the line broadening to F1 direction, indicating that the coordination structures around Al are not strongly distorted.

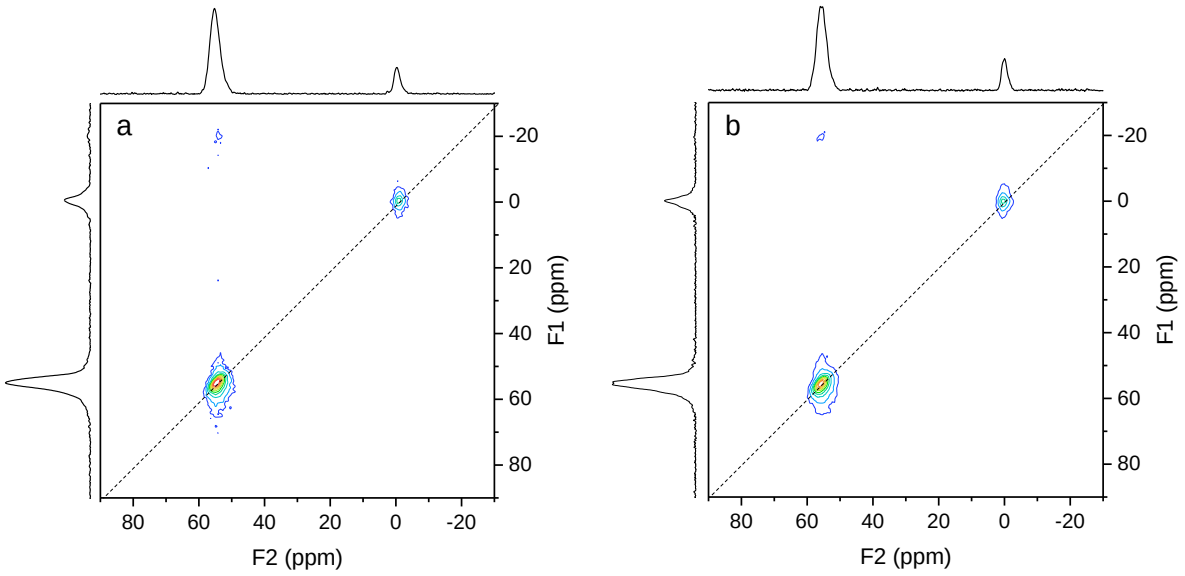

Figure 3-3. 2D ^{27}Al 3QMAS NMR spectra of H-MOR-*A* (a) and H-MOR-*B* (b) samples and their positive projections on the vertical and horizontal frequency axes. F1 and F2. The spectra were measured on the 500 MHz instrument.

3.3.3. Distribution of Exchanged Cu Cations

Distribution of the exchanged Cu^{2+} in H-MOR was investigated by looking at the consumption of the band attributed to BAS by IR spectroscopy. As described in the former section, the band at ca. 3600 cm^{-1}, attributed to BAS, was deconvoluted into two bands located at 3612 cm^{-1} and 3590 cm^{-1}, corresponding to BAS in 12 MR main channel and 8 MR side pocket, respectively.[38] It is known that ion-exchange in MOR occurs preferentially in the more constrained 8 MR side pockets.[43] In the case of Cu-MOR-*B* catalysts, formation of $[Cu_3(\mu\text{-}O)_3]^{2+}$ in MOR was also observed to occur selectively at the pore mouth of 8 MR side pockets, and the consumption of 2 BAS per 3 Cu atoms was observed.[10] Given the similarity in the distribution of BAS in H-MOR-*A* and H-MOR-*B*, we expect that the distribution of exchanged Cu^{2+} is also similar. Indeed, consumption of BAS upon Cu-exchange in H-MOR-*B* also shows that Cu is preferably exchanged at the 8 MR side pocket of MOR, while BAS located at 12 MR main channel stay unoccupied (Figure 3-4). However, the slope of 0.89 for the total consumption of BAS indicates that approximately one BAS is consumed by exchanging a Cu cation. These results suggest different coordination structures around Cu cation in Cu-MOR-*A* and Cu-MOR-*B* catalysts.

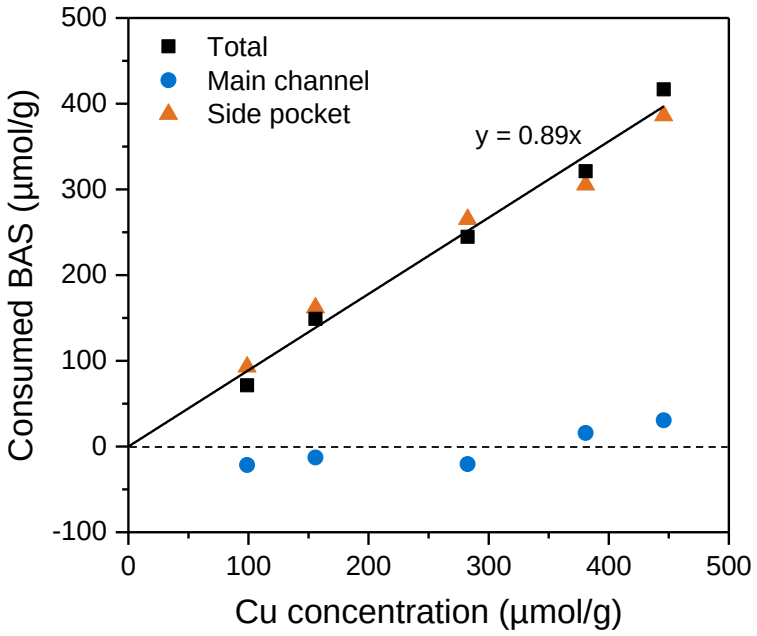

Figure 3-4. Consumption of BAS at 12 MR main channel and 8 MR side pockets with different Cu loading in Cu-MOR-*B* catalysts.

3.3.4. Interaction of EFAl and Cu-Oxo Active Species

Dyballa et al. have observed that the population of octahedral Al decreases upon Cu-exchange of MOR, and it was attributed to realumination of MOR framework in mildly acidic solution.[26] Formation of octahedral EFAl species was observed upon reaction cycles of selective oxidation of methane to methanol. Although it was mentioned that the fraction of octahedral EFAl might affect the yield of CH_4 oxidation on Cu-MOR catalysts,[26] how EFAl governs the properties of exchanged Cu^{2+} species has not been yet studied in detail. Since the Cu-exchange of MOR samples are performed in mildly acidic solution of $Cu(CH_3COO)_2$ (pH 5.7), H-MOR-*B* sample was treated in an aqueous solution of CH_3COOH to study the effect of ion exchange on the Al sites of the zeolite. Figure 3-5 shows weight-normalized ^{27}Al MAS NMR spectra of H-MOR-*B* before and after the treatment in the aqueous solution of CH_3COOH. Two prominent peaks are observed at 55 ppm and 0 ppm, attributed to Al in tetrahedral and octahedral coordination structure, respectively. Identical spectra of H-MOR-*B* before and after the acid treatment indicate that Al sites in MOR are not affected by the Cu-exchange, thus realumination of MOR framework can be excluded under the tested conditions.

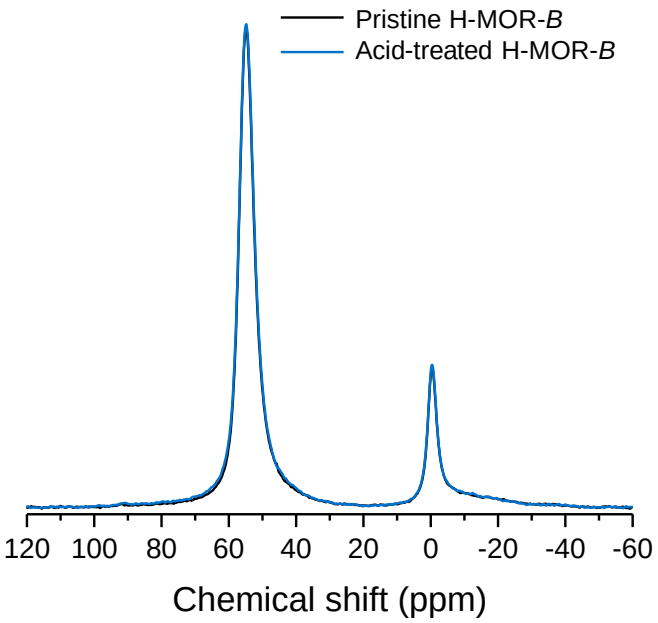

Figure 3-5. ^{27}Al MAS NMR spectra (measured on the 500 MHz instrument) of H-MOR-*B* before and after mildly acidic treatment in an aqueous solution of CH_3COOH at pH 5.7.

Figure 3-6 (a) shows ^{27}Al MAS NMR spectra of Cu-MOR-*B* catalysts at various Cu loadings. Height of the peak at 55 ppm, assigned to tetrahedral Al, decreased with increasing Cu loading, while simultaneous line broadening was observed due to the interaction of paramagnetic Cu^{2+} with framework Al sites. Peak area of tetrahedral Al was constant at different Cu loadings (Figure 3-6 (b)), even though paramagnetic Cu^{2+} cations are exchanged at tetrahedral framework Al sites as observed by IR spectroscopy (Figure 3-4). This is probably due to the weak electron dipole-nuclei dipole interaction between Cu and Al in fully hydrated catalysts.[26] On the other hand, the peak intensity of octahedral Al at 0 ppm linearly diminished with increasing Cu loading. This is either due to the strong interaction of Cu^{2+} with octahedral Al species making some Al "NMR-silent", or due to the actual change in the coordination structure around Al by the introduction of Cu^{2+}. As a consequence, total Al concentration calculated from the total peak area of ^{27}Al MAS NMR spectra linearly decreased upon increasing Cu concentration, while Al concentration determined by elemental analysis was constant (Table A 3-1 in Appendix). These results suggest that strong interaction of EFAl species with paramagnetic Cu^{2+} is present, leading to the formation of NMR-silent Al species.[26, 44]

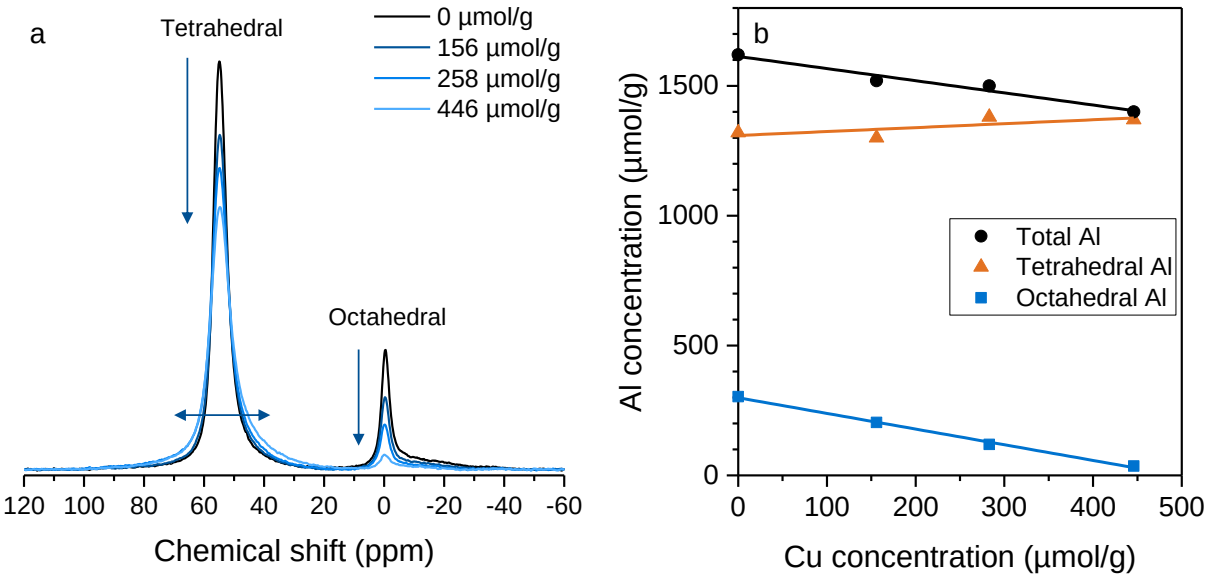

Figure 3-6. ^{27}Al MAS NMR spectra of Cu-MOR-*B* catalysts with different Cu loading measured on the 500 MHz instrument (a) and concentrations of Al in tetrahedral and octahedral coordination structure derived from the peak areas of ^{27}Al MAS NMR spectra.

In order to obtain further information on the coordination structure around Al, Al K-edge XAS study was carried out. Vjunov et al. have shown that the intensity of the feature at 1568 eV in Al K-edge XANES provides quantitative information of octahedral Al species.[45] Unlike ^{27}Al MAS NMR spectroscopy, Al K-edge XAS is not affected by the paramagnetic effect of Cu^{2+}, thus real structural information is obtained. Figure 3-7 (a) shows Al K-edge XANES of Cu-MOR-*B* catalysts with different Cu loading. A small pre-edge peak at 1560.5 eV seen in the spectrum of dehydrated H-MOR-*B* is due to the delocalization of H^+ at negatively charged framework Al sites due to the loss of ligated H_2O molecules.[45] Decrement in the intensity of the feature at ca. 1568 eV, attributed to octahedral Al, is observed with increasing Cu loading. Linear combination fitting (LCF) analysis of this feature of Cu-MOR-*B* catalysts was performed to determine the concentration of Al in tetrahedral and octahedral coordination structures. The spectrum of H-MOR-*B* dehydrated by thermal treatment at 450 °C in the presence of O_2 for 1 h was used as a reference for 0% octahedral Al, since it is known that octahedral Al changes its coordination structure to tetrahedral upon losing hydrating H_2O molecules by thermal treatment.[45-46] H-MOR-*B* in hydrated state was used as a reference for octahedral Al content of 20.4%, as determined by ^{27}Al MAS NMR at high magnetic field (Table 3-3). Figure 3-7 (b) exhibits the concentrations of Al in tetrahedral and octahedral coordination structures. It can be seen that the concentration of

octahedral Al linearly decreases with increasing Cu concentration, as also observed by ^{27}Al MAS NMR (Figure 3-6). Consequently, the concentration of tetrahedral Al shows linear increase according to the Cu concentration. These results indicate that the linear decrease with Cu loading of the concentration of octahedral Al seen by ^{27}Al MAS NMR is due to a change in coordination structure around Al from octahedral to tetrahedral. Octahedral Al species are transformed into tetrahedral upon introduction of Cu^{2+} or they become NMR-silent due to strong interaction with paramagnetic Cu^{2+}. In both cases, results indicate an important interaction between Cu and EFAl at least in the hydrated state of the zeolite. It should be noted that Cu exchanged on BAS would be surrounded by H_2O molecules in the hydrated state of Cu-MOR sample and thus the paramagnetic shield of Al NMR signal of framework Al might have been attenuated by those H_2O molecules.

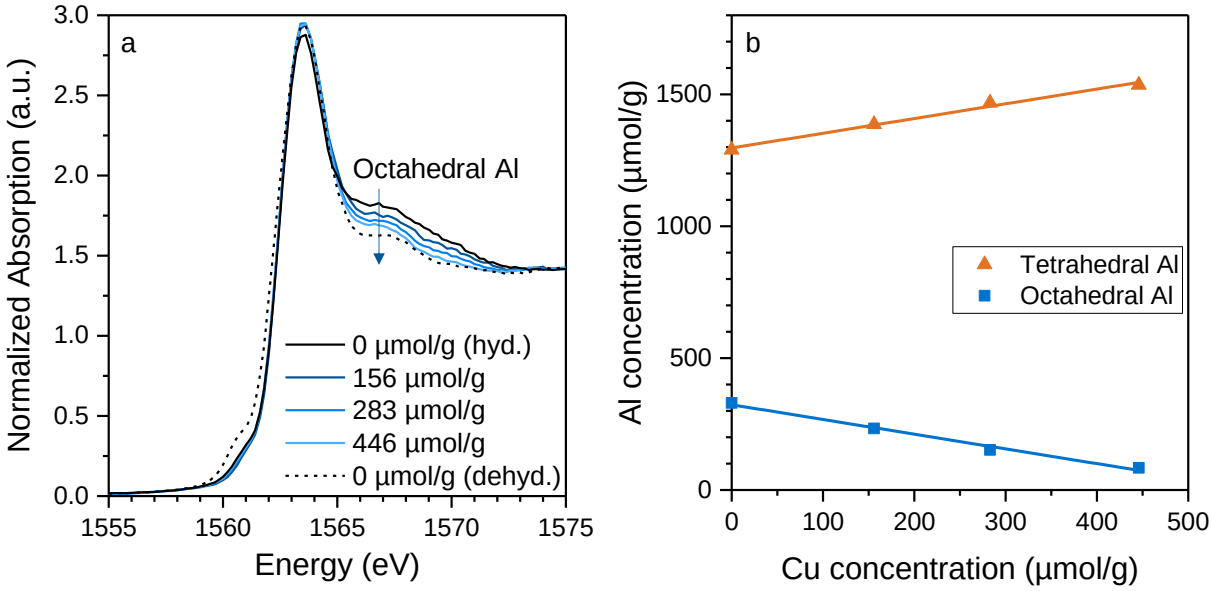

Figure 3-7. Al K-edge XANES of Cu-MOR-*B* catalysts with different Cu loading plotted with H-MOR-*B* in hydrated (hyd.) and dehydrated (dehyd.) state (a). Measurements were performed in hydrated states unless stated “dry”. Concentrations of tetrahedral and octahedral Al obtained by LCF (b).

We have demonstrated that extra-framework octahedral Al species have impact on the nature of Cu-oxo clusters formed in Cu-MOR for the selective oxidation of methane to methanol. In order to further confirm this effect, Cu-exchange of pristine NH_4-MOR-*B* sample was performed. Since H-MOR-*B* is obtained by the calcination of NH_4-MOR-*B*,

it is expected that the distributions of framework Al sites in these two samples are very similar. On the other hand,NH_4-MOR-*B* sample was found to be free of octahedral EFAl species, as indicated by the absence of the peak at 0 ppm in its ^{27}Al MAS NMR spectrum (Figure 3-8). Therefore, all the octahedral EFAl species observed in Figure 3-5 and characterized in this section are formed upon calcination of the parent NH_4-MOR to decompose NH_4^+ and produce the H- form. The total peak areas of ^{27}Al MAS NMR spectra of the NH_4- and H-MOR-*B* samples were identical, therefore the formation of NMR-invisible Al species upon calcination treatment can be excluded.

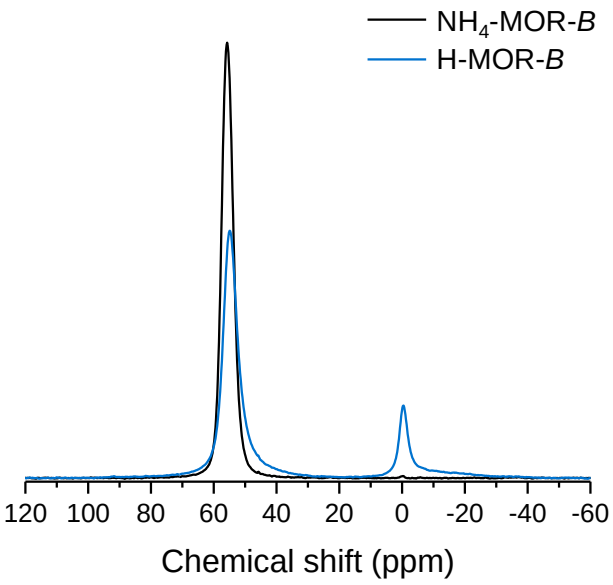

Figure 3-8. Comparison of weight-normalized ^{27}Al MAS NMR spectra of NH_4-MOR-*B* and H-MOR-*B*.

As shown in Figure 3-9, Cu(NH_4)-MOR-*B* catalysts, prepared by Cu-exchange of NH_4-form of MOR, show much lower Cu efficiency of 0.25 compared to Cu-MOR-*B* catalysts, corresponding to ca. 1 CH_4 molecule activated by 4 Cu atoms. This is only half of the activity of Cu-MOR-*B* catalysts, which show the average Cu efficiency of 0.58 (corresponding to 1 CH_4 molecule activated by approximately 2 Cu atoms) at Cu loadings up to 283 µmol/g. Approximately 90% of the Cu in the Cu(NH_4)-MOR-*B* samples were back-exchanged by Na^+, indicating that majority of the Cu species in the catalysts are cationic. Although it has been reported that the presence of co-cations decreases the Cu efficiency of Cu-MOR catalysts,[22] since NH_4^+ cations are

decomposed to form H^+ during activation of the catalyst at 500 °C in the presence of O_2, effect of the different cations in the catalysts can be excluded. Extra-framework metal cations are known to have stabilization effect against dealumination.[47-49] Therefore, it is not surprising that Cu^{2+} cations exchanged in NH_4-form of MOR have similar stabilization effect on the MOR framework upon calcination treatment. Indeed, larger concentration of tetrahedral Al in Cu(NH_4)-MOR-*B* catalyst with 189 µmol/g Cu loading compared to H-MOR-*B* sample suggests that dealumination of MOR framework is suppressed by the presence of Cu^{2+} (Table 3-4). Moreover, the total concentration of Al in calcined Cu(NH_4)-MOR-*B* (189 µmol/g Cu) determined by ^{27}Al MAS NMR spectroscopy was identical to that in H-MOR-*B* (Table 3-4), indicating the absence of NMR-silent Al species. Taking into account the formation of NMR-silent Al species upon interaction of paramagnetic Cu^{2+} and extra-framework octahedral Al and weak electron dipolar-nuclei dipolar interaction between Cu and Al,[26] Cu^{2+} cations in the calcined Cu(NH_4)-MOR-*B* catalyst seem to be solely interacting with framework tetrahedral Al sites.

It is also possible that Cu^{2+} exchanges in NH_4-MOR in different Al framework positions than in H-MOR, due to a competition of available cations for sites.[22] On the other hand, it is known that H_2O steam treatment during product desorption as well as thermal activation at high temperatures facilitate the mobilization of Cu cations in micropores of zeolites.[14, 16, 50-51] Thus, after calcination of Cu-NH_4-MOR, ammonia cations are removed and a Cu-H-MOR is generated and, in principle, after one cycle the oxidative activation of the wet spent catalyst should allow for organization of the Cu clusters in a similar way to a Cu-H-MOR reference material. *Ab initio* thermodynamic study has shown that $[Cu_3(\mu\text{-}O)_3]^{2+}$ species is the most thermodynamically stable species under the used reaction conditions.[10] Therefore, it is expected that, in absence of any co-cations after calcination of Cu-NH_4-MOR to form Cu-H-MOR, re-distribution of Cu cations in micropores of MOR during steam treatment and reactivation would facilitate the formation of the tricopper-oxo clusters. In that case, a second catalytic cycle on Cu-NH_4-MOR should restore the stoichiometry of 1 CH_4 molecule activated by 3 Cu atoms.[16, 52] However, two consecutive reaction cycles on the Cu(NH_4)-MOR-*B* catalyst (232 µmol/g Cu) resulted in constant yield of CH_4 oxidation and methanol selectivity (Figure 3-9 (b)), suggesting that the structure of the Cu-oxo clusters formed in both reaction cycles are identical. These results support the hypothesis that it is a strong

effect of EFAl species in MOR on the distribution or structure of Cu cations what determines the differences in activity observed for the MOR-*B* series.

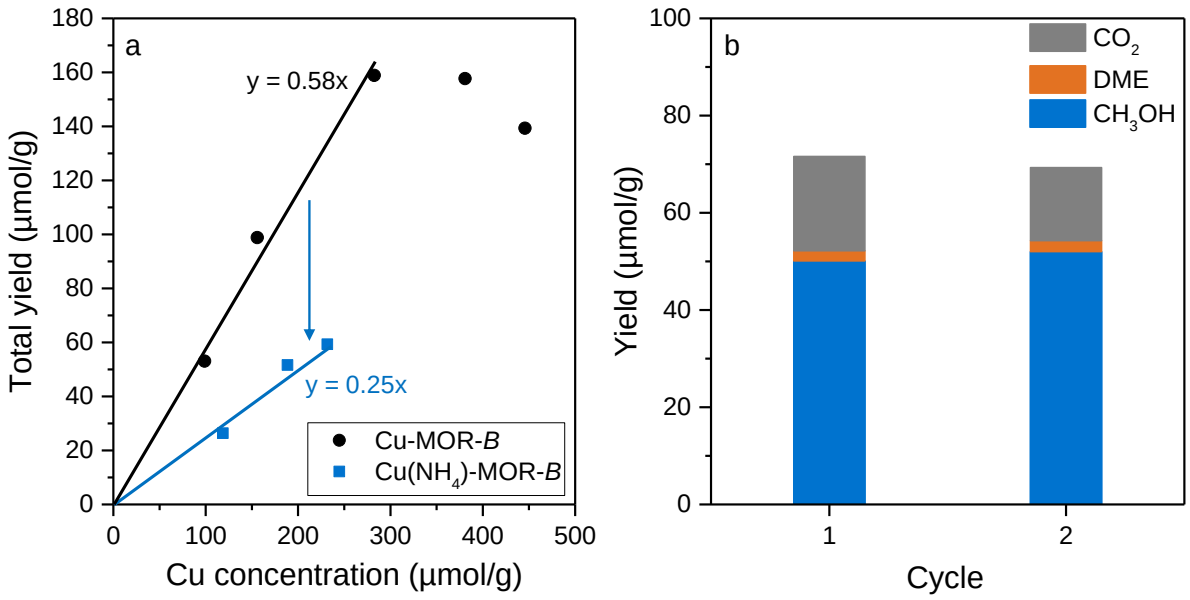

Figure 3-9. Total yield of CH_4 oxidation on Cu-MOR-*B* catalysts prepared from parent MOR in H- and NH_4-forms (a) and the results of two consecutive reaction cycles on Cu(NH_4)-MOR-*B* catalyst (232 µmol/g Cu).

Table 3-4. Concentration of Al in tetrahedral and octahedral coordination structures determined by ^{27}Al MAS NMR spectroscopy.

Sample	Tetrahedral Al (µmol/g)	Octahedral Al (µmol/g)	Total Al (µmol/g)
H-MOR-*B*	1320	300	1620
NH_4-MOR-*B*	1620	0	1620
Cu-MOR-*B* (156 µmol/g Cu)	1300	200	1500
Cu(NH_4)-MOR-*B* (189 µmol/g), calcined	1450	170	1620

3.3.5. Possible Structure of the Active Cu-Oxo Clusters in Cu-MOR-*B* Catalysts

Cu-MOR-*B* catalysts have shown average Cu efficiency of 0.58 below the Cu loading of 283 μmol/g, with the maximum value of 0.63 (Figure 3-1). These values are larger than any expected Cu efficiency assuming the formation of Cu dimer or trimer as single site. Taking into account that the ratio of BAS consumed per Cu cation has also increased from the theoretical 2/3 obtained for Cu-oxo trimers[10] to 0.89 (Figure 3-4), we discuss here the possible structures of Cu species that could achieve such high Cu efficiency.

Kulkarni et al. have carried out periodic DFT calculations combined with thermodynamic analysis to show that $[CuOH]^+$ species in 8 MR of CHA can activate CH_4.[53] Recent study has also shown that mononuclear Cu(II) species on alumina prepared by surface organometallic chemistry are able to oxidize methane into methanol.[54] However, considering the large fraction of paired Al sites on the parent H-MOR-*B* and preferential exchange of Cu cations at the 8 MR side pockets, formation of $[CuOH]^+$ monomers is unlikely. It is known that condensation of two adjacent $[CuOH]^+$ species is favorable at high temperatures to form $[Cu\text{-}O\text{-}Cu]^{2+}$ species.[16, 55] However, the observed Cu efficiencies above 0.5 imply that such $[Cu\text{-}O\text{-}Cu]^{2+}$ clusters are not the predominant species for the high activity of Cu-MOR-*B* catalysts. On the other hand, considering that methane oxidation to methanol requires transfer of two electrons from methane to Cu species, $[Cu^{II}OH]^+$ species would result in the formation of metallic Cu. However, the formation of metallic Cu species was not detected by HERFD-XANES (Figure A 3-3 in Appendix).

Another possibility is the activation of two CH_4 molecules on a tricopper-oxo cluster. DFT calculations of the electronic structures of $[Cu_3(\mu\text{-}O)_3]^{2+}$ supported on MOR have shown that one O atom in $[Cu_3(\mu\text{-}O)_3]^{2+}$ cluster is more reactive than the other two O atoms.[56] However, it was also recently reported that different geometric confinement of $[Cu\text{-}O\text{-}Cu]^{2+}$ clusters results in different reactivity with CH_4.[57] Therefore, it is not surprising that the reactivity of $[Cu_3(\mu\text{-}O)_3]^{2+}$ clusters are also affected by geometric confinement effect or different electronic structures. Since two Cu atoms in the $[Cu_3(\mu\text{-}O)_3]^{2+}$ cluster are in the formal oxidation state of Cu(III), oxidation of two CH_4 molecules is possible with accompanying the formation of two Cu(I). The BAS/Cu of near 1 and CH_4/Cu stoichiometry of 0.63 would be also compatible with the formation of a *trans*-

1,2-μ-peroxo dicopper clusters, as proposed by Pappas et al.[21] However, presence of such species would imply the formation of some inactive clusters or the same species with different reactivities.

Based on our results, we hypothesize that the presence of EFAl inside 8 MR side pockets of MOR-*B* contributes to a change in the electronic structure and/or in the geometric confinement of active Cu-oxo clusters. Such change allows for the activation of a second CH_4 molecule by the multinuclear Cu cluster, resulting in roughly doubling the activity of the catalyst compared to those without the effect of EFAl. Evolution of Cu efficiencies from 0.58 for low Cu concentrations, passing by a maximum of 0.63 and the decrease of Cu efficiency for higher loadings (even though 90% of the Cu species are exchanged as cationic species) implies that Cu speciation is not homogeneous in presence of additional EFAl species located inside 8 MR side pockets of MOR. An optimal EFAl-Cu interaction is achieved at 283 µmol/g of Cu and 260 µmol/g EFAl in 8 MR pockets.

3.4. Conclusions

We have prepared Cu-MOR catalysts at different Cu loading from different parent H-MOR samples. Two parent samples, H-MOR-*A* and H-MOR-*B*, were shown to possess very similar distribution of framework Al sites, while H-MOR-*B* contains more EFAl species inside 8 MR side pockets of MOR compared to H-MOR-*A*. Cu-MOR-*A* catalysts show the Cu efficiency of 0.33 in CH_4 oxidation corresponding to the formation of single site $[Cu_3(\mu\text{-}O)_3]^{2+}$ species. On the other hand, Cu-MOR-*B* catalysts exhibit Cu efficiency of up to 0.63, which is the highest value reported so far. The yield of CH_4 oxidation of Cu-MOR-*B* catalysts increased linearly up to a Cu loading of ca. 300 µmol/g and leveled off at larger Cu concentrations. We have quantitatively shown that octahedral Al is transformed to tetrahedral upon Cu loading in H-MOR-*B*. The transformed Al sites seem to become NMR-silent due to the strong interaction with paramagnetic Cu^{2+}. Cu-exchange in the pristine NH_4-MOR-*B* as a parent sample, which does not possess octahedral EFAl species, resulted in much lower Cu efficiencies of ca. 0.25 despite almost identical distribution of framework Al sites. These results demonstrate that the interaction of Cu species with EFAl species inside 8 MR side pockets of MOR results in the enhanced reactivity of Cu clusters. Though the Cu species formed in Cu-MOR-*B* catalysts seem to be heterogeneous, we hypothesize that dimeric and/or trimeric Cu species, such as *trans-1,2-µ*-peroxo dicopper clusters and $[Cu_3(\mu\text{-}O)_3]^{2+}$ species, which are able to activate two CH_4 molecules per cluster, are responsible for the high Cu efficiency of the catalysts. We propose that the unusually high reactivity of the Cu clusters stems from their interaction with EFAl species in micropores of MOR, especially inside the 8 MR side pockets, resulting in the change in electronic structures or geometric confinement of the Cu species.

3.5. Acknowledgement

The financial support from the Deutsche Forschungsgemeinschaft DFG under project LE1187/13-1 is acknowledged. Part of the research was supported by the TUM International Graduate School of Science and Engineering (IGSSE) and the Max-Buchner Forschungsstiftung from DECHEMA (Grant number 3568). The author acknowledge DESY (Hamburg, Germany), a member of the Helmholtz Association HGF, for the provision of experimental facilities. Parts of this research were carried out at PETRA III and we would like to thank Dr. Wolfgang Caliebe and Dr. Alexandr Kalinko for assistance in using beamline P 64. Dr. Thomas Huthwelker and Dr. Camelia Nicoleta Borca at beamline Phoenix II in Swiss Light Source at Paul-Scherrer-Institute are also gratefully acknowledged for the support in measurements. The

3.6. Appendix

Table A 3-1. Si/Al ratios of Cu-MOR-*B* catalysts and Cu concentrations after Na back-exchange.

Cu concentration (µmol/g)	Si/Al after Cu-exchange (-)	Cu concentration after Na back-exchange (µmol/g)	Remaining Cu after Na back-exchange (%)
99	9.6	6.3	6.4
156	9.4	10	6.4
283	9.3	20	7.0
381	10.2	25	6.6
446	9.4	32	7.1

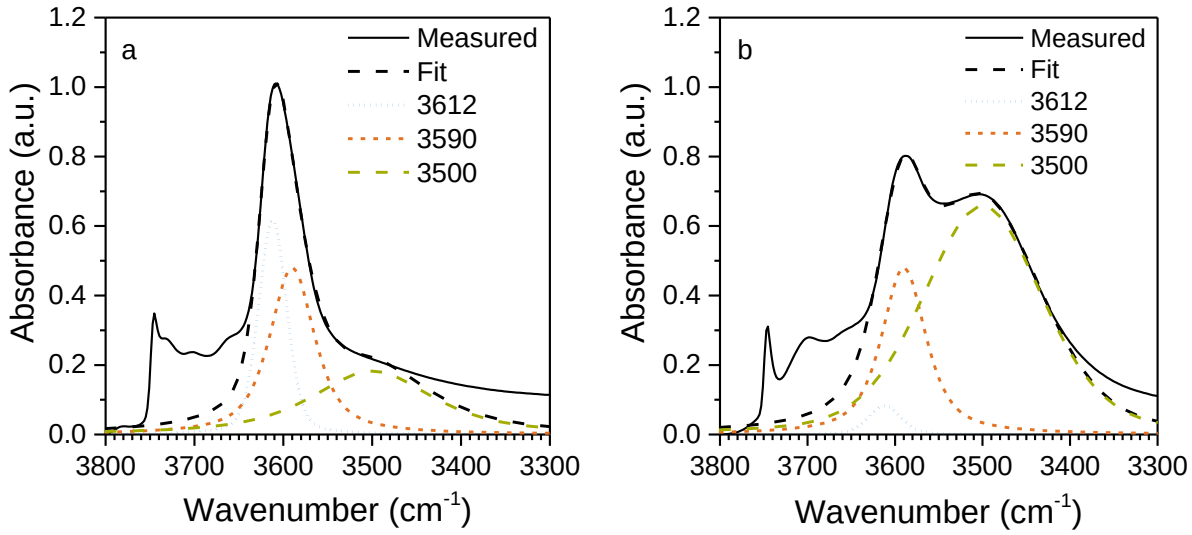

Figure A 3-1. Deconvolution of IR spectra of H-MOR-*B* before adsorption of *n*-hexane (a) and after adsorption of *n*-hexane at 1.0 mbar (b).

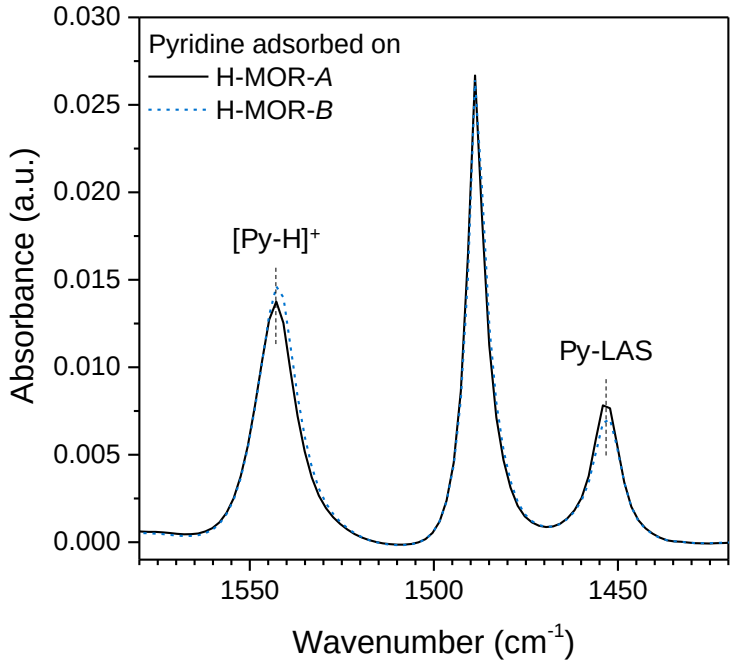

Figure A 3-2. IR spectra of pyridine adsorbed on H-MOR-*A* and H-MOR-*B* samples.

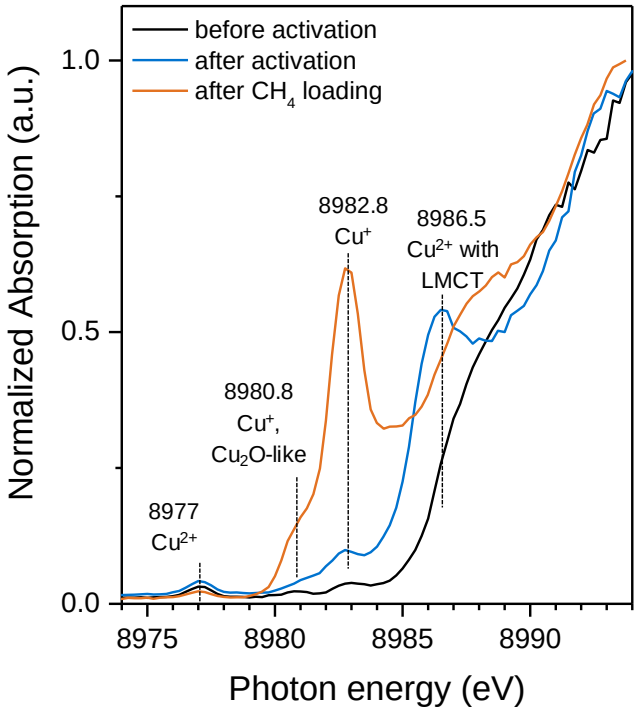

Figure A 3-3. HERFD-XANES of a Cu-MOR-*B* catalyst with 283 µmol/g Cu loading.

Reaction of CH_4 on different Cu-zeolite catalysts was monitored in-situ by UV-Vis spectroscopy. Figure A 3-4 shows the UV-Vis difference spectra of Cu-MOR-*B* catalysts at different Cu loading after CH_4 loading for 30 min. These spectra indicate the change in the Cu species with CH_4 reaction at different Cu concentrations. In the spectrum of the Cu-MOR-*B* catalyst with 156 µmol/g Cu loading, a negative as well as a positive bands are observed at ca. 12,600 cm^{-1} and at ca. 17,500 cm^{-1}, respectively. These bands can be attributed to d-d transition of Cu^{2+} in square-pyramidal and pyramidal coordination structures.[58, 59] Decreasing intensity of the band at 12,600 cm^{-1} suggests the reduction of Cu^{2+} in specific coordination structure to Cu^{+} upon CH_4 reaction, as frequently observed by XANES.[10-11, 14, 21] On the other hand, increase of the band at 17,500 cm^{-1} could be due to the transformation of Cu^{2+} species upon reaction with CH_4 into new coordination structures. In the LMCT region of the UV-Vis spectra of Cu-MOR-*B* catalysts with 156 and 283 µmol/g Cu loading, two negative bands are observed at ca. 39,500 and 29,500 cm^{-1}, indicating the cleavage of Cu-O bond and/or reduction of Cu^{2+} to Cu^{+}. While the band at 29,500 cm^{-1} is associated with $[Cu_3(\mu\text{-}O)_3]^{2+}$,[10] it has been hypothesized that the band at 39,500 cm^{-1} is also due to this Cu species, since the tricopper-oxo cluster contains Cu and O atoms with different electron spin densities.[10, 56] The area ratio of these two peaks were almost identical at lower Cu loadings. However, on the Cu-MOR-*B* catalyst with the highest Cu loading of 446 µmol/g, the relative area of the band at 29,500 cm^{-1} has increased, while the band at 39,500 cm^{-1} has red-shifted, suggesting the transformation of active Cu-oxo clusters at high Cu concentration. It is worth noting that the Cu efficiency of the Cu-MOR-*B* with the highest Cu loading was ca. 0.3, while the other two catalysts show CH_4/Cu stoichiometry above 0.5, and it was proposed that the high Cu efficiency stems from reaction of second CH_4 molecule on an active Cu cluster. UV-Vis bands cannot be unambiguously attributed to Cu species with defined structures because they are in general very broad and one species could show bands at multiple positions.[60] However, these results suggest that such Cu species with high reactivity, if present, show a dominant band at ca. 40,000 cm^{-1} and the $[Cu_3(\mu\text{-}O)_3]^{2+}$ cluster shows a dominant band at ca. 30,000 cm^{-1}.

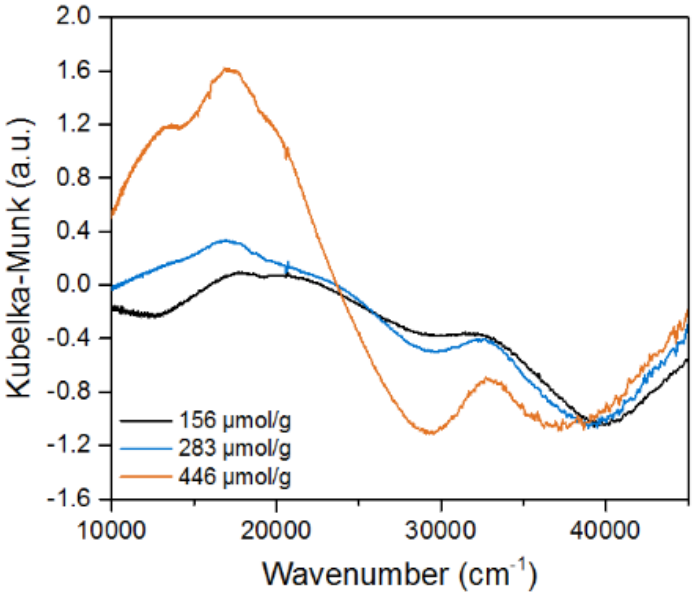

Figure A 3-4. Diffuse-reflectance UV-Vis difference spectra of Cu-MOR-*B* catalysts at different Cu loading, recorded after CH_4 reaction for 30 min. The spectra taken at 0 min CH_4 loading were subtracted. The spectra are normalized to the intensity of the band at 37,000-39,500 cm^{-1} for comparison.

3.7. Reference

1. Malakoff, D., The gas surge. *Science* **2014**, *344*, 1464.
2. Wang, V. C. C.; Maji, S.; Chen, P. P. Y.; Lee, H. K.; Yu, S. S. F.; Chan, S. I., Alkane Oxidation: Methane Monooxygenases, Related Enzymes, and Their Biomimetics. *Chem. Rev.* **2017**, *117*, 8574.
3. Lieberman, R. L.; Rosenzweig, A. C., Crystal Structure of a Membrane-Bound Metalloenzyme that Catalyses the Biological Oxidation of Methane. *Nature* **2005**, *434*, 177.
4. Merkx, M.; Kopp, D. A.; Sazinsky, M. H.; Blazyk, J. L.; Müller, J.; Lippard, S. J., Dioxygen Activation and Methane Hydroxylation by Soluble Methane Monooxygenase: A Tale of Two Irons and Three Proteins. *Angew. Chem. Int. Ed.* **2001**, *40*, 2782.
5. Snyder, B. E. R.; Böttger, L. H.; Bols, M. L.; Yan, J. J.; Rhoda, H. M.; Jacobs, A. B.; Hu, M. Y.; Zhao, J.; Alp, E. E.; Hedman, B.; Hodgson, K. O.; Schoonheydt, R. A.; Sels, B. F.; Solomon, E. I., Structural Characterization of a Non-Heme Iron Active Site in Zeolites that Hydroxylates Methane. *Proc. Natl. Acad. Sci.* **2018**, *115*, 4565.
6. Snyder, B. E. R.; Vanelderen, P.; Bols, M. L.; Hallaert, S. D.; Bottger, L. H.; Ungur, L.; Pierloot, K.; Schoonheydt, R. A.; Sels, B. F.; Solomon, E. I., The Active Site of Low-Temperature Methane Hydroxylation in Iron-Containing Zeolites. *Nature* **2016**, *536*, 317.
7. Mahyuddin, M. H.; Staykov, A.; Shiota, Y.; Yoshizawa, K., Direct Conversion of Methane to Methanol by Metal-Exchanged ZSM-5 Zeolite (Metal = Fe, Co, Ni, Cu). *ACS Catal.* **2016**, *6*, 8321.
8. Starokon, E. V.; Parfenov, M. V.; Pirutko, L. V.; Abornev, S. I.; Panov, G. I., Room-Temperature Oxidation of Methane by alpha-Oxygen and Extraction of Products from the FeZSM-5 Surface. *J. Phys. Chem. C* **2011**, *115*, 2155.
9. Narsimhan, K.; Iyoki, K.; Dinh, K.; Román-Leshkov, Y., Catalytic Oxidation of Methane into Methanol over Copper-Exchanged Zeolites with Oxygen at Low Temperature. *ACS Cent. Sci.* **2016**.
10. Grundner, S.; Markovits, M. A. C.; Li, G.; Tromp, M.; Pidko, E. A.; Hensen, E. J. M.; Jentys, A.; Sanchez-Sanchez, M.; Lercher, J. A., Single-Site Trinuclear Copper Oxygen Clusters in Mordenite for Selective Conversion of Methane to Methanol. *Nat. Commun.* **2015**, *6*, 7546.
11. Alayon, E. M.; Nachtegaal, M.; Ranocchiari, M.; van Bokhoven, J. A., Catalytic Conversion of Methane to Methanol over Cu-Mordenite. *Chem. Commun.* **2012**, *48*, 404.
12. Vanelderen, P.; Hadt, R. G.; Smeets, P. J.; Solomon, E. I.; Schoonheydt, R. A.; Sels, B. F., Cu-ZSM-5: A Biomimetic Inorganic Model for Methane Oxidation. *J. Catal.* **2011**, *284*, 157.
13. Groothaert, M. H.; Smeets, P. J.; Sels, B. F.; Jacobs, P. A.; Schoonheydt, R. A., Selective Oxidation of Methane by the Bis(μ-oxo)dicopper Core Stabilized on ZSM-5 and Mordenite Zeolites. *J. Am. Chem. Soc.* **2005**, *127*, 1394.

14. Pappas, D. K.; Borfecchia, E.; Dyballa, M.; Pankin, I. A.; Lomachenko, K. A.; Martini, A.; Signorile, M.; Teketel, S.; Arstad, B.; Berlier, G.; Lamberti, C.; Bordiga, S.; Olsbye, U.; Lillerud, K. P.; Svelle, S.; Beato, P., Methane to Methanol: Structure–Activity Relationships for Cu-CHA. *J. Am. Chem. Soc.* **2017**, *139*, 14961.

15. Wulfers, M. J.; Teketel, S.; Ipek, B.; Lobo, R. F., Conversion of Methane to Methanol on Copper-Containing Small-Pore Zeolites and Zeotypes. *Chem. Commun.* **2015**, *51*, 4447.

16. Ikuno, T.; Grundner, S.; Jentys, A.; Li, G. N.; Pidko, E.; Fulton, J.; Sanchez-Sanchez, M.; Lercher, J. A., Formation of Active Cu-oxo Clusters for Methane Oxidation in Cu-Exchanged Mordenite. *J. Phys. Chem. C* **2019**, *123*, 8759.

17. Kim, Y.; Kim, T. Y.; Lee, H.; Yi, J., Distinct activation of Cu-MOR for Direct Oxidation of Methane to Methanol. *Chem. Commun.* **2017**, *53*, 4116.

18. Ipek, B.; Wulfers, M. J.; Kim, H.; Göltl, F.; Hermans, I.; Smith, J. P.; Booksh, K. S.; Brown, C. M.; Lobo, R. F., Formation of $[Cu_2O_2]^{2+}$ and $[Cu_2O]^{2+}$ toward C–H Bond Activation in Cu-SSZ-13 and Cu-SSZ-39. *ACS Catal.* **2017**, 4291.

19. Alayon, E. M. C.; Nachtegaal, M.; Bodi, A.; van Bokhoven, J. A., Reaction Conditions of Methane-to-Methanol Conversion Affect the Structure of Active Copper Sites. *ACS Catal.* **2014**, *4*, 16.

20. Smeets, P. J.; Hadt, R. G.; Woertink, J. S.; Vanelderen, P.; Schoonheydt, R. A.; Sels, B. F.; Solomon, E. I., Oxygen Precursor to the Reactive Intermediate in Methanol Synthesis by Cu-ZSM-5. *J. Am. Chem. Soc.* **2010**, *132*, 14736.

21. Pappas, D. K.; Martini, A.; Dyballa, M.; Kvande, K.; Teketel, S.; Lomachenko, K. A.; Baran, R.; Glatzel, P.; Arstad, B.; Berlier, G.; Lamberti, C.; Bordiga, S.; Olsbye, U.; Svelle, S.; Beato, P.; Borfecchia, E., The Nuclearity of the Active Site for Methane to Methanol Conversion in Cu-Mordenite: A Quantitative Assessment. *J. Am. Chem. Soc.* **2018**, *140*, 15270.

22. Grundner, S.; Luo, W.; Sanchez-Sanchez, M.; Lercher, J. A., Synthesis of Single-Site Copper Catalysts for Methane Partial Oxidation. *Chem. Commun.* **2016**, *52*, 2553.

23. Markovits, M. A. C.; Jentys, A.; Tromp, M.; Sanchez-Sanchez, M.; Lercher, J. A., Effect of Location and Distribution of Al Sites in ZSM-5 on the Formation of Cu-Oxo Clusters Active for Direct Conversion of Methane to Methanol. *Top. Catal.* **2016**, *59*, 1554.

24. Dědeček, J.; Wichterlová, B., Role of Hydrated Cu Ion Complexes and Aluminum Distribution in the Framework on the Cu Ion Siting in ZSM-5. *J. Phys. Chem. B* **1997**, *101*, 10233.

25. Dedecek, J.; Sobalik, Z.; Tvaruazkova, Z.; Kaucky, D.; Wichterlova, B., Coordination of Cu Ions in High-Silica Zeolite Matrixes. Cu^+ Photoluminescence, IR of NO Adsorbed on Cu^{2+}, and Cu^{2+} ESR Study. *J. Phys. Chem.* **1995**, *99*, 16327.

26. Dyballa, M.; Pappas, D. K.; Kvande, K.; Borfecchia, E.; Arstad, B.; Beato, P.; Olsbye, U.; Svelle, S., On How Copper Mordenite Properties Govern the Framework Stability and Activity in the Methane-to-Methanol Conversion. *ACS Catal.* **2019**, *9*, 365.

27. Zhang, Y.; Zhao, R.; Sanchez-Sanchez, M.; Haller, G. L.; Hu, J.; Bermejo-Deval, R.; Liu, Y.; Lercher, J. A., Promotion of Protolytic Pentane Conversion on H-MFI Zeolite by

Proximity of Extra-Framework Aluminum Oxide and Brønsted Acid Sites. *J. Catal.* **2019**, *370*, 424.

28. Schallmoser, S.; Ikuno, T.; Wagenhofer, M. F.; Kolvenbach, R.; Haller, G. L.; Sanchez-Sanchez, M.; Lercher, J. A., Impact of the Local Environment of Brønsted Acid Sites in ZSM-5 on the Catalytic Activity in n-Pentane Cracking. *J. Catal.* **2014**, *316*, 93.
29. Almutairi, S. M. T.; Mezari, B.; Filonenko, G. A.; Magusin, P. C. M. M.; Rigutto, M. S.; Pidko, E. A.; Hensen, E. J. M., Influence of Extraframework Aluminum on the Brønsted Acidity and Catalytic Reactivity of Faujasite Zeolite. *ChemCatChem* **2013**, *5*, 452.
30. Dědeček, J.; Sobalík, Z.; Wichterlová, B., Siting and Distribution of Framework Aluminium Atoms in Silicon-Rich Zeolites and Impact on Catalysis. *Catal. Rev.* **2012**, *54*, 135.
31. Brown, S. P.; Wimperis, S., Two-Dimensional Multiple-Quantum MAS NMR of Quadrupolar Nuclei: A Comparison of Methods. *J. Magn. Res.* **1997**, *128*, 42.
32. Amoureux, J.-P.; Fernandez, C.; Steuernagel, S., ZFiltering in MQMAS NMR. *J. Magn. Res., Ser A* **1996**, *123*, 116.
33. Szlachetko, J.; Nachtegaal, M.; Boni, E. d.; Willimann, M.; Safonova, O.; Sa, J.; Smolentsev, G.; Szlachetko, M.; Bokhoven, J. A. v.; Dousse, J.-C.; Hoszowska, J.; Kayser, Y.; Jagodzinski, P.; Bergamaschi, A.; Schmitt, B.; David, C.; Lücke, A., A von Hamos X-Ray Spectrometer Based on a Segmented-Type Diffraction Crystal for Single-Shot X-Ray Emission Spectroscopy and Time-Resolved Resonant Inelastic X-Ray Scattering Studies. *Rev. Sci. Instrum.* **2012**, *83*, 103105.
34. v. Hámos, L., Röntgenspektroskopie und Abbildung mittels gekrümmter Kristallreflektoren. *Naturwiss.* **1932**, *20*, 705.
35. Brezicki, G.; Kammert, J. D.; Gunnoe, T. B.; Paolucci, C.; Davis, R. J., Insights into the Speciation of Cu in the Cu-H-Mordenite Catalyst for the Oxidation of Methane to Methanol. *ACS Catal.* **2019**, *9*, 5308.
36. Dědeček, J.; Wichterlová, B., Co^{2+} Ion Siting in Pentasil-Containing Zeolites. I. Co2+ Ion Sites and Their Occupation in Mordenite. A Vis−NIR Diffuse Reflectance Spectroscopy Study. *J. Phys. Chem. B* **1999**, *103*, 1462.
37. Dedecek, J.; Kaucky, D.; Wichterlova, B.; Gonsiorova, O., Co^{2+} Ions as Probes of Al Distribution in the Framework of Zeolites. ZSM-5 Study. *Phys. Chem. Chem. Phys.* **2002**, *4*, 5406.
38. Eder, F.; Stockenhuber, M.; Lercher, J. A., Brønsted Acid Site and Pore Controlled Siting of Alkane Sorption in Acidic Molecular Sieves. *J. Phys. Chem. B* **1997**, *101*, 5414.
39. Moreau, F.; Ayrault, P.; Gnep, N. S.; Lacombe, S.; Merlen, E.; Guisnet, M., Influence of Na Exchange on the Acidic and Catalytic Properties of an HMOR Zeolite. *Microporous Mesoporous Mater.* **2002**, *51*, 211.
40. Fyfe, C. A.; Bretherton, J. L.; Lam, L. Y., Detection of the 'Invisible Aluminium' and Characterisation of the Multiple Aluminium Environments in Zeolite USY by High-Field Solid-State NMR. *Chem. Commun.* **2000**, 1575.

41. Hu, J. Z.; Wan, C.; Vjunov, A.; Wang, M.; Zhao, Z.; Hu, M. Y.; Camaioni, D. M.; Lercher, J. A., ^{27}Al MAS NMR Studies of HBEA Zeolite at Low to High Magnetic Fields. *J. Phys. Chem. C* **2017**, *121*, 12849.

42. Triantafillidis, C. S.; Vlessidis, A. G.; Evmiridis, N. P., Dealuminated H−Y Zeolites: Influence of the Degree and the Type of Dealumination Method on the Structural and Acidic Characteristics of H−Y Zeolites. *Ind. Eng. Chem. Res.* **2000**, *39*, 307.

43. Veefkind, V. A.; Smidt, M. L.; Lercher, J. A., On the Role of Strength and Location of Brønsted Acid Sites for Ethylamine Synthesis on Mordenite Catalysts. *Appl. Catal. A* **2000**, *194-195*, 319.

44. Song, J.; Wang, Y.; Walter, E. D.; Washton, N. M.; Mei, D.; Kovarik, L.; Engelhard, M. H.; Prodinger, S.; Wang, Y.; Peden, C. H. F.; Gao, F., Toward Rational Design of Cu/SSZ-13 Selective Catalytic Reduction Catalysts: Implications from Atomic-Level Understanding of Hydrothermal Stability. *ACS Catal.* **2017**, *7*, 8214.

45. Vjunov, A.; Wang, M.; Govind, N.; Huthwelker, T.; Shi, H.; Mei, D.; Fulton, J. L.; Lercher, J. A., Tracking the Chemical Transformations at the Brønsted Acid Site upon Water-Induced Deprotonation in a Zeolite Pore. *Chem. Mater.* **2017**, *29*, 9030.

46. Omegna, A.; Prins, R.; van Bokhoven, J. A., Effect of Temperature on Aluminum Coordination in Zeolites H−Y and H−USY and Amorphous Silica−Alumina: An in Situ Al K Edge XANES Study. *J. Phys. Chem. B* **2005**, *109*, 9280.

47. Dyballa, M.; Obenaus, U.; Lang, S.; Gehring, B.; Traa, Y.; Koller, H.; Hunger, M., Brønsted Sites and Structural Stabilization Effect of Acidic Low-Silica Zeolite A Prepared by Partial Ammonium Exchange. *Microporous Mesoporous Mater.* **2015**, *212*, 110.

48. Deng, C.; Zhang, J.; Dong, L.; Huang, M.; Bin, L.; Jin, G.; Gao, J.; Zhang, F.; Fan, M.; Zhang, L.; Gong, Y., The Effect of Positioning Cations on Acidity and Stability of the Framework Structure of Y zeolite. *Sci. Rep.* **2016**, *6*, 23382.

49. Sousa-Aguiar, E. F.; Trigueiro, F. E.; Zotin, F. M. Z., The Role of Rare Earth Elements in Zeolites and Cracking Catalysts. *Catal. Today* **2013**, *218-219*, 115.

50. Pappas, D. K.; Borfecchia, E.; Lomachenko, K. A.; Lazzarini, A.; Gutterød, E. S.; Dyballa, M.; Martini, A.; Berlier, G.; Bordiga, S.; Lamberti, C.; Arstad, B.; Olsbye, U.; Beato, P.; Svelle, S., Cu-Exchanged Ferrierite Zeolite for the Direct CH_4 to CH_3OH Conversion: Insights on Cu Speciation from X-Ray Absorption Spectroscopy. *Top. Catal.* **2019**.

51. Bozbag, S. E.; Alayon, E. M. C.; Pecháček, J.; Nachtegaal, M.; Ranocchiari, M.; van Bokhoven, J. A., Methane to Methanol over Copper Mordenite: Yield Improvement through Multiple Cycles and Different Synthesis Techniques. *Catal. Sci. Technol.* **2016**, *6*, 5011.

52. Kwak, J. H.; Varga, T.; Peden, C. H. F.; Gao, F.; Hanson, J. C.; Szanyi, J., Following the Movement of Cu Ions in a SSZ-13 Zeolite during Dehydration, Reduction and Adsorption: A Combined in Situ TP-XRD, XANES/DRIFTS Study. *J. Catal.* **2014**, *314*, 83.

53. Kulkarni, A. R.; Zhao, Z. J.; Siahrostami, S.; Norskov, J. K.; Studt, F., Monocopper Active Site for Partial Methane Oxidation in Cu-Exchanged 8MR Zeolites. *ACS Catal.* **2016**, *6*, 6531.

54. Meyet, J.; Searles, K.; Newton, M. A.; Wörle, M.; van Bavel, A. P.; Horton, A. D.; van Bokhoven, J. A.; Copéret, C., Monomeric Copper(II) Sites Supported on Alumina Selectively Convert Methane to Methanol. *Angew. Chem. Int. Ed.* **2019**, *0*.

55. Llabrés i Xamena, F. X.; Fisicaro, P.; Berlier, G.; Zecchina, A.; Palomino, G. T.; Prestipino, C.; Bordiga, S.; Giamello, E.; Lamberti, C., Thermal Reduction of Cu^{2+}−Mordenite and Re-oxidation upon Interaction with H_2O, O_2, and NO. *J. Phys. Chem. B* **2003**, *107*, 7036.

56. Vogiatzis, K. D.; Li, G.; Hensen, E. J. M.; Gagliardi, L.; Pidko, E. A., Electronic Structure of the $[Cu_3(\mu\text{-}O)_3]^{2+}$ Cluster in Mordenite Zeolite and Its Effects on the Methane to Methanol Oxidation. *J. Phys. Chem. C* **2017**, *121*, 22295.

57. Snyder, B. E. R.; Vanelderen, P.; Schoonheydt, R. A.; Sels, B. F.; Solomon, E. I., Second-Sphere Effects on Methane Hydroxylation in Cu-Zeolites. *J. Am. Chem. Soc.* **2018**.

58. Vanelderen, P.; Vancauwenbergh, J.; Tsai, M.-L.; Hadt, R. G.; Solomon, E. I.; Schoonheydt, R. A.; Sels, B. F., Spectroscopy and Redox Chemistry of Copper in Mordenite. *ChemPhysChem* **2014**, *15*, 91.

59. Delabie, A.; Pierloot, K.; Groothaert, M. H.; Weckhuysen, B. M.; Schoonheydt, R. A., The Siting of Cu(II) in Mordenite: a Theoretical Spectroscopic Study. *Phys. Chem. Chem. Phys.* **2002**, *4*, 134.

60. Li, H.; Paolucci, C.; Khurana, I.; Wilcox, Laura N.; Göltl, F.; Albarracin-Caballero, J. D.; Shih, A. J.; Ribeiro, F. H.; Gounder, R.; Schneider, W. F., Consequences of Exchange-Site Heterogeneity and Dynamics on the UV-Visible Spectrum of Cu-Exchanged SSZ-13. *Chem. Sci.* **2019**, *10*, 2373.

4. Selective Oxidation of Methane to Methanol on Cu Clusters Hosted in Different Support Materials

Abstract

Cu-exchanged zeolites are known to convert methane selectively into methanol at moderate reaction temperatures. Establishing a correlation between zeolite framework structure and CH_4 oxidation activity of the Cu-zeolites could facilitate the strategical design of the catalysts. In this chapter,[3] Cu-exchanged MOR, MEL and FER are applied to the methane oxidation reaction. Presence of 8 MR structure on the wall of larger main channels as well as high concentrations of paired Al sites seem to facilitate the formation of active Cu-oxo clusters. Cu-hydroxo clusters synthesized via atomic layer deposition on the nodes of the metal-organic framework (MOF) NU-1000 are also active for oxidation of methane to methanol under mild reaction conditions. Tuning of the reaction conditions was carried out by testing the stability of the Cu-NU-1000 under reaction conditions. Investigation of the various Cu-based catalysts supported on porous materials has revealed that structural confinement effect, well-defined pore structure and anchoring sites and high thermal stability and redox resistance are the important factors of the support materials.

[3] This chapter is adapted with permission from the following publication in the Journal of American Chemical Society: Ikuno, T.; Zheng, J.; Vjunov, A.; Sanchez-Sanchez, M.; Ortuño, M. A.; Pahls, D. R.; Fulton, J. L.; Camaioni, D. M.; Li, Z.; Ray, D.; Mehdi, B. L.; Browning, N. D.; Farha, O. K.; Hupp, J. T.; Cramer, C. J.; Gagliardi, L.; Lercher, J. A., Methane Oxidation to Methanol Catalyzed by Cu-Oxo Clusters Stabilized in NU-1000 Metal–Organic Framework. *J. Am. Chem. Soc.* **2017**, *139*, 10294.

4.1. Introduction

Cu-oxo clusters supported on zeolites are known to be able to oxidize methane selectively into methanol at moderate temperatures.[1-14] Especially, Cu-exchanged MOR catalysts have been extensively studied and major improvement in CH_4 oxidation yield per Cu atom (Cu efficiency) has been achieved.[1, 3-4, 7, 15-16] Activity has been attributed to the formation of Cu-dimers and trimers, with nominal Cu efficiency of 0.5 and 0.33, respectively.[4, 15] Recent study on Cu-FER catalysts has also achieved Cu efficiency of 0.33, while the effect of Cu concentration on the Cu efficiency has not been discussed.[13] Formation of active Cu dimer or larger clusters has been also proposed in Cu-MAZ catalysts, while the formation of active Cu species was not observed at the Cu loading below 300 µmol/g.[14] Some comparative studies of Cu-zeolites with various frameworks structures (mainly medium- and large-pore zeolites) have been reported, where the presence of 8 MR channel is proposed to be responsible for the formation of active Cu-oxo clusters active in methane oxidation.[5, 8, 17] Si/Al ratios of most of the tested zeolites were approximately 5 or below and Na-type of zeolites were used to prepare most of the catalysts. Relatively low Si/Al ratio resulted in high Cu loading, and consequently, formation of CuO nanoparticles was observed in some catalysts after catalyst activation at high temperatures, which makes it difficult to determine the CH_4 oxidation yield that stems from cationic ion-exchanged Cu species. In addition, it has been demonstrated that the presence of Na^+ and other co-cations in Cu-MOR catalysts has negative effect on the Cu efficiency of Cu-MOR catalysts.[18] Moreover, dependence of Cu efficiency on Cu concentration has been observed for Cu-MFI catalysts.[1, 19] Therefore, preparation of Cu-zeolite catalysts has to be performed considering the effect of co-cations and various Cu loadings have to be examined.

Despite extensive study on Cu-zeolite with different framework structures, high Cu efficiency of Cu-zeolite catalysts have been achieved only on Cu-FER and Cu-MOR catalysts.[4, 13, 15, 20] Understanding the effect of zeolite framework structure on the activity of Cu-zeolite catalysts could make it possible to design the Cu-zeolite catalysts more strategically.

Strong adsorption of H_2O on the hydrophilic zeolites is another challenging aspect of selective oxidation of methane to methanol, which requires Cu-zeolite catalyst regeneration at high temperatures.[6, 21] Activation of Cu-zeolite catalysts at lower

temperatures, such as 200 °C, typically results in lower methanol yields compared to those achieved by activation at high temperature.[6, 12, 21-22] Thus, the use of less hydrophilic porous materials to support the highly active Cu-oxo clusters could allow the catalyst regeneration at lower temperatures. Metal-organic-frameworks (MOFs) are a family of crystalline porous organic-inorganic composite materials, consisting of metal nodes and organic linkers. Possibility of selecting different metal cations and organic linkers has led to a vast number of MOFs with unique structures with different physicochemical properties.[23] Among others, NU-1000 MOF, $Zr_6(\mu_3\text{-}OH)_8(OH)_8$(1,3,6,8-tetrakis(*p*-benzoate)pyrene)$_2$, possesses high thermal stability up to 350 °C and well-defined hydroxyl groups on Zr_6 nodes, that allows for post-synthetic deposition of metal cations.[24] Its relatively large cylindrical mesopores (34 Å diameter) are suitable for the application of atomic layer deposition (ALD) which employs relatively large metal complexes as precursors.[25-26] For instance, it has been shown that Ni-loaded NU-1000 MOF achieves high catalytic activity and stability in ethylene hydrogenation since strong interaction between Ni cations and Zr_6 nodes of NU-1000 as well as the organic linkers prevent Ni cations from sintering.[25]

In this chapter, the effect of the support for Cu clusters on the CH_4 oxidation activity is discussed. Cu-zeolite catalysts were prepared from H-type of 8 MR containing zeolites (Si/Al ~ 10 or higher) under well-controlled conditions at various Cu loadings, in order to obtain further understanding on the relationship between Cu efficiency of Cu-zeolite catalysts with zeolite framework structure. Cu-loaded NU-1000 was prepared via ALD and was applied as a direct methane-to-methanol catalyst to study the effect of different support materials on the activity of the Cu clusters.

4.2. Experimental Methods

4.2.1. Aqueous Ion-Exchange of Zeolites

Parent H-MOR and H-FER samples were obtained by the calcination of commercial NH_4-MOR (Clariant, Si/Al = 10, 11) and NH_4-FER (Tosoh, Si/Al = 9) in a flow of synthetic air (100 mL/min) at 550 °C for 6 h. H-MEL samples (Si/Al = 19, 27 and 33) were kindly provided by Prof. Dr. Miroslaw Derewinski from Pacific Northwest National Laboratory (PNNL).

Cu-exchange was performed under well-controlled conditions to avoid the precipitation of CuO and $Cu(OH)_2$ nanoparticles.[18] A parent H-zeolite sample was exchanged in a aqueous solution of $Cu(CH_3COO)_2$ (0.001-0.01 M, 60 $mL/g_{zeolite}$) at room temperature for 20 h. The pH of the solution was adjusted to 5.7 by adding aqueous HNO_3 before the addition of a zeolite. Solid phase was collected by centrifugation after the ion-exchange and rinsed by re-dispersion in doubly deionized water (50 $mL/g_{zeolite}$) and subsequent centrifugation. The rinsing step was repeated four times and the products were dried at 100 °C for 24 h.

Na-exchange was performed in an aqueous solution of $NaNO_3$ (0.5 M, 100 $mL/g_{zeolite}$) at 60 °C for 24 h. In the case of back-exchange of Cu-zeolite samples with Na^+, the samples were calcined at 500 °C for 2 h in the flow of synthetic air (100 mL/min) in advance.

Co-exchange of Na-type of zeolites was performed in aqueous $Co(NO_3)_2$ (0.05 M, 150 $mL/g_{zeolite}$) at ambient temperature for 24 h, following the conditions reported by Dedecek et al.

Atomic compositions of the samples were determined by atomic absorption spectroscopy (AAS) on a UNICAM 939 AA spectrometer after dissolution of the samples in boiling hydrofluoric acid.

4.2.2. Preparation of Cu-NU-1000 MOF

The NU-1000 MOF was synthesized following the procedure reported in a literature.[26] Cu-loaded NU-1000 was prepared by ALD using bis-(dimethylamino-2-propoxy)copper(II), $Cu(dmap)_2$ (reactant A) as a precursor. Room-temperature deionized H_2O was used as the co-reactant (reactant B). In a typical experiment, a

custom-made stainless steel powder sample holder containing microcrystalline NU-1000 (60.0 mg, 0.028 mmol) was placed in the ALD chamber, which was held at 110 °C for 30 min to remove any physisorbed water before dosing with the Cu precursor. A cylinder containing $Cu(dmap)_2$ was held at 100 °C, and each of its pulses followed the time sequence of t_1-t_2-t_3, where t_1 is the precursor pulse time, t_2 is the substrate exposure time, and t_3 is the N_2 purge time (t_1 = 1 s, t_2 = t_3 = 240 s). To ensure full metalation of the Zr_6 sites throughout the microcrystals, the $Cu(dmap)_2$ pulsing cycle was repeated 80 times before exposure of the MOF to H_2O pulses, using the same time sequence as for the Cu pulse (t_1 = 0.015 s, t_2 = t_3 = 120 s). The concentration of Cu in Cu-NU-1000 samples was determined from inductively coupled plasma-atomic emission spectroscopy (ICP-AES) measurements.

4.2.3. Selective Oxidation of Methane to Methanol

The activity of the catalysts for methane oxidation to methanol was tested at atmospheric pressure. The reaction was performed in a stainless-steel plug flow reactor with a 4 mm inner diameter. The catalytic reaction included three consecutive steps: (i) activation in O_2, (ii) reaction with CH_4, and (iii) H_2O steam-assisted product desorption.

In a typical experiment for Cu-zeolite catalysts, 50 mg of a catalyst (pressed and sieved to 250-400 µm particle size) was loaded in the reactor and activated in O_2 flow (16 mL/min) at 500 °C for 1 h, and cooled down to 200 °C in O_2 flow. Following the flushing in He, CH_4 was loaded in the flow (16 mL/min) for up to 4 h at 200 °C. After cooling to 135 °C in He flow, H_2O steam-assisted product desorption was performed in a 50/50 mixture of H_2O/He purged at a flow rate of 20 mL/min for up to 1 h.

In the case for Cu-NU-1000, 20 mg of a catalyst was loaded in the reactor and activated in O_2 flow (16 mL/min) at 200 °C, followed by flushing in He. CH_4 was loaded subsequently in the flow (16 mL/min) as a mixture of 90% CH_4 and 10% He for up to 4 h at 150 °C. After cooling to 135 °C in He flow, steam-assisted product desorption was performed in either 50/50 or 10/90 mixture of H_2O/He purged at a flow rate of 20 mL/min for up to 2 h.

The oxidation products were identified and quantified using online mass spectrometry and by monitoring the time-dependent evolution of signals at m/z 31, 44 and 46,

characteristic for methanol, CO_2 and dimethyl ether, respectively. The He signal (m/z = 4) was used as an internal standard. Selectivity and yield were determined from the integral of the product concentrations as a function of time. Dimethyl ether was assumed to form by condensation of two molecules of methanol via loss of water.

4.2.4. In-Situ Ultraviolet-Visible Spectroscopy

Ultraviolet–visible (UV-Vis) spectra of Cu-zeolite samples were measured on an Avaspec 2048 spectrometer (Avantes) with a light source AvaLight-DH-S-BAL (Avantes) in the diffuse reflectance mode. The samples were pressed and sieved into a size of 250-400 µm and placed in a quartz flow reactor (6 mm inner diameter) with square optical-grade quartz windows, sandwiched between quartz wool. The reactor was placed horizontally in a lab-made heating chamber with an 8-mm diameter hole at the bottom, where a high-temperature optical fiber (Avantes FCR-7UV400 2ME-HTX) can be vertically directed to the reactor. In a typical experiment, the sample was first activated in pure O_2 flow (16 mL/min) at 450 °C for 1 h with a heating rate of 10 °C/min. After the thermal activation step, the catalyst was cooled down to 200 °C and purged with He for 30 min, and then CH_4 reaction was performed for 30 min in pure CH_4 (16 mL/min). Spectra were measured periodically throughout the experimental procedure (every 5 min during thermal activation, every minute during CH_4 reaction). The spectra are presented as Kubelka-Munk function, defined as $F(R) = (1-R)^2/2R$, where $R = R_s/R_r$. R_s and R_r refer to the signal intensity of the sample and reference, respectively. H-type of the zeolite used for Cu-exchange was used as a reference.

4.2.5. Thermogravimetric Analysis

Thermogravimetric analysis and differential scanning calorimetry (TGA-DSC) were performed on a SENSYS EVO TG-DSC (SETARAM Instrumentation) at the ramp rate of 3 K/min.

4.2.6. N_2-Physisorption

N_2-physisorption for surface area and pore volumes was obtained on a Micromeritics ASAP 2020 instrument. The carbon slit pore model with a NL-DFT method was used.

Single-point adsorption close to P/P_0 = 0.99 was used to determine the total pore volume.

4.2.7. X-Ray Diffraction

X-ray diffraction (XRD) patterns of Cu-NU-1000 were recorded on EMPYREAN (PANalytical) with Cu Kα radiation (λ = 1.5406 Å, 45 kV, 40 mA).

4.3. Results and Discussion

4.3.1. Effect of the Framework Structure on the Activity in Selective Oxidation of Methane to Methanol on Cu-Zeolites

Series of MOR, FER and MEL zeolites with different Cu loadings were prepared to study the effect of zeolite framework structures on the activity for selective oxidation of methane to methanol. In addition, Cu-MEL catalysts with different Si/Al ratios were also studied.

First, Co^{2+} ion exchange of the parent zeolites was performed to estimate the concentration of Al sites separated by one or two Si tetrahedral .[27] It showed that more than 60% of Al sites in MOR are paired, while 79% of the Al sites in FER sample are isolated or separated by at least three Si tetrahedra (Table 4-1). For MEL samples, approximately half of the Al sites are paired at various Si/Al ratios. However, substantial increase of Si/Al ratio upon ion-exchange steps indicates the dealumination of ca. 20% of total Al.

In order to assess the concentration of exchanged Cu species in each sample, back-exchange of Cu-MOR and Cu-FER catalysts with Na^+ was performed. In this way, it is possible to quantify the concentration of Cu forming undesired CuO or $Cu(OH)_2$ nanoparticles. While cationic Cu species can be hydrolyzed and back-exchanged by Na^+, charge-neutral CuO and $Cu(OH)_2$ nanoparticles remain in the zeolite pore.[18] It has been found out that more than 85% of the Cu in Cu-MOR and Cu-FER catalysts was back-exchanged by Na^+, indicating that most of the Cu species are in cationic form.

Table 4-1. Compositions of the zeolites before and after Co-exchange and the fraction of Al sites balancing Co^{2+}, corresponding to the fraction of paired Al sites.

Zeolite	Si/Al before Co-exchagne (-)	Si/Al after Co-exchange (-)	2*Co/Al (-)
MOR	11	11	0.66
FER	9.4	8.8	0.21
MEL	19	27	0.50
	27	34	0.49
	33	46	0.43

Figure 4-1 shows the yield of CH_4 oxidation measured on Cu-zeolites at various Cu loadings and different framework structures. The measurements were performed under optimized three-stage reaction conditions, allowing enough contact time for all the active sites to react, and therefore CH_4 oxidation yields provide a quantitative measure of the concentration of active Cu-oxo clusters. Cu efficiency of CH_4 activation is defined as [Total yield]/[Cu concentration]. In Figure 4-1, the theoretical Cu efficiencies corresponding to trimeric Cu clusters are represented as dashed lines with slopes of 0.33. Cu-MOR catalysts show CH_4 oxidation yields corresponding to the formation of single-site tricopper-oxo clusters within the range of Cu loading tested.[4]

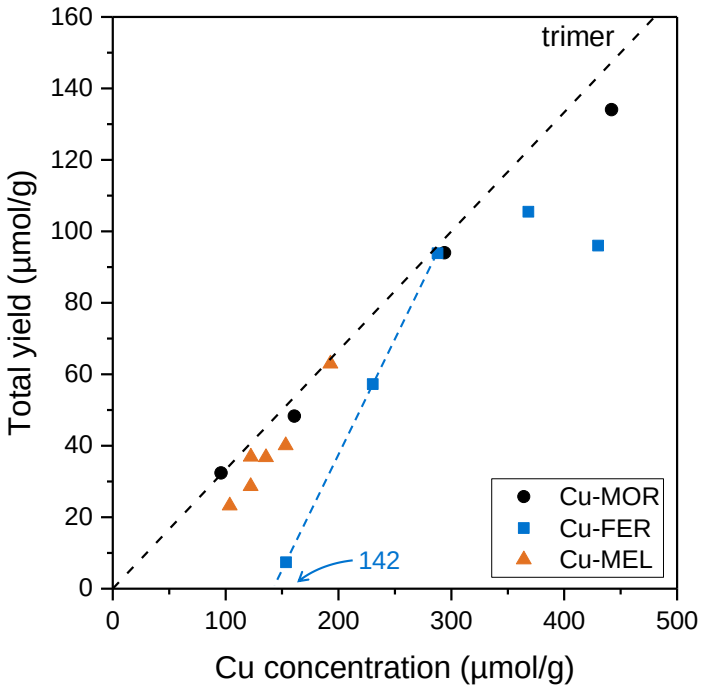

Figure 4-1. CH_4 oxidation yield of various Cu-zeolite catalysts at different Cu loadings. The black dashed line indicates the Cu efficiency corresponding to the presence of only active trimers. The blue dashed line shows the linear correlation of CH_4 oxidation yield to Cu concentration in the Cu-FER catalysts.

Cu-MEL catalysts show Cu efficiencies of approximately 0.33 at various Si/Al ratios and Cu loadings, similar to Cu-MOR materials. This suggests the formation of Cu-oxo clusters with Cu nuclearity of three or smaller. MEL zeolite possesses intersecting 10 MR straight channels, which have shallow 8 MR cavities on their wall (Figure 4-2). It has been demonstrated that $[Cu_3(\mu\text{-}O)_3]^{2+}$ clusters in MOR form at pore mouths of 8

MR side pockets.[4] The same tricopper-oxo clusters supported on MFI, which does not possesses 8 MR, have been proposed to have lower reactivity due to the less constrained local environment.[19] Considering these results, it is plausible that 1 CH_4/3 Cu ratio achieved on Cu-MEL catalysts stems from the same $[Cu_3(\mu\text{-}O)_3]^{2+}$ clusters anchored at 8 MR.

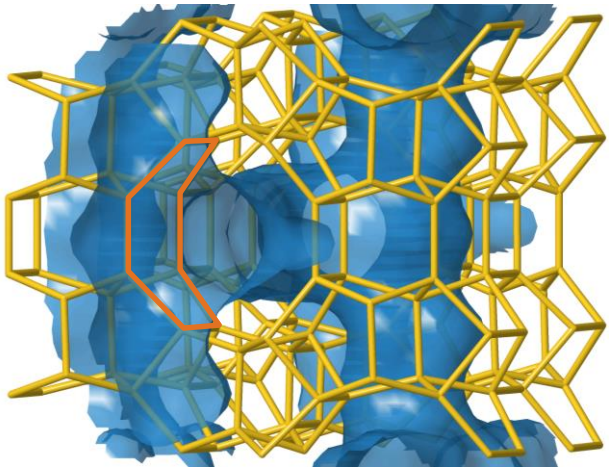

Figure 4-2. Channel structure of MEL zeolite. An 8 MR cavity located near an intersection of two 10 MR channels is highlighted orange.

Cu-FER catalysts, however, seem to have a threshold Cu concentration to start forming active Cu-oxo clusters. At the Cu concentration of 154 µmol/g, the Cu-FER catalyst show a very small CH_4 oxidation yield that correspond to the Cu efficiency of only 0.048. CH_4 oxidation yield then increases linearly up to the Cu concentration of 288 µmol/g, and it starts declining at Cu concentrations above 368 µmol/g. The maximum Cu efficiency was observed at 288 µmol/g to be 0.33, and the threshold Cu concentration for the formation of the active Cu-oxo clusters was found to be 142 µmol/g. It is worth noting that more than 85% of total Cu are exchanged as cationic species in the tested Cu loadings, as determined by Na^+ back-exchange. For various Cu-zeolites with different framework structures, it has been often observed that CH_4 oxidation yield increases with Cu concentration approximately linearly when Cu-exchange is performed under well-controlled conditions.[4, 6, 15, 18-19] Cu concentration-dependent structure of Cu clusters was observed in Cu-MFI catalysts, where the formation of monomeric and dimeric Cu species seems to be preferred at lower Cu concentrations, and the formation of $[Cu_3(\mu\text{-}O)_3]^{2+}$ species at higher Cu

concentrations.[19] The slope of increasing CH_4 oxidation observed for the Cu-FER catalysts is 0.64. If we assume the threshold of 142 µmol/g of Cu as a constant concentration of inactive Cu, this slope could be assigned to the formation of Cu trimer that is able to activate two CH_4 molecules, similar to the high reactivity described for some MOR samples in the chapter 3. However, in this case we cannot exclude the transformation of inactive Cu to active species at higher Cu loadings. It has been shown that the existence of paired Al sites can facilitate the stabilization of multinuclear Cu-oxo clusters, such as $[Cu\text{-}O\text{-}Cu]^{2+}$ or $[Cu_3(\mu\text{-}O)_3]^{2+}$ species, at low Cu concentrations.[4, 19] The low fraction of paired Al sites in FER (21%, determined by Co-exchange) is likely to direct the Cu speciation towards formation of isolated $[CuOH]^+$ species anchored to isolated Al sites. The maximum Cu efficiency of 0.33 achieved for Cu-FER catalysts at medium Cu loadings suggests the formation of Cu-oxo clusters with Cu nuclearity of three or smaller. Therefore, we hypothesize that isolated monomeric Cu species can be transformed into active multinuclear Cu clusters at increasing Cu concentrations. Decrement of the CH_4 oxidation yield at Cu concentrations above 430 µmol/g is attributed to further changes in the nuclearity or structure of Cu species in FER, which transforms active species into inactive ones.

Reaction of CH_4 on different Cu-zeolite catalysts was monitored in-situ by UV-Vis spectroscopy. First, UV-Vis spectra of a Cu-MOR catalyst (Cu loading 406 µmol/g) was recorded during CH_4 reaction in order to observe the consumption of $[Cu_3(\mu\text{-}O)_3]^{2+}$ (Figure 4-3). The bands in the range of 20,000-45,000 cm^{-1} correspond to $Cu^{2+} \leftarrow O^{2-}$ ligand-to-metal charge transfer (LMCT). The bands at 10,000-20,000 cm^{-1} are attributed to d-d transition in Cu^{2+}. In the measured spectrum at 0 min CH_4 loading (Figure 4-3 (a)), in the region of d-d transition, an outstanding band was observed at 13,000 cm^{-1} with a shoulder at 16,000 cm^{-1}, which can be attributed to d-d transition of square-pyramidal or pyramidal and square-planar Cu^{2+} species.[28-29] Under exposure of the catalyst to CH_4, an increase in the intensity of the bands at 13300 cm^{-1}, 16400 cm^{-1} and 19600 cm^{-1} is observed (Figure 4-3 (b)). An increase of the bands in the d-d transition region during CH_4 oxidation was reported also by Narshiman et al. in Cu-MOR samples.[11] In the LMCT region, broad bands were observed at ca. 39,500 cm^{-1} and 30,000 cm^{-1}. Upon reaction with CH_4, two broad bands at ca. 30,000 cm^{-1} and 38,000 cm^{-1} decrease their intensities. It has been indicated that the $[Cu_3(\mu\text{-}O)_3]^{2+}$ cluster hosted in MOR exhibits a UV-Vis absorption band at ca. 30,000 cm^{-1} during CH_4 loading, and it was attributed to the consumption of the Cu clusters upon reaction

with CH_4.[4] Since the tricopper-oxo cluster contains Cu and O atoms with different electron spin densities, we hypothesize that the band at 38,000 cm^{-1} is also due to a $Cu^{2+} \leftarrow O^{2-}$ charge transfer in the trimer.[4, 30]

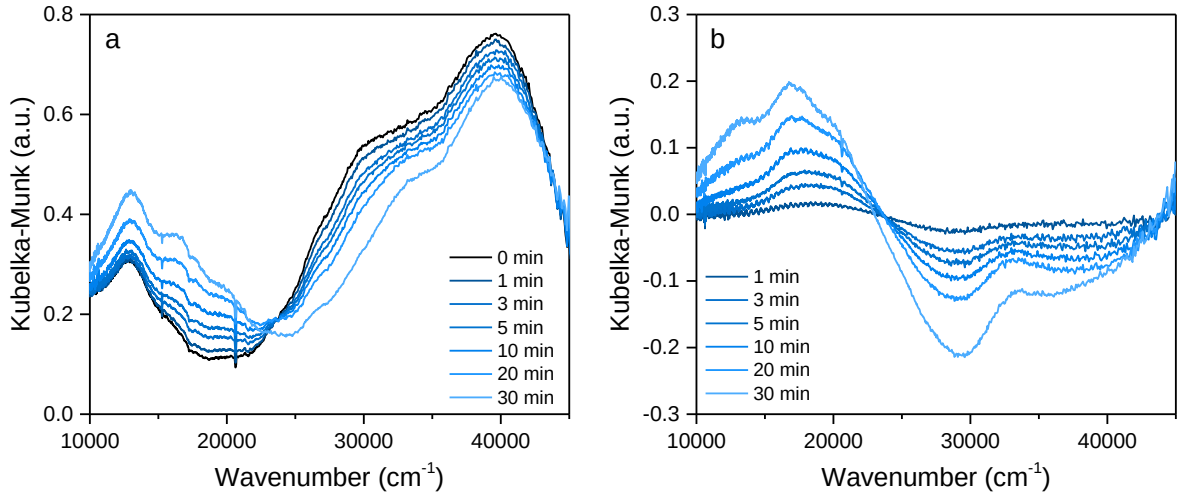

Figure 4-3. UV-Vis spectra of a Cu-MOR catalyst with 406 µmol/g Cu loading recorded during CH_4 reaction (a) and the difference spectra obtained by subtracting the spectrum at 0 min CH_4 loading (b).

Similar behavior of Cu-MEL catalysts upon reaction with CH_4 is observed in the d-d transition range of Cu^{2+}, showing the consumption of a band at ca. 13,200 cm^{-1}, due to the reduction of Cu^{2+} to Cu^{+} upon CH_4 reaction (Figure 4-4 (a)). Bands in this region have been attributed both to monomeric and to dimeric Cu species.[29, 31] The consumption of the bands at ca. 28,600 cm^{-1} and 40,000 cm^{-1} in the LMCT region was also observed. The positions of these bands are similar to those in Cu-MOR catalysts. However, the relative contribution of the band at ca. 39,500 cm^{-1} in Cu-MOR is larger than the one at ca. 29,500 cm^{-1}. Conversely, Cu-MEL catalysts show a larger contribution of the band at 28,600 cm^{-1}, and its relative area increased with Cu loading (Figure 4-4 (a)). On the other hand, the Cu efficiencies of Cu-MEL catalysts are similar at different Cu loadings, as shown in Figure 4-1. These results suggests that there are active Cu-oxo clusters with different structures in Cu-MEL catalysts, which show more dominant UV-Vis LMCT bands at ca. 30,000 cm^{-1} or 40,000 cm^{-1}, and the concentration of the site which shows more dominant UV-Vis band at ca. 30,000 cm^{-1} increases with Cu loading.

In the UV-Vis spectra of Cu-FER catalysts (Figure 4-4 (b)), a broad negative band and a broad positive band are observed at ca. 12,000 cm^{-1} and 20,000 cm^{-1}, respectively. These results point to the reduction of Cu^{2+} to Cu^{+} and the change in the coordination structure around Cu^{2+} upon CH_4 reaction. Consumption of the bands in LMCT region at ca. 29,000 cm^{-1} and at 35,500-39,000 cm^{-1} are also observed, similar to the Cu-MOR and the Cu-MEL catalysts. The intensity of the band at 29,000 cm^{-1} is roughly constant at lower Cu concentrations of up to 288 µmol/g. CH_4 oxidation yield linearly increased with Cu concentration in this range of Cu loadings. However, at the higher Cu concentrations (when Cu efficiency started to drop, Figure 4-1), the intensity of the band at 29,000 cm^{-1} increased drastically and a red shift of the band at ca. 39,000 cm^{-1} was observed (Figure 4-4 (b)). Cu-MOR-*B* catalysts (chapter 3) also showed an increase of the UV-Vis band at ca. 29,000 cm^{-1} at higher Cu loadings while Cu efficiency dropped. These similarities of the UV-Vis features in Cu-MOR-*B* (chapter 3) and Cu-FER catalysts suggest that similar Cu-oxo clusters are formed in these two catalysts; i.e., those that are able to activate up to two CH_4 molecules per cluster. Such Cu-oxo clusters are transformed into less reactive species at higher Cu loading in Cu-FER catalysts.

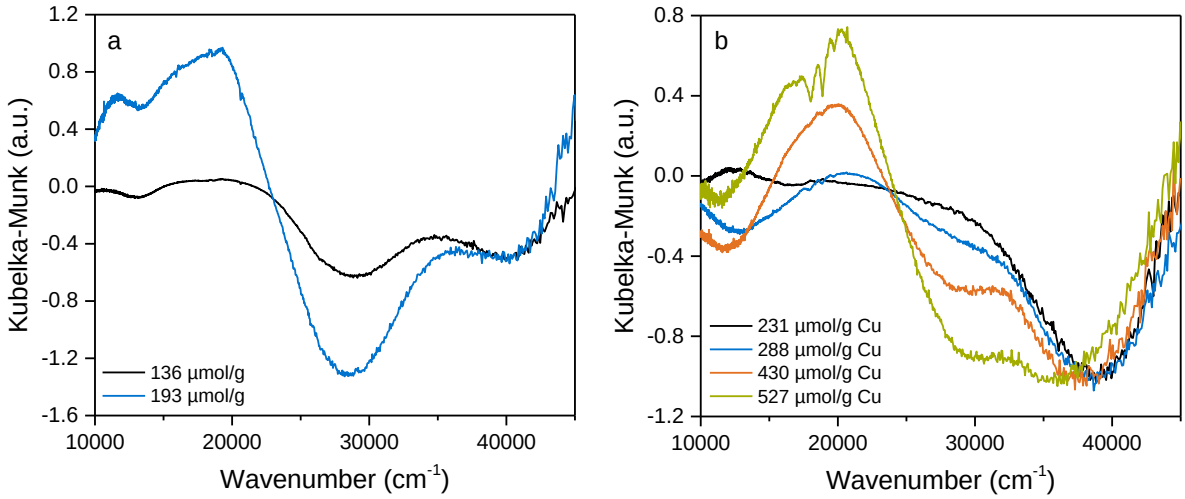

Figure 4-4. UV-Vis difference spectra of Cu-MEL catalysts with Si/Al = 19 (a) and Cu-FER catalysts (b) at different Cu loading, recorded after CH_4 reaction for 30 min. The spectra taken at 0 min CH_4 loading were subtracted. The spectra are normalized to the intensity of the band at 37,000-39,500 cm^{-1} for comparison.

4.3.2. Cu-NU-1000 MOF as a Catalyst for the Selective Oxidation of Methane to Methanol

Cu-NU-1000 catalyst was prepared via ALD following the procedure reported for Ni-NU-1000 by Li et al.[25] The crystallinity and porosity of NU-1000 after Cu deposition were tested by XRD, scanning transmission electron microscopy (STEM) and N_2 physisorption analysis. It was found that the crystallinity as well as the pore structures of NU-1000 has been retained after Cu loading. The concentration of Cu was 10 wt.% (1660 µmol/g), corresponding to an average of approximately 4 Cu atoms per node. In-situ EXAFS analyses during methane oxidation step combined with DFT computational modelling have shown that the most likely structure for Cu active species in NU-1000 is a trimeric Cu-hydroxo species, $[Cu^{II}(OH)_2]_3 \cdot 2H_2O$ (Figure 4-5).[32] However, large uncertainty in Cu coordination number suggests the presence of other Cu clusters, which are likely inactive or unselective in the oxidation of methane to methanol.

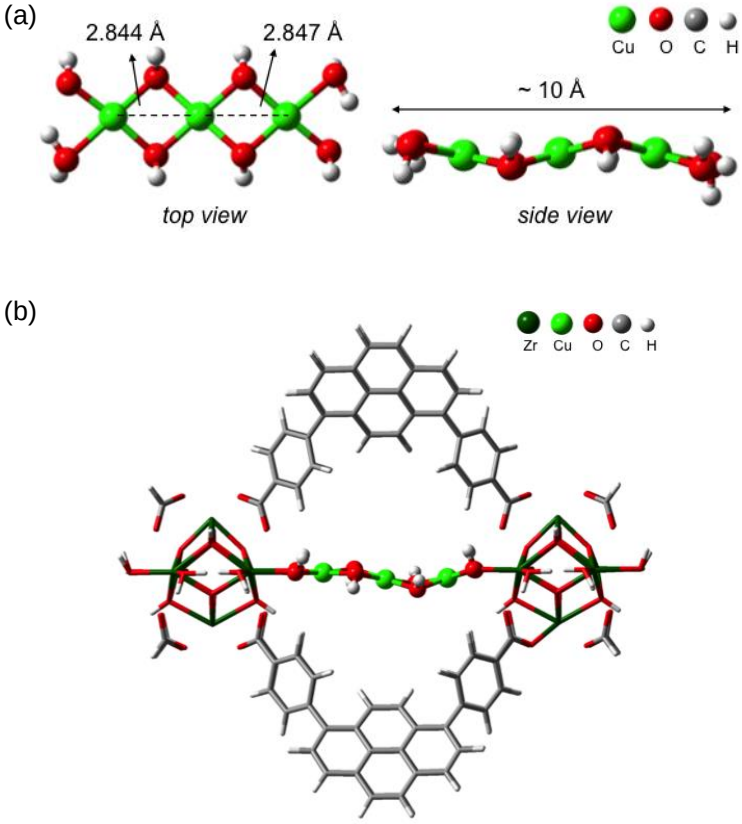

Figure 4-5. DFT-optimized structure of a trimeric Cu-hydroxo cluster (a) and the same species supported on NU-1000 (b). In the structural model supported on NU-1000, the two Cu-Cu distances to the central metal atom are 2.968 and 2.990 Å.

Thermal stability of the Cu-NU-1000 catalyst was investigated under O_2 and inert environments in order to optimize the catalyst activation conditions. Figure 4-6 shows the TGA-DSC results obtained for NU-1000 before Cu-loading in the flow of synthetic air and N_2, respectively. In both cases, the weight loss is primarily due to desorption of the physisorbed water from the MOF pores, which is observed already at 50 °C and is an endothermic process. Subsequent weight loss is observed at much higher temperatures (~310 °C) and is attributed to the removal of H_2O-ligands from the nodes of NU-1000.[24] Finally, at temperatures above ~350 °C we observe further changes: exothermic in synthetic air flow and endothermic in N_2 flow. These are due to the deformation of NU-1000, specifically through the oxidation (exothermic) and the pyrolysis (endothermic) of the linkers in the presence and the absence of O_2, respectively.

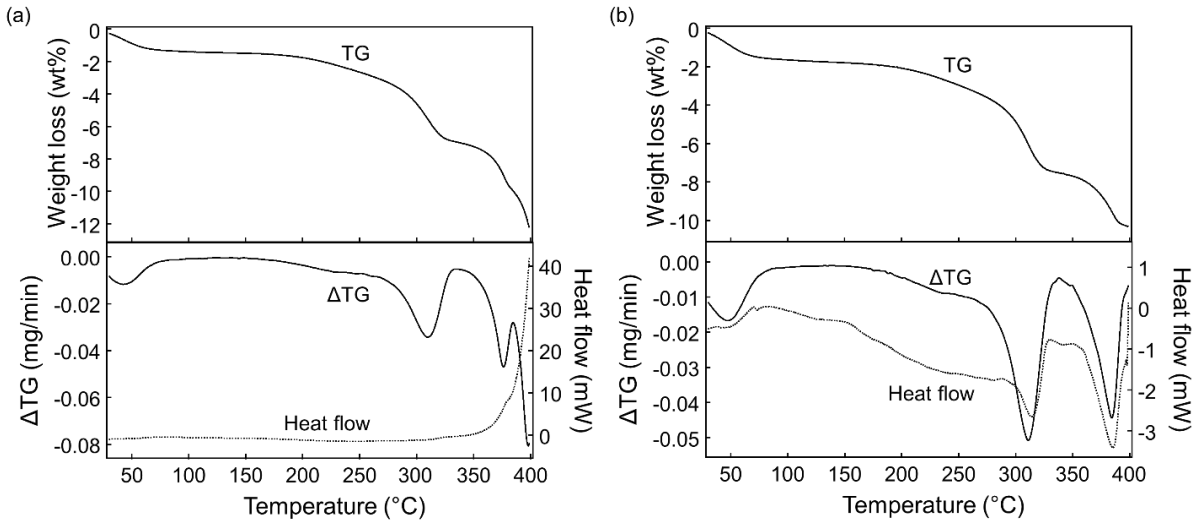

Figure 4-6. TGA-DSC curves measured for NU-1000 in the flow of synthetic air (a) and in N_2 (b) with temperature ramp of 3 K/min.

Comparison of the thermal stability of Cu-NU-1000 and NU-1000 in pure O_2 was also performed by TGA (Figure 4-7). It can be seen that the decomposition of NU-1000 proceeds between 400 °C and 500 °C due to the oxidation of the linkers. On the other hand, Cu-NU-1000 decomposition takes place between 300 °C and 400 °C, indicating that Cu loading on NU-1000 decreases its thermal stability in the presence of O_2. Overall, Cu-NU-1000 shows good stability in the presence of O_2 up to ~300 °C.

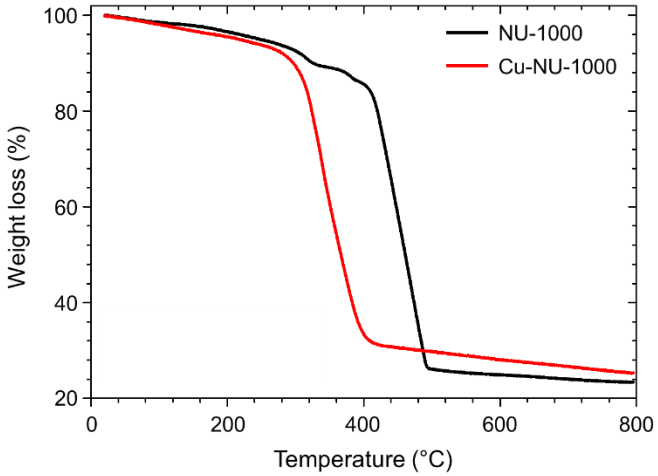

Figure 4-7. TGA of NU-1000 and Cu-NU-1000 in the flow of pure O_2. The curves were obtained with temperature ramp of 3 K/min from room temperature to 800 °C.

As a next step, thermal stability of Cu-NU-1000 in CH_4 flow was investigated in order to determine the appropriate temperature for CH_4 reaction. Figure 4-8 (a) shows the TGA-DSC curves obtained for Cu-NU-1000 in CH_4 flow. In this measurement, a mass spectrometer (MS) was connected to the outlet of TGA-DSC analyzer in order to monitor the formed/desorbed compounds. Cu-NU-1000 was activated at 150 °C in the flow of synthetic air for 1 h and then flushed with CH_4 prior to starting the temperature ramp in CH_4 flow. Changes were not detected for temperatures below 150 °C. A substantial weight loss is observed at 213 °C accompanied by exothermic and endothermic processes at 210 °C and 220 °C, respectively. Formation of CH_3OH and CO_2, m/z = 31 and 44, respectively, is observed at 216 °C (Figure 4-8 (b)). Because under the experiment conditions there is not any O_2 in the gas phase, the exothermic reaction is attributed to the oxidation of CH_4 to CO_x and H_2O by the previously O_2-activated Cu-species deposited in NU-1000. We also observe further fragments (m/z = 28, 41, 42, 43. due to CO, CO_2 and possibly acetic acid) at 221 °C as result of an endothermic process (DSC peak at 220 °C), which could stem from the decarboxylation of organic linkers of NU-1000 in the presence of Cu cations.[33] These results suggest that CH_4 loading reaction has to be performed below 200 °C in order to avoid the over-oxidation of CH_4 by the Cu clusters in NU-1000 and to prevent the structural destruction of the MOF.

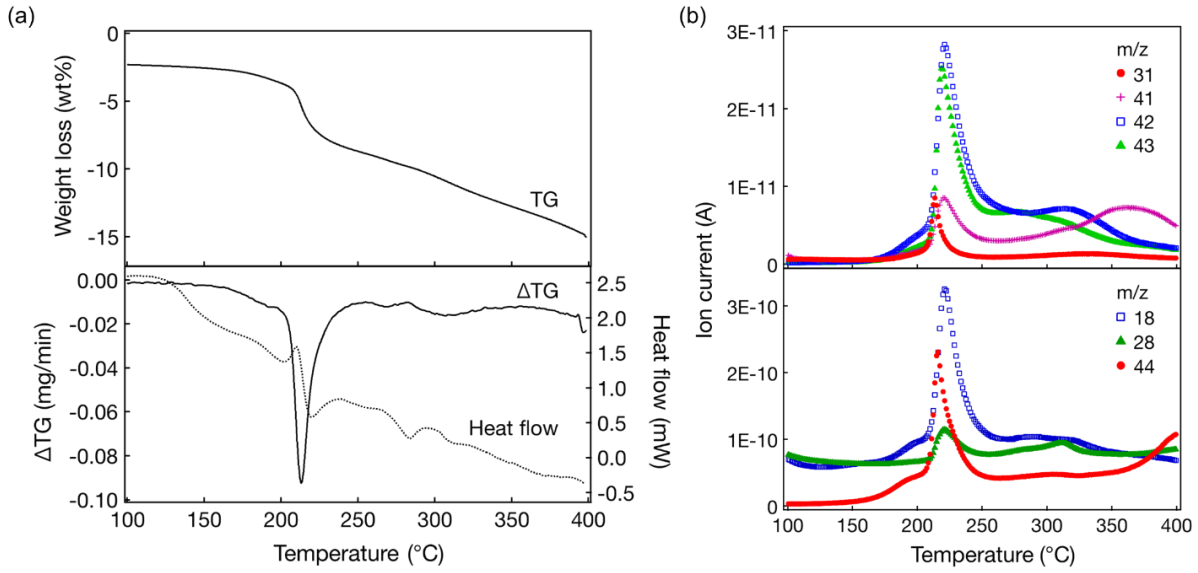

Figure 4-8. TGA-DSC curves obtained for Cu-NU-1000 in CH_4 flow after activation in synthetic air flow (a) and the corresponding MS-signals of the observed TG-DSC test desorption products (b). The catalyst was heated up at 3 K/min temperature ramp.

The stability of Cu-NU-1000 was analyzed along the activation treatment in the presence of O_2. Figure 4-9 shows TGA curve as well as MS signals during activation of the catalyst at 200 °C. A weight loss of ca. 4% was observed during heating of the catalyst, which can also be seen in Figure 4-7. When the temperature was kept at 200 °C for 3 hours, additional weight loss of ca. 4% was observed. Analysis of the gas products during the activation treatment in the thermobalance showed that the overall weight loss is due not only to dehydration but also to the decomposition of remnants from the Cu complex used for the synthesis of Cu-NU-1000. Besides dehydration of the catalyst (m/z = 18), the fragments m/z = 28, 30, 44, 45 were observed (Figure 4-10), which correspond to fragmentation of dimethylamino-2-propoxy ligand and its partial oxidation products. These fragments were only detected for fresh samples under oxidative activation and were not detected during methane activation or steam treatment.

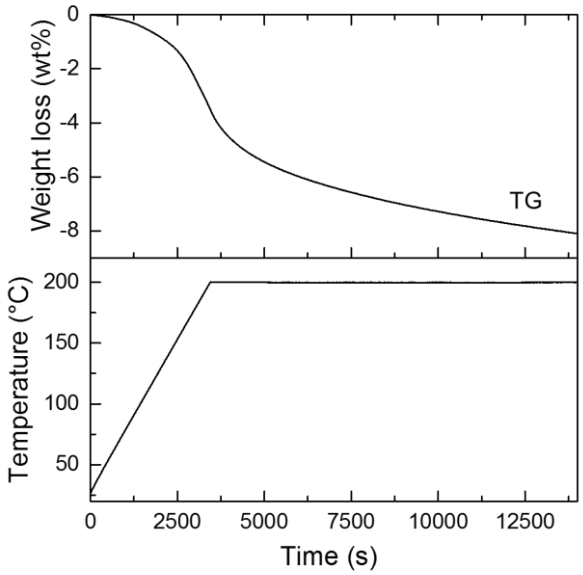

Figure 4-9. TGA curve obtained during the thermal activation of Cu-NU-1000 in the flow of synthetic air.

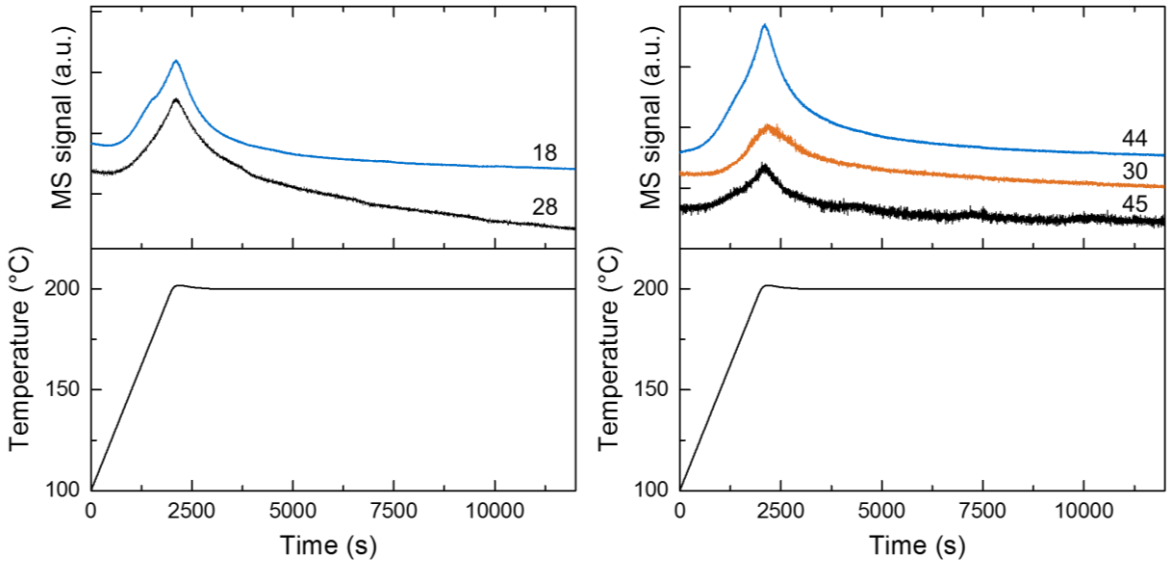

Figure 4-10. MS signals obtained during the thermal activation of Cu-NU-1000 in the flow of pure O_2.

Based on these results, the stepwise oxidation of methane to methanol on Cu-NU-1000 was performed as following. First, Cu-NU-1000 was pretreated in O_2 flow at 200 °C for 3 h to remove physisorbed water. Then, the reactor was cooled to 150 °C and purged with pure He. In the second step, the pretreated Cu-NU-1000 was exposed

to a flow of pure CH_4 at 150 °C for 3 h. During this step, partial reduction of Cu^{2+} into Cu^{+} was observed by XANES.[32] The weight of the Cu-NU-1000 sample was monitored under CH_4 loading conditions by TGA analysis and it was determined that thermal decomposition of Cu-NU-1000 does not occur under the selected conditions. In the final step, water was introduced in the form of 10% steam in He at 135 °C to desorb the products methanol, dimethyl ether and CO_2. It should be noted that water is also produced during CH_4 oxidation. However, the amount is negligible in comparison to the steam concentration used in the extraction step, and therefore quantification is not performed. We performed three consecutive cycles of the three-stage reaction in order to determine the activity and the stability of Cu-NU-1000. As shown in Table 4-2 (condition A), in the first cycle we observed CH_4 oxidation products equivalent to 43.9 µmol/g and a selectivity to methanol and DME (17.7 and 2.0 µmol, respectively) of ca. 45 %. We note a decrease in activity in the subsequent two cycles, with overall yields of 30.7 and 21.8 µmol/g, respectively. However, the yield of CO_2 decreased by 40% per cycle, while the methanol and DME yields decreased only 14% per cycle. Thus, the selectivity towards methanol and DME increased to 53% and 61 %, respectively. On the other hand, if the methane-loading step is omitted (condition B), neither methanol nor DME were produced, but ca. 12 µmol/g of CO_2 was detected. This indicates that a part of CO_2 observed during H_2O steam-assisted product desorption stems from the catalyst itself.

We have also tested the methane to methanol reaction with 50 % steam and 50 % He to desorb the products in the third step in order to investigate the effect of steam treatment conditions on the catalyst deactivation. Under higher H_2O steam concentration, more CO_2 was produced, and less methanol and DME formed (condition C in Table 4-2). While total products equivalent to 60 µmol/g were obtained in the first catalytic cycle, the combined yield of methanol dimethyl ether was only approximately 8 µmol/g (14 % selectivity). Since activation and CH_4 loading conditions are identical and only the H_2O concentration has been changed, we speculate that the additional amount of CO_2 formed stems mainly from decarboxylation of linkers in Cu-NU-1000.[34] Indeed, 60 % of the pore volume was lost after the first cycle of methane reaction with H_2O-assisted product desorption with 50% H_2O/50% He (Table 4-3). It was found that NU-1000 without Cu content also produced CO_2 when subjected to the same reaction conditions (condition D in Table 4-2). In contrast, when 10% steam in He was used, the change in the pore volume and surface area of the Cu-NU-1000 was

only 1-2 %. These results indicate that the H_2O steam treatment has to be performed at lower H_2O concentration, e.g. 10% in He, in order to prevent the partial decomposition of Cu-NU-1000.

Table 4-2. The activity and selectivity for the oxidation of methane on (Cu-)NU-1000 for multiple cycles.

Conditions[a]	Cycle	Carbon yield (μmol/g)				Carbon selectivity (%)	
		Methanol	DME	CO_2	Total	Methanol + DME	CO_2
A	1	17.7	2.0	24.2	43.9	44.9	55.1
	2	15.8	0.6	14.3	30.7	53.4	46.6
	3	13.2	0.1	8.5	21.8	61.0	39.0
B	1	0	0	11.8	11.8	0	100
C	1	6.9	1.3	51.7	59.9	13.7	86.3
	2	2.9	0.7	31.7	35.4	10.3	89.7
	3	2.2	0.7	30.1	33.0	8.9	91.1
D	1	0.5	0.5	34.5	35.5	2.8	97.2
	2	0.4	0.6	21.7	22.7	4.5	95.5

[a]reaction conditions: (A) 3 cycles on the Cu-NU-1000 with activation in O_2 at 200 °C for 3 h, CH_4 loading at 150 °C for 3 h, and steam-assisted product desorption in the flow of 10% H_2O and 90% He for 2 h at 135 °C. (B) 1 cycle on the Cu-NU-1000 under the same conditions as A but without CH_4 loading step. (C) 3 cycles on the Cu-NU-1000 with activation in O_2 at 150 °C for 1 h, CH_4 loading at 150 °C for 3 h, and steam-assisted product desorption in the flow of 50% H_2O and 50% He for 30 min at 135 °C. (D) 2 cycles on the NU-1000 with activation in O_2 at 150 °C for 1 h, CH_4 loading at 150 °C for 3 h, and steam-assisted product desorption in the flow of 50% H_2O and 50% He for 30 min at 135 °C.

Table 4-3. N_2 physisorption properties of Cu-NU-1000 before and after reaction cycles.

Sample	BET surface area (m^2/g)	Pore volume (cm^3/g)
NU-1000	2290	1.55
Cu-NU-1000	1749	1.15
Cu-NU-1000 after 1 cycle [a]	1712	1.14
Cu-NU-1000 after 3 cycle [a]	1689	1.10
Cu-NU-1000 after 1 cycle [b]	570	0.46

[a]Steam:helium = 1:9; [b]Steam:helium = 1:1.

The stability of Cu-NU-1000 catalyst under the reaction conditions was further tested by TGA of fresh and spent Cu-NU-1000 in N_2 flow with H_2O steam-assisted product desorption in 10% H_2O and 90% He flow (Figure 4-11). It can be seen that the thermal stability of the material was not affected after a catalytic cycle. Analysis of XRD patterns of the Cu-NU-1000 before and after reaction was also done (Figure 4-12) and decrease in the crystallinity of Cu-NU-1000 was not observed after reaction of the catalyst with CH_4 or H_2O steam-assisted product desorption, in good agreement with the results from N_2 adsorption and TGA. All these results show that Cu-NU-1000 material is stable under the reaction conditions applied for methane oxidation to methanol.

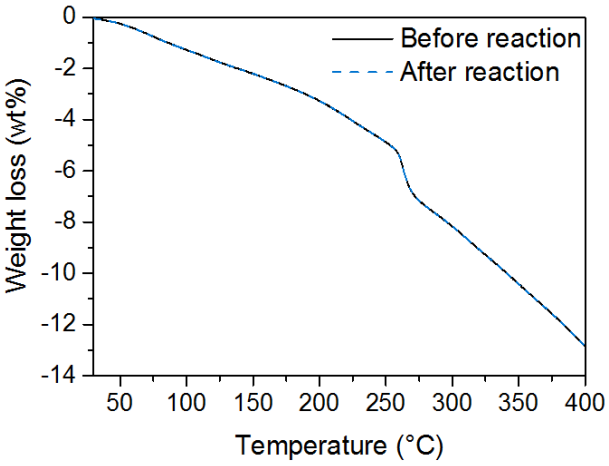

Figure 4-11. TGA curves of Cu-NU-1000 before and after a reaction cycle. The measurements were carried out during ramping at 3 K/min from room temperature to 400 °C in N_2 flow.

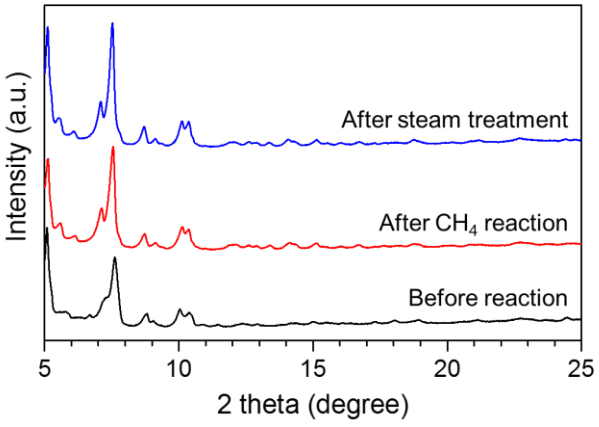

Figure 4-12. XRD patterns of the Cu-NU-1000 catalyst before reaction, after reaction with CH_4 and after desorption of the products by steam treatment in 10% H_2O and 90% helium.

As a next step, the origin of the Cu-activity in Cu-NU-1000 in relation to the fraction of Cu(II) is discussed. It was observed that ~15% of total Cu is present as Cu^{+} and ~85% in Cu^{2+}, and only ca. 9% of Cu^{2+} is reduced into Cu^{+} upon reaction with CH_4.[32] We suggest that the 15 % Cu^{+} already present under ambient conditions does not contribute to methane conversion because the formation of Cu^{0} was not observed by XANES upon CH_4 reaction.[32] Increase of Cu^{+} species by 9% during CH_4 reaction is suggested to be the consequence of reduction of Cu(II) by reaction with methane.[35-36] We surmise that the extent of Cu^{2+} reduction in Cu-clusters of a few atoms via methane loading at 150 °C is thermodynamically limited.[37] We, hence, conclude that the methane conversion and selectivity attributable to the metal deposited on the MOF nodes are achieved by just a fraction (9 %) of the Cu in Cu-NU-1000. This fraction amounts to 149 µmol/g of the total 1660 µmol/g Cu species on the node. The stoichiometries for the redox reaction forming methanol and CO_2 can be calculated by equations 4.1 and 4.2, respectively, where the active Cu(II) species is represented as $Cu(OH)_2$. The oxidation of methane to methanol and methane to CO_2 require 2 and 8 equivalents of $Cu(OH)_2$, respectively.

$$CH_4 + 2Cu(OH)_2 \rightleftharpoons CH_3OH + Cu_2O + 2H_2O \quad (4.1)$$

$$CH_4 + 8Cu(OH)_2 \rightleftharpoons CO_2 + 4Cu_2O + 10H_2O \quad (4.2)$$

Thus, in the first cycle, it requires 43.9 µmol CH_4 to reduce 233 µmol $Cu(OH)_2$ to form 19.7 µmol methanol plus dimethyl ether and 24.2 µmol CO_2, and this is 84 µmol $Cu(OH)_2$ more than the 149 µmol predicted to be converted by the XANES analysis.[32] Thus, it is concluded that the excess CO_2 is produced during the steaming step via decarboxylation of Cu-NU-1000. We note that there are precedents for decarboxylation of carboxylic acids by Cu(II) ions[38] and the proto decarboxylation of aromatic carboxylic acids is catalyzed by Cu(I) ions.[33, 39] Thus, assuming that approximately 150 µmol of $Cu(OH)_2$ are converted during the methane loading step, which transform 33.5 µmol CH_4 to 19.7 µmol methanol plus dimethyl ether and 13.8 µmol CO_2, the 10.4 µmol CO_2 is attributed to the decarboxylation of linkers. Indeed, in line with this estimation, 11.8 µmol/g of CO_2 was observed as a sole product during steam treatment in 10% H_2O and 90% helium in a blank test in which the catalyst was not contacted with methane. Taken this into account, the selectivity for methane oxidation to methanol and dimethyl ether in the first cycle is as high as 56 %, which is comparable to the selectivity measured in the subsequent cycles. As the yields of CO_2 in the second and third cycles

are much lower than in the first cycle, we conclude that decarboxylation of linkers becomes less significant in subsequent cycles. It should be noted that nevertheless a partial deactivation of the catalyst along the cycles is evident from the decrease in methanol and DME yield from 19.7 µmol/g to 13.3 µmol/g. We tentatively attribute this to the deactivation of a fraction of the active Cu species. The evidence raises interesting questions about why only a small fraction (~0.5%) of the available carboxylates seems susceptible to degradation. It might be, for example, that a minor fraction of carboxylates in Cu-NU-1000 feature metal coordination that differs from that indicated by the single-crystal X-ray structure of the parent material.

4.3.3. Comparison of Different Support Materials for the Selective Oxidation of Methane to Methanol on Cu Species

Framework structures of the tested zeolites, MOR, MEL and FER, all possess 8 MR structures on the wall of 10 MR or 12 MR channel. It has been demonstrated that tricopper-oxo clusters in MOR are stabilized preferably at the pore mouths of 8 MR side pockets.[4] On the other hand, substantial amount of spectator species were observed in Cu-MFI catalysts, even if the catalysts were prepared under well-controlled conditions.[19] The lack of 8 MR in MFI-type zeolite suggests that the formation of Cu-oxo clusters which are active in CH_4 oxidation are preferably formed at 8 MR. It has been proposed that 8 MR pore structures are preferred for the formation of active Cu-oxo clusters due to the structure confinement effect.[5] However, Cu efficiency of 1/3 obtained also for Cu-MEL catalysts, which has 8 MR shallow dents on the wall of 10 MR channel instead of 8 MR pores, suggests that 8 MR pores are not essential for the formation of active Cu species. It seems that the presence of 8 MR on the wall of larger channels such as 10 MR and 12 MR are more important for the formation of active Cu-oxo clusters. In addition, higher fraction of paired Al sites seems to be preferred for the active sites formation. Study on Cu-MFI catalysts has shown that higher concentration of paired Al sites results in the higher concentration of multinuclear Cu-oxo clusters formed.[19] In the Cu-MOR and Cu-MEL catalysts, which possess higher fraction of paired Al sites, almost linear increase of CH_4 oxidation yield with the Cu concentration was observed. This indicates that the presence of Al pairs facilitates the formation of active multinuclear Cu-oxo clusters at low Cu concentrations. On the other hand, in Cu-FER catalysts, where only 21% of Al sites are paired, a threshold Cu concentration was observed before starting to form active Cu species. Therefore, to sum up, the

formation of active Cu-oxo clusters in zeolites is enhanced by the presence of 8 MR structure on the wall of larger main channels as well as high fraction of paired Al sites are essential.

Cu clusters on a metal organic framework with good thermal stability, such as NU-1000, are also able to oxidize CH_4 to methanol. The activity is attributed to the Cu-hydroxo-like species in NU-1000 MOF, bridging the Zr_6 nodes.[32] Overall process temperature was reduced; in particular the catalyst activation can be performed at only 200 °C. The yield of methanol and DME over Cu-NU-1000 was ca. 20 µmol/g at the first reaction cycle, which is much greater than the yield of some Cu-zeolite catalysts at the same conditions.[12, 22] A highly active Cu-MOR catalyst which forms single-site $[Cu_3(\mu\text{-}O)_3]^{2+}$ at 500 °C has been reported to show the methanol yield in the same order of magnitude when activated at 200 °C.[21] However, large fraction of spectator Cu species are present in the Cu-NU-1000 catalyst. Deactivation of the catalyst over reaction cycles was also observed.

This study on the Cu-zeolite catalysts as well as on a Cu-MOF catalyst points out the important requirements of the support material for the preparation of Cu-based catalysts with high CH_4 oxidation activity. First, the importance of structural confinement effect is reflected as the preference of the presence of 8 MR in the zeolite structure as well as paired framework Al sites. Low methanol yield on Cu-oxide clusters supported on silica also indicates that the well-defined micropores in zeolites are advantageous on the formation of active Cu clusters.[40] Secondly, well-defined pore structure and anchoring sites in zeolites are excellent environment to form active Cu-oxo clusters. Even though NU-1000 MOF provides highly defined anchoring sites at Zr_6 nodes, presence of pores with very different size (from the range of micropore to mesopore) seems to end up in the formation of spectator species as well as large Cu oxide particles.[32] Lastly, high thermal stability and redox resistance of support materials are required to retain high methanol yield over the reaction cycles. It has been shown that Cu-zeolite catalysts show excellent stability during CH_4 oxidation reaction cycles.[4, 19] On the other hand, organic linkers in NU-1000 MOF can be decarboxylated by Cu clusters, which causes the deactivation of the catalyst.

4.4. Conclusions

Selective oxidation of methane to methanol was carried out on Cu-zeolites with different framework structures and on Cu-NU-1000 MOF. Cu-MOR, Cu-MEL and Cu-FER catalysts with various Cu loading were prepared by aqueous ion-exchange under well-controlled conditions to study the effect of zeolite framework structure on the formation of active Cu-oxo clusters. Cu-MOR catalysts with Si/Al = 11 have shown 1 CH_4/3 Cu stoichiometry due to the formation of single-site $[Cu_3(\mu\text{-}O)_3]^{2+}$ species, which shows a dominant UV-Vis band at ca. 30,000 cm^{-1}. Cu-MEL catalysts have shown Cu efficiency of ca. 0.33 at various Si/Al ratios and Cu loadings, while UV-Vis spectroscopy has suggested the presence of active Cu-oxo clusters with different structures. Cu-FER catalysts have shown a threshold Cu concentration of 142 µmol/g to start forming active Cu-oxo clusters, possibly due to the small fraction of paired Al sites that stabilize dimeric and trimeric Cu clusters. Above the threshold Cu concentration, similarities in the UV-Vis spectra of Cu-FER catalysts to Cu-MOR catalysts suggest the formation of Cu-oxo clusters with high reactivity at medium Cu concentrations and their transformation into less reactive form with increasing Cu loading in the Cu-FER catalysts.

In Cu-NU-1000 catalyst, Cu species have a trimeric Cu-hydroxide-like structure that bridges two nodes across the c-pore of the MOF. Cu-NU-1000 has been shown to be able to oxidize methane into methanol under milder conditions, although a significant fraction of the Cu atoms in Cu-NU-1000 appears to be spectators. Active Cu species deposited in NU-1000 convert methane at 150 °C with a 45-60% selectivity to methanol and DME, when H_2O steam-assisted product desorption is performed in 10% H_2O in inert. Excess CO_2 produced during the first cycle derives from partial decarboxylation of the NU-1000 linkers under reaction conditions, while the framework structure of Cu-NU-1000 was retained. High H_2O concentration during product desorption resulted in the collapse of the MOF structure, producing larger amount of CO_2.

Three essential aspects have to be considered for choosing support materials for Cu-clusters: (i) structural confinement effect, (ii) well-defined pore structure and anchoring sites and (iii) high thermal stability and oxidation resistance. Lacking one of these properties could result in the poor performance or the stability of the Cu-loaded catalysts.

4.5. Acknowledgement

The financial support from the Deutsche Forschungsgemeinschaft DFG under project LE1187/13-1 is acknowledged. Part of the research was supported by the TUM International Graduate School of Science and Engineering (IGSSE) and the Max-Buchner Forschungsstiftung from DECHEMA (Grant number 3568). Insu Lee and Lei Tao are acknowledged for the support in experiments. The author thanks Xaver Hecht for N_2 physisorption measurements. Part of this work was supported by the Inorganometallic Catalyst Design Center, and EFRC funded by the U.S. Department of Energy (DoE), Office of Science, Office of Basic Energy Sciences (DE-SC0012702).

4.6. Appendix

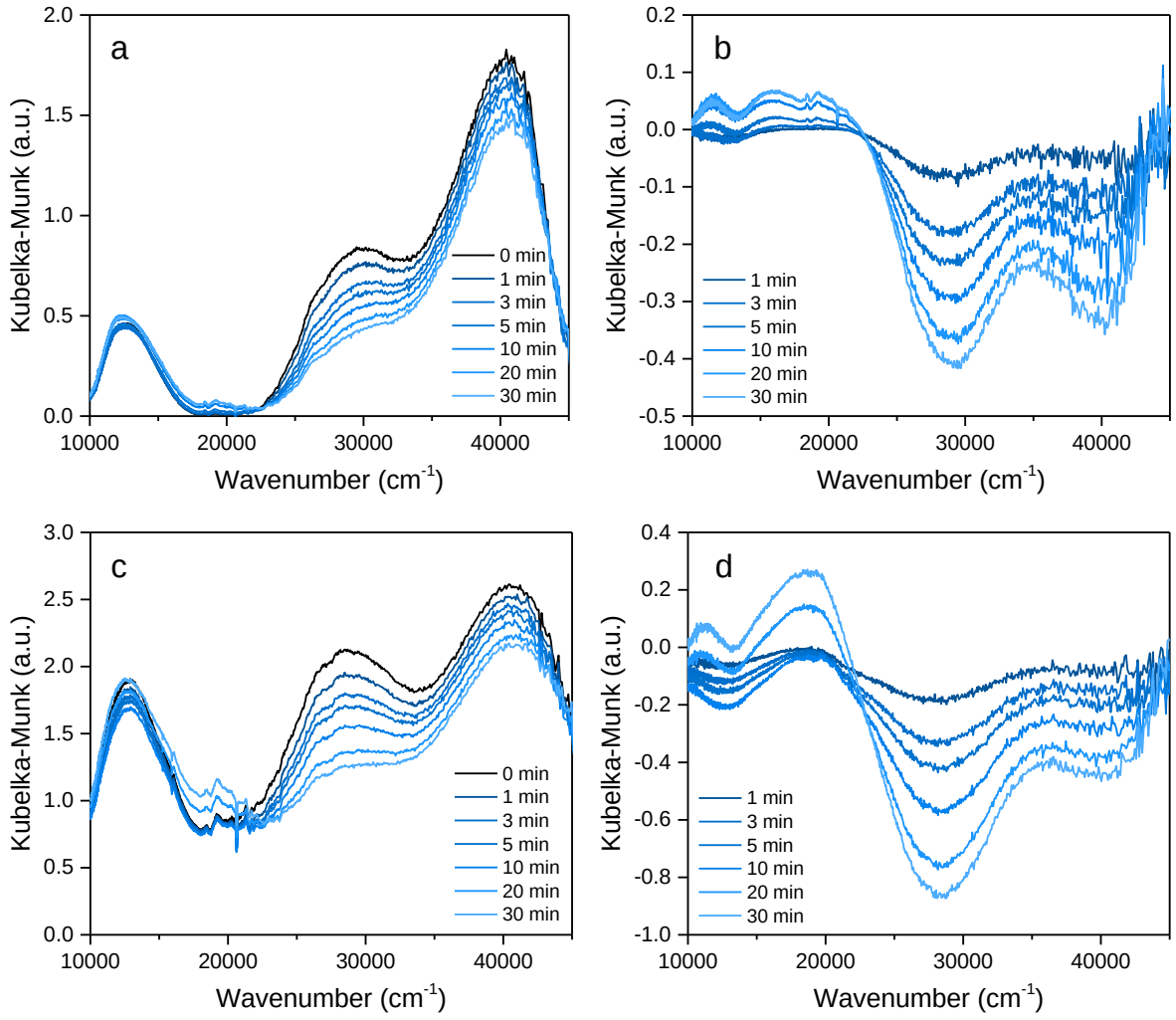

Figure A 4-1. In-situ UV-Vis spectra (a,c) and difference spectra (b,d) of Cu-MEL catalysts (Si/Al = 19) with Cu loadings of 136 µmol/g (a,b) and 193 µmol/g (c,d) measured during CH_4 loading.

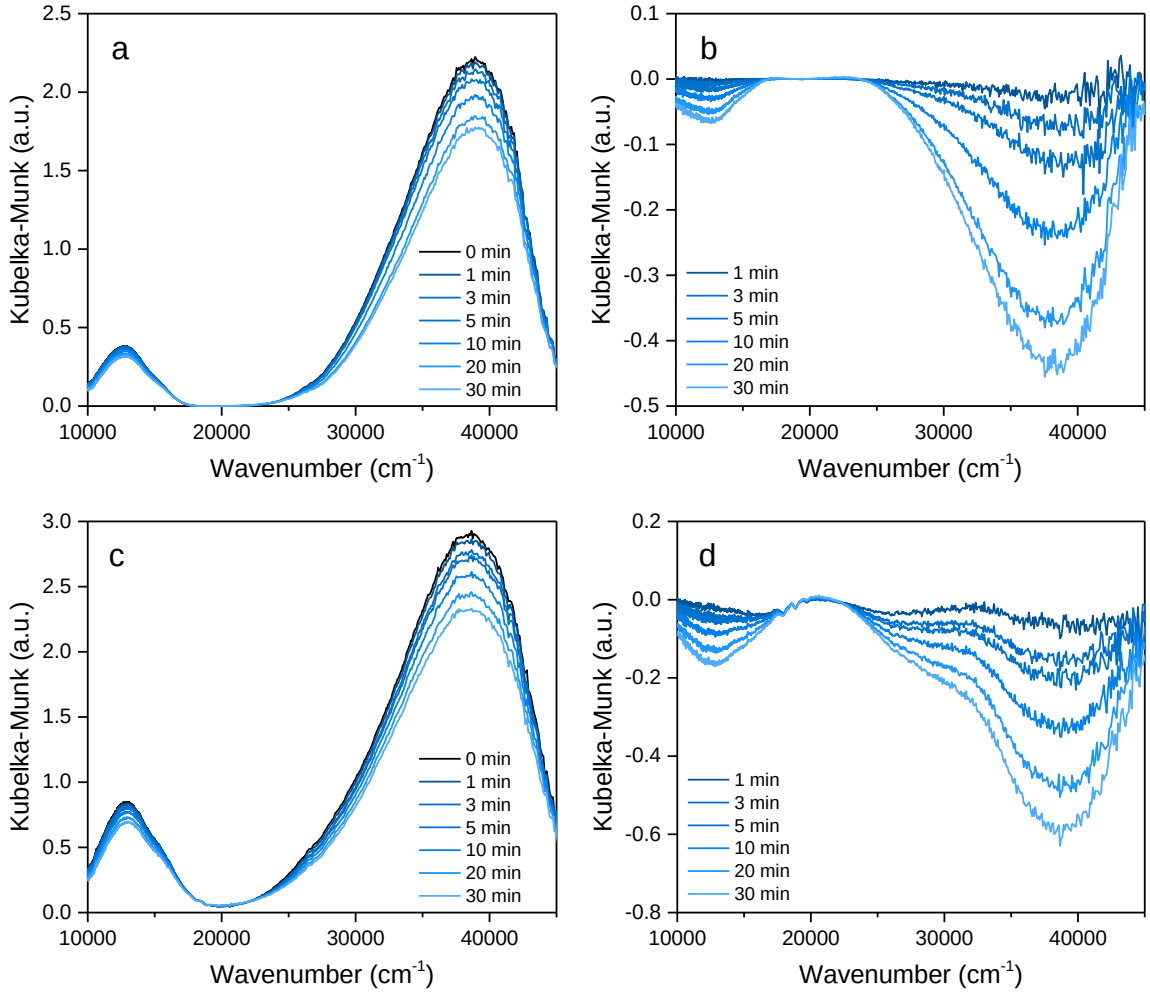

Figure A 4-2. In-situ UV-Vis spectra (a,c) and difference spectra (b,d) of Cu-FER catalysts with Cu loadings of 231 µmol/g (a,b) and 288 µmol/g (c,d) measured during CH_4 loading.

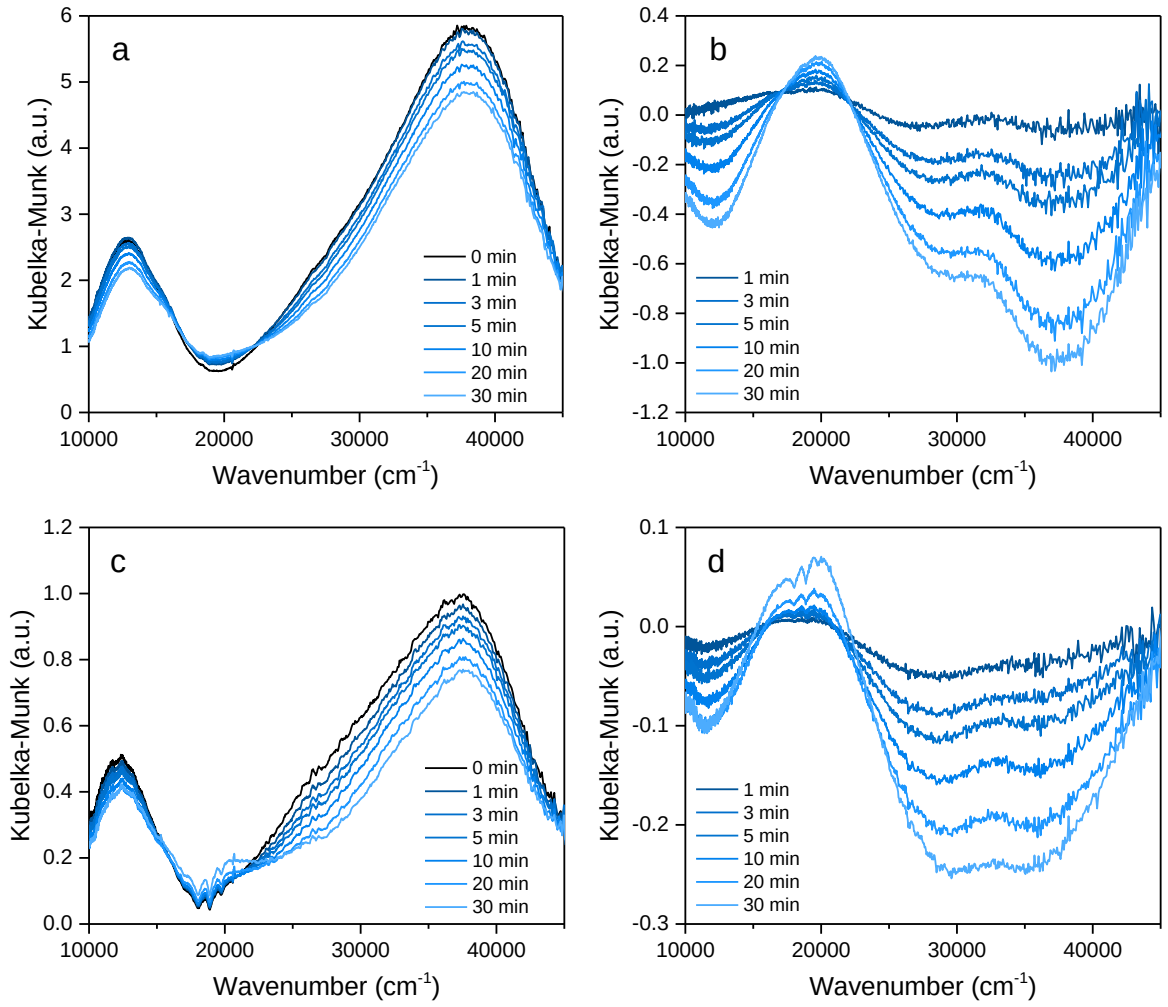

Figure A 4-3. In-situ UV-Vis spectra (a,c) and difference spectra (b,d) of Cu-FER catalysts with Cu loadings of 430 µmol/g (a,b) and 527 µmol/g (c,d) measured during CH_4 loading.

4.7. Reference

1. Groothaert, M. H.; Smeets, P. J.; Sels, B. F.; Jacobs, P. A.; Schoonheydt, R. A., Selective Oxidation of Methane by the Bis(μ-oxo)dicopper Core Stabilized on ZSM-5 and Mordenite Zeolites. *J. Am. Chem. Soc.* **2005**, *127*, 1394.
2. Vanelderen, P.; Hadt, R. G.; Smeets, P. J.; Solomon, E. I.; Schoonheydt, R. A.; Sels, B. F., Cu-ZSM-5: A Biomimetic Inorganic Model for Methane Oxidation. *J. Catal.* **2011**, *284*, 157.
3. Alayon, E. M.; Nachtegaal, M.; Ranocchiari, M.; van Bokhoven, J. A., Catalytic Conversion of Methane to Methanol over Cu-Mordenite. *Chem. Commun.* **2012**, *48*, 404.
4. Grundner, S.; Markovits, M. A. C.; Li, G.; Tromp, M.; Pidko, E. A.; Hensen, E. J. M.; Jentys, A.; Sanchez-Sanchez, M.; Lercher, J. A., Single-Site Trinuclear Copper Oxygen Clusters in Mordenite for Selective Conversion of Methane to Methanol. *Nat. Commun.* **2015**, *6*, 7546.
5. Park, M. B.; Ahn, S. H.; Mansouri, A.; Ranocchiari, M.; van Bokhoven, J. A., Comparative Study of Diverse Copper Zeolites for the Conversion of Methane into Methanol. *ChemCatChem* **2017**, *9*, 3705.
6. Pappas, D. K.; Borfecchia, E.; Dyballa, M.; Pankin, I. A.; Lomachenko, K. A.; Martini, A.; Signorile, M.; Teketel, S.; Arstad, B.; Berlier, G.; Lamberti, C.; Bordiga, S.; Olsbye, U.; Lillerud, K. P.; Svelle, S.; Beato, P., Methane to Methanol: Structure–Activity Relationships for Cu-CHA. *J. Am. Chem. Soc.* **2017**, *139*, 14961.
7. Le, H. V.; Parishan, S.; Sagaltchik, A.; Göbel, C.; Schlesiger, C.; Malzer, W.; Trunschke, A.; Schomäcker, R.; Thomas, A., Solid-State Ion-Exchanged Cu/Mordenite Catalysts for the Direct Conversion of Methane to Methanol. *ACS Catal.* **2017**, 1403.
8. Ipek, B.; Wulfers, M. J.; Kim, H.; Göltl, F.; Hermans, I.; Smith, J. P.; Booksh, K. S.; Brown, C. M.; Lobo, R. F., Formation of $[Cu_2O_2]^{2+}$ and $[Cu_2O]^{2+}$ toward C–H Bond Activation in Cu-SSZ-13 and Cu-SSZ-39. *ACS Catal.* **2017**, 4291.
9. Ipek, B.; Lobo, R. F., Catalytic Conversion of Methane to Methanol on Cu-SSZ-13 using N_2O as Oxidant. *Chem. Commun.* **2016**, *52*, 13401.
10. Wulfers, M. J.; Teketel, S.; Ipek, B.; Lobo, R. F., Conversion of Methane to Methanol on Copper-Containing Small-Pore Zeolites and Zeotypes. *Chem. Commun.* **2015**, *51*, 4447.
11. Narsimhan, K.; Michaelis, V. K.; Mathies, G.; Gunther, W. R.; Griffin, R. G.; Román-Leshkov, Y., Methane to Acetic Acid over Cu-Exchanged Zeolites: Mechanistic Insights from a Site-Specific Carbonylation Reaction. *J. Am. Chem. Soc.* **2015**, *137*, 1825.
12. Sheppard, T.; Hamill, C. D.; Goguet, A.; Rooney, D. W.; Thompson, J. M., A Low Temperature, Isothermal Gas-Phase System for Conversion of Methane to Methanol over Cu-ZSM-5. *Chem. Commun.* **2014**, *50*, 11053.
13. Pappas, D. K.; Borfecchia, E.; Lomachenko, K. A.; Lazzarini, A.; Gutterød, E. S.; Dyballa, M.; Martini, A.; Berlier, G.; Bordiga, S.; Lamberti, C.; Arstad, B.; Olsbye, U.; Beato, P.; Svelle, S., Cu-Exchanged Ferrierite Zeolite for the Direct CH_4 to CH_3OH Conversion: Insights on Cu Speciation from X-Ray Absorption Spectroscopy. *Top. Catal.* **2019**.

14. Knorpp, A. J.; Pinar, A. B.; Newton, M. A.; Sushkevich, V. L.; van Bokhoven, J. A., Copper-Exchanged Omega (MAZ) Zeolite: Copper-concentration Dependent Active Sites and its Unprecedented Methane to Methanol Conversion. *ChemCatChem* **2018**, *10*, 5593.

15. Pappas, D. K.; Martini, A.; Dyballa, M.; Kvande, K.; Teketel, S.; Lomachenko, K. A.; Baran, R.; Glatzel, P.; Arstad, B.; Berlier, G.; Lamberti, C.; Bordiga, S.; Olsbye, U.; Svelle, S.; Beato, P.; Borfecchia, E., The Nuclearity of the Active Site for Methane to Methanol Conversion in Cu-Mordenite: A Quantitative Assessment. *J. Am. Chem. Soc.* **2018**, *140*, 15270.

16. Kim, Y.; Kim, T. Y.; Lee, H.; Yi, J., Distinct Activation of Cu-MOR for Direct Oxidation of Methane to Methanol. *Chem. Commun.* **2017**, *53*, 4116.

17. Zhao, Z. J.; Kulkarni, A.; Vilella, L.; Norskov, J. K.; Studt, F., Theoretical Insights into the Selective Oxidation of Methane to Methanol in Copper-Exchanged Mordenite. *ACS Catal.* **2016**, *6*, 3760.

18. Grundner, S.; Luo, W.; Sanchez-Sanchez, M.; Lercher, J. A., Synthesis of Single-Site Copper Catalysts for Methane Partial Oxidation. *Chem. Commun.* **2016**, *52*, 2553.

19. Markovits, M. A. C.; Jentys, A.; Tromp, M.; Sanchez-Sanchez, M.; Lercher, J. A., Effect of Location and Distribution of Al Sites in ZSM-5 on the Formation of Cu-Oxo Clusters Active for Direct Conversion of Methane to Methanol. *Top. Catal.* **2016**, *59*, 1554.

20. Kulkarni, A. R.; Zhao, Z.-J.; Siahrostami, S.; Nørskov, J. K.; Studt, F., Cation-Exchanged Zeolites for the Selective Oxidation of Methane to Methanol. *Catal. Sci. Technol.* **2017**.

21. Ikuno, T.; Grundner, S.; Jentys, A.; Li, G. N.; Pidko, E.; Fulton, J.; Sanchez-Sanchez, M.; Lercher, J. A., Formation of Active Cu-oxo Clusters for Methane Oxidation in Cu-Exchanged Mordenite. *J. Phys. Chem. C* **2019**, *123*, 8759.

22. Tomkins, P.; Mansouri, A.; Bozbag, S. E.; Krumeich, F.; Park, M. B.; Alayon, E. M.; Ranocchiari, M.; van Bokhoven, J. A., Isothermal Cyclic Conversion of Methane into Methanol over Copper-Exchanged Zeolite at Low Temperature. *Angew. Chem. Int. Ed.* **2016**, *55*, 5467.

23. Furukawa, H.; Cordova, K. E.; O'Keeffe, M.; Yaghi, O. M., The Chemistry and Applications of Metal-Organic Frameworks. *Science* **2013**, *341*, 1230444.

24. Planas, N.; Mondloch, J. E.; Tussupbayev, S.; Borycz, J.; Gagliardi, L.; Hupp, J. T.; Farha, O. K.; Cramer, C. J., Defining the Proton Topology of the Zr_6-Based Metal–Organic Framework NU-1000. *J. Phys. Chem. Lett.* **2014**, *5*, 3716.

25. Li, Z.; Schweitzer, N. M.; League, A. B.; Bernales, V.; Peters, A. W.; Getsoian, A.; Wang, T. C.; Miller, J. T.; Vjunov, A.; Fulton, J. L.; Lercher, J. A.; Cramer, C. J.; Gagliardi, L.; Hupp, J. T.; Farha, O. K., Sintering-Resistant Single-Site Nickel Catalyst Supported by Metal Organic Framework. *J. Am. Chem. Soc.* **2016**, *138*, 1977.

26. Mondloch, J. E.; Bury, W.; Fairen-Jimenez, D.; Kwon, S.; DeMarco, E. J.; Weston, M. H.; Sarjeant, A. A.; Nguyen, S. T.; Stair, P. C.; Snurr, R. Q.; Farha, O. K.; Hupp, J. T., Vapor-Phase Metalation by Atomic Layer Deposition in a Metal–Organic Framework. *J. Am. Chem. Soc.* **2013**, *135*, 10294.

27. Dědeček, J.; Sobalík, Z.; Wichterlová, B., Siting and Distribution of Framework Aluminium Atoms in Silicon-Rich Zeolites and Impact on Catalysis. *Catal. Rev.* **2012**, *54*, 135.

28. Vanelderen, P.; Vancauwenbergh, J.; Tsai, M.-L.; Hadt, R. G.; Solomon, E. I.; Schoonheydt, R. A.; Sels, B. F., Spectroscopy and Redox Chemistry of Copper in Mordenite. *ChemPhysChem* **2014**, *15*, 91.

29. Delabie, A.; Pierloot, K.; Groothaert, M. H.; Weckhuysen, B. M.; Schoonheydt, R. A., The Siting of Cu(II) in Mordenite: a Theoretical Spectroscopic Study. *Phys. Chem. Chem. Phys.* **2002**, *4*, 134.

30. Vogiatzis, K. D.; Li, G.; Hensen, E. J. M.; Gagliardi, L.; Pidko, E. A., Electronic Structure of the $[Cu_3(\mu\text{-}O)_3]^{2+}$ Cluster in Mordenite Zeolite and Its Effects on the Methane to Methanol Oxidation. *J. Phys. Chem. C* **2017**, *121*, 22295.

31. Li, H.; Paolucci, C.; Khurana, I.; Wilcox, L. N.; Goltl, F.; Albarracin-Caballero, J. D.; Shih, A. J.; Ribeiro, F. H.; Gounder, R.; Schneider, W. F., Consequences of Exchange-Site Heterogeneity and Dynamics on the UV-Visible Spectrum of Cu-Exchanged SSZ-13. *Chem. Sci.* **2019**, *10*, 2373.

32. Ikuno, T.; Zheng, J.; Vjunov, A.; Sanchez-Sanchez, M.; Ortuño, M. A.; Pahls, D. R.; Fulton, J. L.; Camaioni, D. M.; Li, Z.; Ray, D.; Mehdi, B. L.; Browning, N. D.; Farha, O. K.; Hupp, J. T.; Cramer, C. J.; Gagliardi, L.; Lercher, J. A., Methane Oxidation to Methanol Catalyzed by Cu-Oxo Clusters Stabilized in NU-1000 Metal–Organic Framework. *J. Am. Chem. Soc.* **2017**, *139*, 10294.

33. Cahiez, G.; Moyeux, A.; Gager, O.; Poizat, M., Copper-Catalyzed Decarboxylation of Aromatic Carboxylic Acids: En Route to Milder Reaction Conditions. *Adv. Synth. Catal.* **2013**, *355*, 790.

34. Darensbourg, D. J.; Longridge, E. M.; Atnip, E. V.; Reibenspies, J. H., A Linear, Monomeric Copper(I) Acetate Derivative, Bis[bis(phenanthroline)copper] bis(acetato)cuprate(1-) Hydrogen Bis(acetate). An Effective Catalyst for the Decarboxylation of Carboxylic Acids. *Inorg. Chem.* **1992**, *31*, 3951.

35. Neylon, M. K.; Marshall, C. L.; Kropf, A. J., In Situ EXAFS Analysis of the Temperature-Programmed Reduction of Cu-ZSM-5. *J. Am. Chem. Soc.* **2002**, *124*, 5457.

36. Vanelderen, P.; Vancauwenbergh, J.; Sels, B. F.; Schoonheydt, R. A., Coordination Chemistry and Reactivity of Copper in Zeolites. *Coord. Chem. Rev.* **2013**, *257*, 483.

37. Navrotsky, A.; Ma, C.; Lilova, K.; Birkner, N., Nanophase Transition Metal Oxides Show Large Thermodynamically Driven Shifts in Oxidation-Reduction Equilibria. *Science* **2010**, *330*, 199.

38. Fitzpatrick, J. H.; Hopgood, D., Metal Ion Catalyzed Decarboxylation. Kinetics and Mechanism of the Oxidative Decarboxylation of Copper(II) Complexes of Aminomalonic Acid in Aqueous Solution. *Inorg. Chem.* **1974**, *13*, 568.

39. Goossen, L. J.; Manjolinho, F.; Khan, B. A.; Rodríguez, N., Microwave-Assisted Cu-Catalyzed Protodecarboxylation of Aromatic Carboxylic Acids. *J. Org. Chem.* **2009**, *74*, 2620.

40. Bozbag, S. E.; Sot, P.; Nachtegaal, M.; Ranocchiari, M.; van Bokhoven, J. A.; Mesters, C., Direct Stepwise Oxidation of Methane to Methanol over Cu–SiO_2. *ACS Catal.* **2018**, *8*, 5721.

5. Conclusions

In this dissertation, it was studied the selective oxidation of methane to methanol on Cu-based catalysts supported on microporous materials.

In the first part (Chapter 2), the formation of $[Cu_3(\mu\text{-}O)_3]^{2+}$ clusters hosted in MOR was investigated in order to understand thermodynamically or kinetically limiting steps of the formation of active Cu-oxo clusters. It is shown that the formation of $[Cu_3(\mu\text{-}O)_3]^{2+}$ species takes place through the formation of precursor species in inert atmosphere, followed by oxidation. The formation of the precursor species was studied by in-situ XAS. First, in the temperature range of 50-300 °C, dehydration of octahedral Cu^{2+} complexes occurs, leading to the formation of μ-oxo bridged Cu^{2+} species coordinated to framework Al sites. These species are auto-reduced into Cu^{+} via thermally driven emission of the bridging oxygen or the generation of OH radicals from $[CuOH]^{+}$. This step occurs already at 200 °C in inert atmosphere, and the maximum concentration of Cu^{+} is reached at 450-500 °C. A small fraction of Cu^{+} was also observed in the presence of O_2, even though Cu^{2+} is thermodynamically more favored under oxidative conditions. We hypothesize that the high mobility of Cu^{+} formed at high temperature is essential to enable the reorganization of Cu cations in MOR pores to form the precursor species of $[Cu_3(\mu\text{-}O)_3]^{2+}$ clusters. Finally, formation of $[Cu_3(\mu\text{-}O)_3]^{2+}$ clusters occurs by the oxidation of the precursor species. It is shown that such oxidation and formation of the active clusters is completed in 1 h even at mild temperatures (50-200 °C). The superior performance of Cu-MOR in methane oxidation compared to other Cu-zeolites is attributed to the high concentration of paired framework Al sites at the pore mouth of 8 MR side pockets of MOR, which is accessible for Cu cations to form Cu-oxo clusters.

In the second part (Chapter 3), it was studied the effect of the presence, type and location of EFAl species on the activity of Cu-MOR. For that, we have prepared series of Cu-MOR materials from two H-MOR zeolites with different EFAl distributions. While distribution of FAl sites is almost identical between the two H-MOR samples, characterization by IR of adsorbed probe molecules showed that one MOR sample (MOR-*B*) possesses more EFAl inside 8 MR side pockets. Cu-MOR catalysts with less EFAl inside 8 MR side pockets (Cu-MOR-*A*) show Cu efficiency of CH_4 activation of ca. 0.33, attributed to the formation of single-site $[Cu_3(\mu\text{-}O)_3]^{2+}$ clusters. On the other hand, Cu-MOR catalysts which contain more EFAl inside 8 MR side pockets (Cu-MOR-

B) have shown the Cu efficiency of up to 0.63. In both series of Cu-MOR catalysts, Cu cations were located at the pore mouth of 8 MR side pockets. In the Cu-MOR catalysts with more EFAl inside 8 MR side pockets, transformation of octahedral Al species to tetrahedral species was observed with increasing Cu concentration by XAS measurements at Al K-edge. The effect of EFAl species on the reactivity of Cu clusters was confirmed by the lower activity of Cu-MOR samples prepared from NH_4-MOR-*B* as a parent sample. In this preparation, FAl sites are protected against dealumination during calcination and, thus, the final Cu-MOR has a lower concentration – and presumably different distribution of EFAl. Although the Cu species formed in the Cu-MOR-*B* catalysts seem to be heterogeneous, we hypothesize that a high concentration of dimeric and/or trimeric Cu species such as *trans-1,2-μ*-peroxo dicopper clusters and $[Cu_3(\mu\text{-}O)_3]^{2+}$ species. The currently achieved CH_4/Cu efficiency of 0.63 can only be explained by the activation of two CH_4 molecules per cluster. The high reactivity of the Cu-oxo clusters are proposed to stem from their interaction with EFAl species located inside 8 MR side pockets of MOR, leading to the change in electronic structures or geometric confinement of the Cu species.

In the third part (Chapter 4), selective oxidation of methane to methanol was performed on various Cu-based catalysts supported on microporous materials, e.g. zeolites and a MOF, in order to investigate the effect of the support materials on the formation of Cu-oxo clusters as well as their reactivity. MOR, MEL and FER were used to prepare Cu-zeolite materials under ion exchange conditions that have been adjusted to avoid the formation of CuO and $Cu(OH)_2$ inactive nanoparticles. Cu-MEL catalysts have shown activated CH_4/Cu stoichiometry of ca. 0.3 at various Si/Al ratio and Cu concentrations, though the presence of active Cu-oxo clusters with different structures is possible. Cu-FER catalysts have shown a threshold Cu concentration of 142 μmol/g, below which the methane oxidation products were not observed. This is hypothesized to be due to a low concentration of paired Al sites, which are able to stabilize active multinuclear Cu-oxo clusters. UV-Vis study of the Cu-FER catalysts has suggested that the highly reactive Cu-oxo clusters, which were proposed in the Cu-MOR catalysts with higher concentration of EFAl inside 8 MR side pockets (Chapter 3), might also form in the Cu-FER catalysts above the threshold Cu concentration. At higher Cu loadings, the additional Cu in the sample might induce the transformation of such highly reactive Cu-oxo clusters into less reactive ones and/or form Cu inactive species. Cu clusters loaded on NU-1000 MOF have also shown methane oxidation activity,

although a significant fraction of Cu is inactive. While some CO_2 forms via decarboxylation of organic linkers of NU-1000 during H_2O steam-assisted product desorption, framework structure of NU-1000 was successfully retained after three cycles of methane oxidation reaction. Our observations on Cu-zeolite and Cu-NU-1000 catalysts suggests that there are three essential aspects to be considered to choose support materials: (i) structural confining environment, (ii) well-defined pore structure and anchoring sites to host Cu-oxo clusters and (iii) high thermal stability and oxidation resistance.

List of Publications

Journal articles

Ikuno, T.; Grundner, S.; Jentys, A.; Li, G. N.; Pidko, E.; Fulton, J.; Sanchez-Sanchez, M.; Lercher, J. A., Formation of Active Cu-oxo Clusters for Methane Oxidation in Cu-Exchanged Mordenite. *J. Phys. Chem. C* **2019**, *123*, 8759.

Ikuno, T.; Zheng, J.; Vjunov, A.; Sanchez-Sanchez, M.; Ortuño, M. A.; Pahls, D. R.; Fulton, J. L.; Camaioni, D. M.; Li, Z.; Ray, D.; Mehdi, B. L.; Browning, N. D.; Farha, O. K.; Hupp, J. T.; Cramer, C. J.; Gagliardi, L.; Lercher, J. A., Methane Oxidation to Methanol Catalyzed by Cu-Oxo Clusters Stabilized in NU-1000 Metal–Organic Framework. *J. Am. Chem. Soc.* **2017**, *139*, 10294.

Ikuno, T.; Chaikittisilp, W.; Liu, Z.; Iida, T.; Yanaba, Y.; Yoshikawa, T.; Kohara, S.; Wakihara, T.; Okubo, T., Structure-Directing Behaviors of Tetraethylammonium Cations toward Zeolite Beta Revealed by the Evolution of Aluminosilicate Species Formed during the Crystallization Process. *J. Am. Chem. Soc.* **2015**, *137*, 14533.

Ishii, H.; Ikuno, T.; Shimojima, A.; Okubo, T., Preparation of Core–Shell Mesoporous Silica Nanoparticles with Bimodal Pore Structures by Regrowth Method. *J. Colloid Interface Sci.* **2015**, *448*, 57.

Schallmoser, S.; Ikuno, T.; Wagenhofer, M. F.; Kolvenbach, R.; Haller, G. L.; Sanchez-Sanchez, M.; Lercher, J. A., Impact of the Local Environment of Brønsted Acid Sites in ZSM-5 on the Catalytic Activity in n-Pentane Cracking. *J. Catal.* **2014**, *316*, 93.

Koike, N.; Ikuno, T.; Okubo, T.; Shimojima, A., Synthesis of Monodisperse Organosilica Nanoparticles with Hollow Interiors and Porous Shells using Silica Nanospheres as Templates. *Chem. Commun.* **2013**, *49*, 4998.

Ikuno, T.; Nomura, A.; Iyoki, K.; Sugawara-Narutaki, A.; Okubo, T.; Shimojima, A., Facile Synthesis of Well-Dispersed Hollow Mesoporous Silica Nanoparticles Using Iron Oxide Nanoparticles as Template. *Chem. Lett.* **2013**, *42*, 316.

Oral Presentations

Ikuno, T.; Grundner, S.; Sanchez-Sanchez, M.; Lercher, J. A. On the Formation of Active Cu-Oxo Clusters in Mordenite for Direct Oxidation of Methane to Methanol. 25th North American Catalysis Society Meeting, Denver, CO, USA, June 2017.

Poster Presentations

Ikuno, T.; Sanchez-Sanchez, M.; Lercher, J. A. Formation of Active Cu-Oxo Clusters in Cu-MOR for Selective Oxidation of Methane to Methanol. 51. Jahrestreffen Deutscher Katalytiker, Weimer, Germany, March 2018.

Ikuno, T.; Sanchez-Sanchez, M.; Lercher, J. A. Formation of Active Cu-Oxo Clusters Hosted in MOR for Selective Oxidation of Methane to Methanol. 30. Deutsche Zeolith-Tagung, Kiel, Germany, February 2018.

Ikuno, T.; Grundner, S.; Sanchez-Sanchez, M.; Lercher, J. A. Selective Oxidation of Methane over Cu-Oxo Clusters Supported on NU1000 Metal Organic Framework. 50. Jahrestreffen Deutscher Katalytiker, Weimer, Germany, March 2017.